Università Politecnica delle Marche
Scuola di Dottorato di Ricerca in Scienze dell'Ingegneria
Corso di Dottorato in Ingegneria Industriale

Tecnologia Bound Metal Deposition: effetto dei parametri di processo sulle proprietà meccaniche delle parti stampate e valutazione dell'impatto ambientale del processo di fabbricazione

Ph.D. Dissertation of:

Tommaso Mancia

Supervisor:

Prof. Archimede Forcellese

Assistant Supervisor:

Prof. Michela Simoncini

Ph.D. Course coordinator:

Prof. G. Di Nicola

XXXV edition - new series

Università Politecnica delle Marche
Scuola di Dottorato di Ricerca in Scienze dell'Ingegneria
Corso di Dottorato in Ingegneria Industriale

Bound Metal Deposition technology: effect of process parameters on the mechanical properties of printed parts and environmental impact evaluation of the printing process

Ph.D. Dissertation of:

Tommaso Mancia

Supervisor:

Prof. Archimede Forcellese

Assistant Supervisor:

Prof. Michela Simoncini

Ph.D. Course coordinator:

Prof. G. Di Nicola

XXXV edition - new series

Università Politecnica delle Marche
Dipartimento di Ingegneria Industriale e Scienze Matematiche
Via Brecce Bianche — 60131 - Ancona, Italy

Abstract

The research project of this work aims at analysing the effect of the process parameters of 3D printing by means of the innovative Bound Metal Deposition (BMD) technology on the mechanical performance of 17-4 PH stainless steel. The investigation involved the realization of tensile specimens, in accordance with the specifications of the ASTM E8 standard, using a 3D printing system based on the BMD technology. The process parameters investigated in the present work were: i) the growth orientation angle with respect to the printing bed, ii) the infill pattern, iii) the printing speed, and iv) the extrusion nozzle diameter. The influence of the aging treatment after the sintering step was also investigated by subjecting some specimens to the H900 aging process, as reported in the MPIF 35 standard.

The tensile tests were carried out according to the ASTM E8 standard. The nominal stress-nominal strain curves, recorded during testing, were analysed in order to obtain the main mechanical properties of 17-4 PH stainless steel, such as elastic modulus, yield strength, ultimate tensile strength and elongation at break. Optical microscopy was carried out on fractured surfaces in order to understand the fracture mechanism. Furthermore, the scanning electron microscopy-energy dispersive X-ray analysis (SEM-EDX) was used in order to obtain detailed information about the chemical composition of samples. A spectrophotometry analysis was also carried out in order to evaluate the constituent elements of the material once sintering phase has taken place. Finally, the environmental sustainability of the 3D printing process of 17-4 PH stainless steel using the BMD technology was studied according to the standardized methodology of Life Cycle Assessment. The effect of the aging heat treatment after the sintering step on the environmental impact was also evaluated.

Summary

List of Figures

List of Tables

Introduction

The evolution of manufacturing technologies in recent years is involving the entire industrial sector worldwide. Even small companies are equipping themselves with manufacturing systems that can make faster manufacturing production, less expensive and that can fully meet the required quality requirements, with the aim of being increasingly competitive in a constantly evolving market. One of the first technological devices to help manufacturing industries was the entry of rapid prototyping that brought an incredible revolution in the creation of prototypes that could take place in much faster times than the standard ones. From rapid prototyping the evolution moved on to rapid casting and then to rapid tooling, able to reduce production times, increasing the quality of the parts produced. In other words, rapid manufacturing has been possible thanks to the advent of Additive Manufacturing (AM), a family of technologies that has revolutionized the concept of traditional production. In fact, if for the concept of standard production, it was expected that to obtain a piece it was necessary to start from a larger part to be processed by removing material to obtain the finished piece, with the AM the start is from the opposite concept, that is to add material only where it is needed to build, layer by layer, the complete part. This has made it possible to significantly reduce the production times of particularly complex parts and to reduce the amount of raw material used and consequently also waste and scrap. The first patent, which provided for a photosensitive thermosetting material that was cured layer by layer with a light source, was introduced in 1984. Since then, the evolution of AM has expanded the technological field, introducing a series of technologies that has allowed it to land in many industrial and non-industrial sectors, greatly increasing the types of materials that can be used. The last frontier that is proving to be of considerable interest at the industrial level concerns metallic materials. If on the one hand traditional technologies still allow to produce metal parts of the highest quality at reduced costs, however, they cannot compete with AM on the complexity of construction. In fact, if the complexity of the part to be realized is too high, traditional technologies, however advanced, may not even allow the generation of the component. AM in this case becomes the predominant technology for the production of complex parts, allowing to obtain details not obtainable otherwise, without increasing production times and costs. This has allowed AM technologies for the production of metal parts to take a key role within many manufacturing industries. However, given the recent development of these technologies, some aspects are still being developed to ensure

high quality of the parts produced. In fact, research in this field is numerous and many researchers worldwide are focusing their studies on AM technologies capable of generating metal parts. Most of them start from the use of metal powder that is welded together by an energy source (laser or electron beam) inside controlled atmosphere chambers. This is because metal powders have very small dimensions and represent one of the limits of use of these printing systems, as in addition to the machinery itself, precautions must be taken in terms of safety of the working environment such as ad hoc systems and personal protective equipment that must be worn by operators on board the machine. With the evolution of technologies, this safety problem in the environments where AM machinery is installed has been taken into consideration and solved with the advent of a technique that allows the use of metal powder but consolidated together with a binder that allows it not to be dispersed in the environment. The production process, named Bound Metal Deposition (BMD) is totally new and completely different from those that provide an energy source for powder welding. In fact, it is a material extrusion system and, once the part is obtained, it is placed in a sintering furnace where the powders are welded together, and the binder is vaporized in order to obtain the completely metallic part. Being a completely new technology, however, it presents some problems. Some mainly concern the aspects of deformation of the parts and the shrinkage stresses during the sintering phase, while others concern the same problems of 3D printing related to Material Extrusion (ME) as a very similar technology, where the choice of process parameters plays a key role.

Being a totally new technology, in the scientific literature there are no adequate studies that can make an effective contribution to the improvement of this technology. For this reason, these aspects have been deepened in the present work, in particular the mechanical properties of the material taken into consideration for this study as a function of the choice of the parameters of the 3D printing process.

The objective of this work, in fact, was to analyze the effect of main parameters and heat treatment of the 3D printing process using BMD technology on the tensile mechanical performance of 17-4 PH stainless steel, metal material used for this study.

To obtain a complete analysis, tensile specimens were made, whose dimensions are in accordance with what is reported in the ASTM E8 standard, through the choice of the main parameters of the ME process that could contribute most to the variation of the mechanical properties of the material, such as the growth orientation angle, the type of infill pattern, the printing speed and the size of the diameter of the extrusion nozzle. Some of the tensile specimens thus made have also been subjected to an

aging process, according to the indications reported in the MPIF standard 35 standard, before being subjected, together with all those relating to the different conditions studied, to tensile tests always following what is indicated in the ASTM E8 standard. The results were then analyzed and reported both in the form of graphs and tables, so as to be able to compare the tensile mechanical properties of 17-4 PH stainless steel obtained in the different 3D printing conditions considered. Stainless steel specimens were also observed using a stereomicroscope at different magnification levels, in order to observe the fracture surfaces, and a scanning electron microscope, with which it was possible carried out an Energy Dispersive X-ray (EDX) analysis. A spectrophotometry analysis was also carried out in order to evaluate the constituent elements of 17-4 PH material once sintering phase has taken place. Finally, the environmental evaluation of the 17-4 PH stainless steel 3D printing process was conducted following the standardized methodology of Life Cycle Assessment, with the objective of evaluating and compare the environmental impacts related to the production and postprocessing of tensile specimens using the BMD technology.

Chapter 1

1 Literature review

The term "Additive Manufacturing" (AM) indicates the technologies for the realization of objects starting from a computerized 3D model and adding the necessary material one layer on top of the other. It differs greatly from traditional subtractive technologies (e.g. milling or turning) that start from a block of material, which is plastically deformed or from which chip-forming material is mechanically removed. In the case of Additive Manufacturing, starting material is in form of powders, filaments or others that are deposited or welded only where it is necessary and in the necessary quantity, thus guaranteeing a high saving of raw material and production time.

The first use of additive techniques dates back to 1986 with the publication of Chuck Hull's patent for stereolithography. The initial idea of the new system was to create physical models and prototypes (hence the name rapid prototyping) to help the design process with printed objects and not limited to virtual representations or drawings [1]. Over time, these techniques have had a strong development with regard to the use of materials, precision and quality of the parts made. The models have therefore been made with even better features, providing more detailed information regarding the 3F (Form, Fit, and Function). Initially, the models allowed to appreciate only the shape and appearance of the object (Form); the greater precision of the processes has allowed to create models in the tolerance required for assembly processes (Fit) and, finally, the better quality of the materials has guaranteed the realization of usable objects (Function) [2]. From this it follows that additive manufacturing processes are no longer limited to prototyping but completely replace traditional production processes.

Since the first patent of stereolithography, additive manufacturing has had a strong development in terms of technology and possible applications. Starting from a limited use for the prototypes to the realization of finished and semi-finished parts. 3D printing machines have been constructed and equipped with different AM techniques that allow the use of a wide number of materials, such as metals, plastics, and ceramic and composite materials.

Additive manufacturing is used in quite every area of industry, with particular reference to:

- automotive sector, for the production of low weight components, spare parts and accessories;
- medical/pharmaceutical sector, for the production of implants and customizable prostheses, models of human bodies for medical training, reconstructions of organic tissues for the testing phase in the development of new medicinal products etc;
- aerospace sector, for the production of accessories with reduced weight thanks to topological optimization and generative design operations;
- construction sector, with concrete printing processes for the construction of entire or part of houses;
- sport sector, for equipment, protection systems and prototypes.

1.1 Advantages of Additive Manufacturing

AM has been defined as a technology capable of radically changing the development and realization of objects, leading to a real new industrial revolution.

3D printing introduces a new concept: depositing the material only where it is needed and without problems associated with the complexity of the components. These technologies allow the creation of very complicated parts, not achievable with traditional techniques. The increase in complexity, however, does not necessarily lead to an increase in the cost of production of the part, unlike what happens for traditional techniques. For designers, this results in a completely new approach to designing and manufacturing parts realized by 3D printing. The possibility of creating complex shapes with low costs guarantees a strong freedom in design, leading to a new design system capable of optimizing the shapes and the weight of the parts.

Additive manufacturing is a technology that can be considered:

- Environmentally sustainable
    - The material unused in a 3D printing process can be recycled (either directly or after some preparation process). The redesign of the parts lead to lighter components, resulting in a reduction in the material

used in the production processes. In addition, for the components production for the transport sectors (e.g., automotive and aerospace), a reduction in weight allows lower fuel consumption, with a consequent reduction in environmental emissions.

- With a reduced time to market
- With a production on request approach
- With a high degree of customization of the product
    - This feature makes AM particularly suitable for biomedical applications, where product customization is often required for implants and prostheses. Partial modifications of objects can be easily done because the production process doesn't change but acts exclusively on CAD drawings. In this way, it is easy to customize the product for each customer, approaching the concept of "mass customization".
- Reduction of the number of components
    - The possibility of producing great complexity parts allows to significantly reduce the number of components of the assemblies. A case in point is provided by the RF antennas of the Optisys company in which, thanks to AM and appropriate design choices, from 100 assembled pieces, it passes to a single component (Figure 1.1). In that specific case, the new design allowed a weight reduction of more than 95%, with delivery times from 11 months to 2 months and a reduction in production costs of 20-25%.

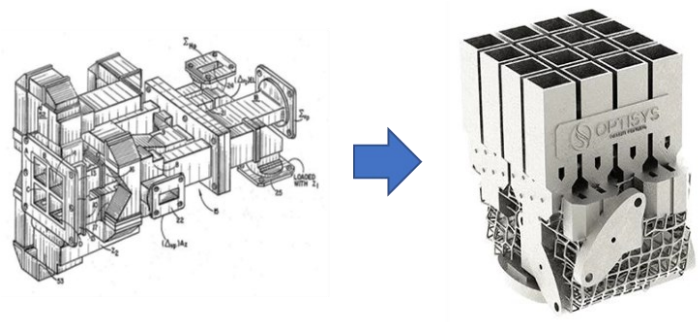

Figure 1.1: Application of AM on an antenna of the company Optisys. Sx) previous solution with 100 assembled parts; Dx) antenna made for AM consisting of a single component

1.2 Comparison between AM and traditional technologies

Additive manufacturing allows the production of parts and products in an automated method and with high customization, but this technology is not suitable for high production volumes due to printing times, that are considered still long. Also, the products cost is an important aspect that must be taken into account, and it can be considered intermediate between mass production and traditional artisanal production. The cost of production is not a function of the complexity of the piece, and this allows great freedom of design. The graph in Figure 1.2 shows a typical trend in the cost of a small production batch for parts of increasing complexity. Parts with low geometric complexity are cheaper with traditional processing methods; in some cases, following a redesign, a new optimized shape could be recreated with better functionality and lower production costs for AM than in the previous case.

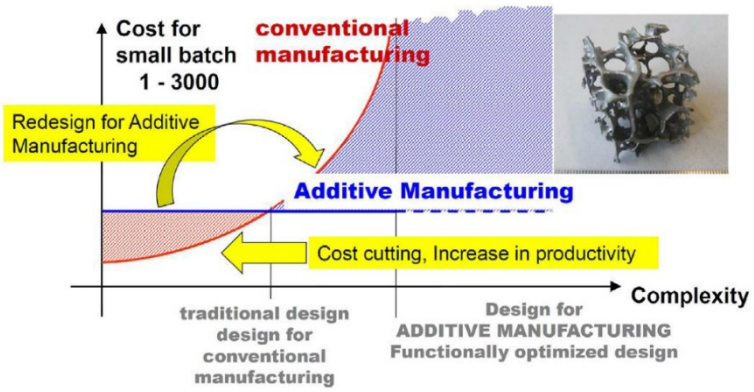

Figure 1.2: Cost of production as parts complexity varies

With traditional methods, an increase in product complexity leads to a significant increase in production costs (a longer production cycle is required with more complex operations); therefore, above a certain level of products complexity to be realized, AM becomes the economically desirable solution. In addition, some geometries such as internal lattices (latex), are not achievable through traditional technologies and 3D printing is the only possible alternative.

Comparing AM with traditional technologies based on the use of numerical control machines (CNC), there is similarity in the use of computers and virtual models. The biggest difference between these systems is the subtractive approach on the one hand and additive approach on the other. Other important differences are observed in terms of:

- Materials
  3D printing was developed around polymeric materials and waxes, and later composite, ceramic and metallic materials were introduced. Regarding the lasts, there are not yet many printable alloys for AM due to the particular process and solidification conditions. The AM process can cause voids and anisotropy in the material. On the other hand, traditional CNCs are suitable for machining metals and hard materials for the production of precise, homogeneous parts with good and predictable properties.
- Speed
  CNC machines typically have a much higher machining speed than those of AM. However, 3D printing is often the only process that can be adopted for the realization of a part, while traditional processes are typically multiphase and require the transport and repositioning of the part on different system.
- Complexity
  As mentioned above, the greater the complexity of a part, the greater the benefit of using additive manufacturing technologies.
- Accuracy
  The accuracy of 3D printing processes, as for traditional processes, depends a lot on the type of process considered. More details on the different processes will be provided in the following paragraphs. However, it can be considered that, typically, the accuracy achievable by employing subtractive manufacturing methods is not achievable with 3D printing systems.
- Programming
  CNC machine programming includes selecting tools, speeds, position and approach angle etc. Errors in programming can cause serious damage to the machine and tools used. The programming of AM machines is less complex and there are no serious repercussions in case of incorrect programming [2].

1.3 Additive Manufacturing Process: workflow

Currently, there are numerous 3D printing processes that exploit different technological principles (Powder Bed Fusion, Direct Energy Deposition, Fused Filament Fabrication, Stereolithography, etc.). In all cases, the production process consists of the following stages:

1. Realization of the CAD model
   All AM processes start from a CAD model that completely describes the geometry of the piece to be realized. For the creation of the model, it can be used a CAD software (e.g. NX, CATIA, Solid Edge etc.) or a tool for reverse engineering (e.g. laser, scanner, etc).
2. Creating an STL model
   From the CAD model, the STL model is processed to define the orientation of the workpiece, the direction of growth and the necessary supports. STL files are used to represent the CAD model exclusively for its geometry; They remove all modeling data and approximate surfaces with a series of triangles (meshes).
3. Model Slicing
   The object is ideally divided into overlapping layers that will then be printed in succession by the machine. The following are defined:
   - The thickness of the layers, a factor that determines the accuracy of the print
   - Process parameters
   - Production times and costs
   - Machine setup

   The machine must be prepared for the printing process. This step may include operations such as loading material and replacing worn extruders and print plates.
4. Printing process
   The printing process is typically carried out in a fully automated way and can be carried out without the need for a supervision. Printing times range from a few minutes to several hours.
5. Further operations
   At the end of the printing process, the part is extracted from the machine, the supports are removed (if any) and further processes are carried out to improve the mechanical and aesthetic properties of the printed part. Among these, it may be necessary to priming and painting processes or machining certain surfaces to

machine tools to obtain, for example, more precise tolerances or to create threaded holes.

In addition, it is important to consider periodic checks and maintenance of AM printers. Although they are suitable for unsupervised work, they have delicate components that must be kept under control and replaced in case of wear.

1.4 Main Additive manufacturing technologies

In the last 40 years there has been a strong development of additive manufacturing technologies. The market has seen the birth of numerous companies and research groups that have proposed design solutions for 3D printing systems. Figure 1.3 shows some of the printing systems developed over the years.

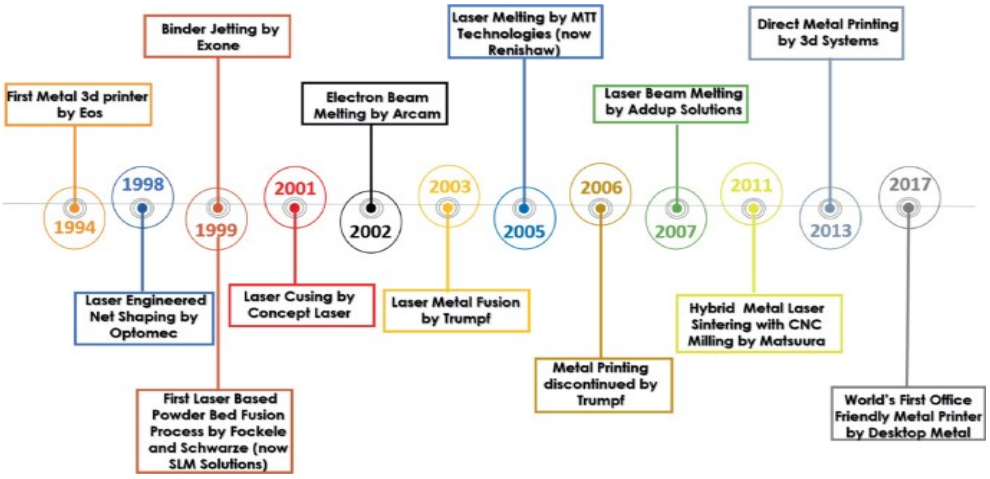

Figure 1.3: Timeline of the development of some additive manufacturing technologies

In order to ensure uniformity in the nomenclature, these technologies have been grouped into 7 macro-categories by ISO/ASTM 52900:

- Photopolymerization (Vat photopolymerization)
- Material extrusion
- Material jetting
- Binder jetting

- Powder bed fusion
- Sheet lamination
- Direct energy deposition

The following paragraphs describe the principles of operation of such systems.

1.4.1 Photopolymerization

The photopolymerization process is based on the use of a liquid resins capable of polymerizing under the effect of a UV light, a scanning laser beam or an image projected at high resolution (photoresin). Photopolymers were developed in the late 60s and were initially used for coatings. The starting material consists of monomers or oligomers, additives and photoinitiators. The latter are molecules that, when exposed to radiation, create reactive species (free radicals), capable of starting a polymerization reaction. Then, following the exposure of the resin to a radiation beam, long polymer chains are formed and subsequently cross-linking takes place, i.e. the formation of covalent bonds between the different polymeric molecules. The material, in this way, solidifies. The distinction that can be evaluated within this category of AM technology is based on the resin supply that consists of a tank containing the liquid for Stereolitography (SLA) Digital Light Processing (DLP) and LCD technologies, while, for Material Jetting (MJ) the resin is released by a printing head on the plane selectively and then polymerized.

SLA – DLP - LCD

In the 80s, Chuck Hull, engineer founder of 3D Systems, during some experiments, managed to obtain solids by curing layers of a photoresin one on top of the other, thus creating the process known as SLA. Nowadays, a typical vertical photopolymerization system includes a resin tank, a mobile construction platform and a light source, usually an ultraviolet (UV) laser diode for SLA, a light projector for DLP and a liquid crystal display for LCD technologies. The UV beam is thus quickly scanned through the resin bath to cover the cross-section of the workpiece for the SLA technology, while for DLP and LCD the light source scans al the section for a specific time step. After scanning each layer, the moving platform is moved along the vertical direction. The 3D object is obtained as an overlap of layers of polymerized resin.

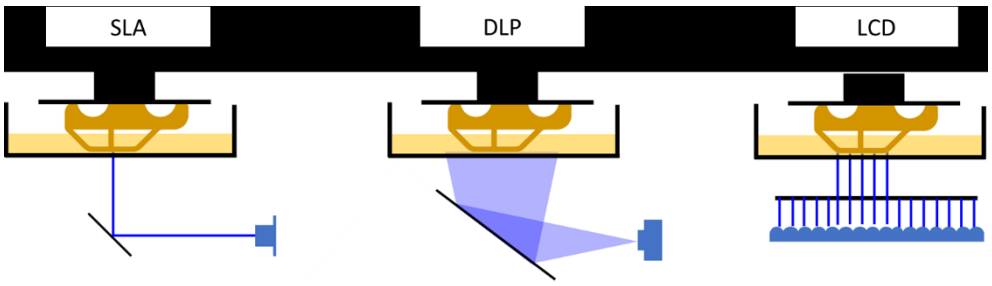

Figure 1.4: Simplified diagram of the operation of photopolymerization technologies

Figure 1.4 is a simplified diagram of the operation of photopolymerization technologies. After the printing process, the parts must be further cured in order to achieve their optimal mechanical properties. Long exposure to ambient light can cause printed resins to become embrittle. This problem can be solved by subjecting the printed parts to surface treatments, for example by applying a layer that absorbs UV rays.
The properties of the material are regulated by the chemistry of the resin monomers and the cross-linking of the polymer mesh. For this reason, it is possible to engineer resin chemistry so as to obtain a wide variety of materials and mechanical properties. It is also possible to reinforce the resin, for example with fibers and particles, so that composite materials can be printed. The parts obtained by photpolimerization are isotropic, can have good precision and good aesthetics. They can have variable dimensions: from meters (as in the case of the Massivit3D printer) to few millimeters with details smaller than a micrometer (for Nanoscribe printers).

Material Jetting

MJ technology is a 3D printing technique in which, starting from an STL file, the object is obtained by depositing drops of material with spatial control. The material jet production machine uses an inkjet head that releases small drops of material onto the print platform.

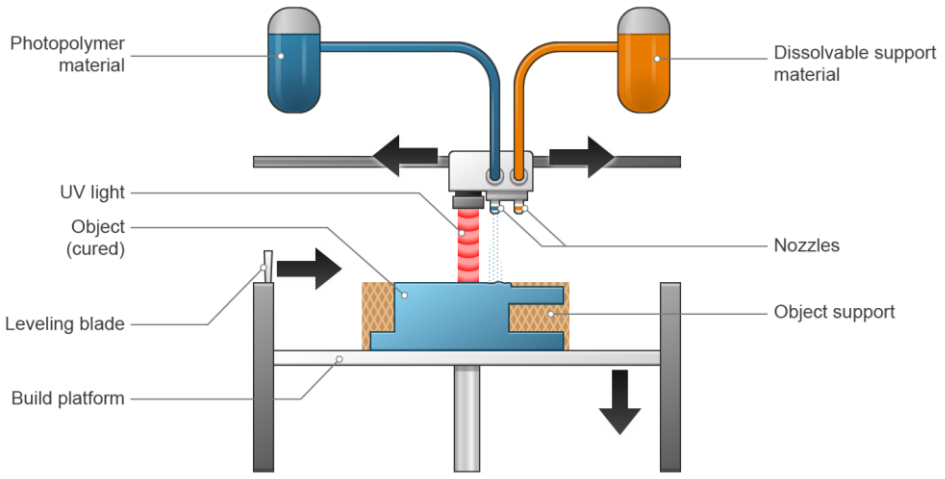

Figure 1.5: Material Jetting process scheme

The basic operation is similar to that of 2d inkjet printers; in this case, however, a three-dimensional object is obtained as an overlay of "images" (layers). The typical process scheme for the material jetting technology for photopolymer is shown in Figure 1.5, where an UV light is used to polymerize the resin in order to create a solid layer for the next deposition, while the printing phase of a resin printer equipped with this technology is shown in Figure 1.6.

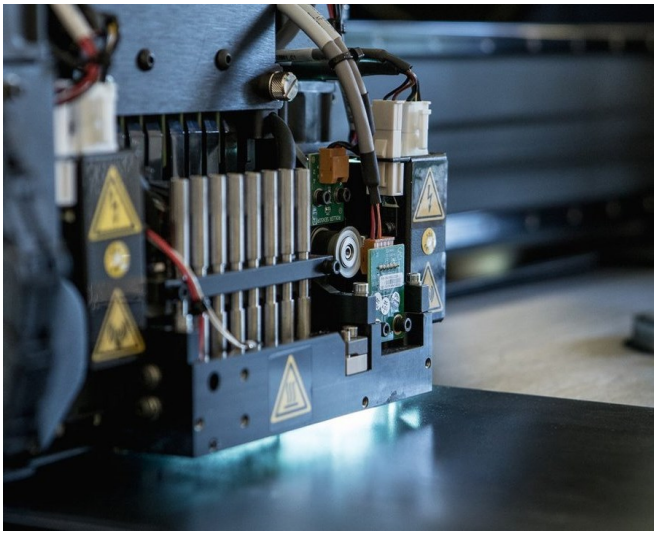

Figure 1.6: Material jetting printing head for photopolymers with UV lamp for the polymerization phase

With MJ it is possible to print different materials, even on the same object, such as photosensitive resins, wax and metals. Photopolymers can be pigmented to vary their color. The material of each 3D "pixel", or "voxel", can be obtained as a combination of different inks that are mixed to obtain locally different colors and/or different stiffness of the material. In this way, multicolored and multi-material parts can be obtained. In addition, ceramic or metal particles can be added to different materials at the nanoscale in order to modify the properties of the finished product. Parts with built-in electronics, such as cables and antennas, can also be realized. In the preparation of the printing process, the printing instructions for each layer must be defined, including the CAD design information together with the specifications of material composition, color and other variables. Parts with details up to about 0.1 mm in size can be produced thanks to a minimum layer height permitted dimensions of nanometers scale, but also large parts (on the meter scale).

Figure 1.7 shows some examples of parts made with this technology that have parts made with different colors in the biomedical field.

Figure 1.7: Example of human organs reconstruction with material jetting technology

1.4.2 Material Extrusion

In the process of material extrusion, the part is realized by depositing layer upon layer an extruded molten material through a nozzle. The nozzle moves following a defined path so as to follow, layer by layer, the geometry of the part. The relative vertical movement between the nozzle and the construction plate allows the creation of the different layers. The state of the material to be printed is usually checked with a temperature changing, but there are also other approaches for the solidification of the material such as, for example, the use of chemical reactions.

There are some features common to all material extrusion systems:

- Material loading: most of the materials used in this process are in the form of continuous filaments, pellets and powders and must be loaded into the machine before the printing process;
- Melting of the material: the material is melted so as to allow its flow through the nozzle of the printer;
- Application of pressure for material handling;

- Extrusion: the nozzle determines the shape and size of the extruded material. Larger nozzles will allow a faster printing phase but with less precision of printed parts;
- Support structures: these are structures that can be removed during the post-processing phase and are necessary to support the part under construction. Typically, AM machines are able to extrude two different materials, one for the part and one for the support material, in order to print another material that makes easier the separation or dissolution of unnecessary material.

Extrusion is compatible with a wide variety of thermoplastics materials ranging from mixtures of raw polymeric materials, for example Polylactic Acid (PLA) and Acrylonitrile Butadiene Styrene (ABS), to high-performance technical materials as Polycarbonate (PC), ULTEM and PPSF. These can be rigid or flexible; the former is the most widely used while the flexible ones (elastomeric) allow the production of components such as gaskets and caps. For these kinds of materials, the reference technology is defined Fused Filament Fabrication (FFF). Within the technology of Material Extrusion there is also another technology, in addition to the FFF, when metal material is considered for the realization of parts. In this case, metal powder was supplied in form of feedstock with a binder and extruded as in the FFF process. This 3D printing methodology, called Bound Metal Deposition (BMD) is increasingly becoming an economical method for making metal parts. For these materials, the process varies from plastics, in fact several post-processing steps must be added.

FFF process

A scheme of the FFF Material Extrusion process is reported in Figure 1.8. FFF consists in the extrusion of a thermoplastic filament that is deposited layer after layer on a heated construction plane to form the desired three-dimensional geometry. The starting material is a filament of thermoplastic material wound in a coil. A driving wheel drives the thermoplastic filament of the coil inside the extruder, which is heated thanks to a series of resistances. The temperature of the extruder is such as to induce softening of the material, while the extrusion pressure is given by the portion of filament that is pushed by the mechanical movement that is generated by the rotation imposed on the coil. In order to obtain a constant flow of material (in terms of filament speed and diameter) the extrusion pressure and the speed of movement of the nozzle in the plane must remain as constant as possible throughout the printing process. Inside the extruder the filament is brought to high temperatures (generally

about 200° – 250° C) in order to reach a viscosity that allows it to be extruded through a nozzle. The material, in the viscous state, is then deposited on the print bed (build platform), also at a controlled temperature, based on the geometry drawn by the movement of the nozzle (nozzle). The material is then allowed to cool and then the part can be removed from the build platform. The next process, if necessary, is to remove supports that may have been generated depending on the geometry of the part. The supports can be generated with the same material as the model and, to facilitate manual removal, a certain gap between the layer of the support and the model is considered, or they can be generated with a second extruder using a water-soluble material that allows the dissolution of the support if the complete part is inserted into a bath of specific salts.
The systems can be configured for molding parts with high details, with layer thickness even less than 0.1 mm, or coarse details, with layer thicknesses approaching 10 mm. It is possible to achieve the realization of components with dimensions up to several meters using thermoplastic materials such as ABS, PPS.

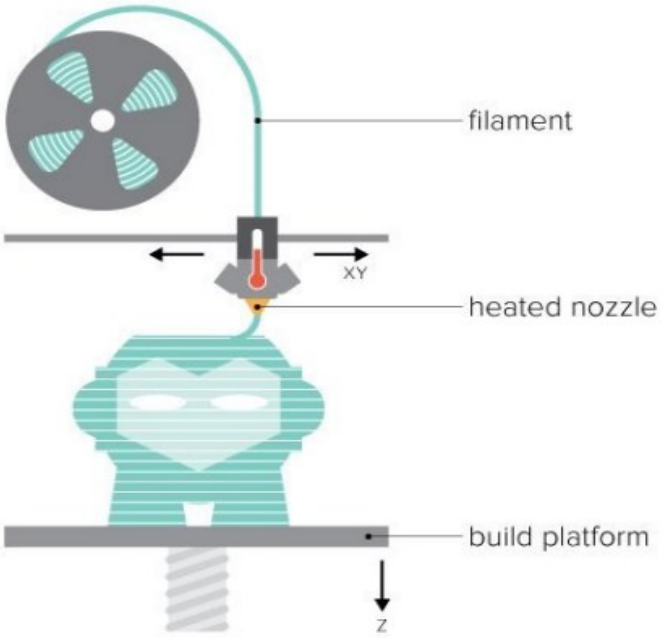

Figure 1.8: Material extrusion process

BMD process

The latest metal additive manufacturing technology presented in this chapter is Bound Metal Deposition (BMD), whose process allows to obtain metal parts through a punctual deposition of material consisting of metal powder and polymer binder. The Figure 1.9 shows the BMD process scheme.
3D printers equipped with this technology uses a material extrusion system similar to that of FFF printers. For printing operations, bound metal rods (feedstocks) are used as starting materials; these derive from metal powder held together by wax and polymer binder. As with 3D printing of plastic materials, the system heats and extrudes the material layer by layer following the geometries of a virtual model. The construction plate is moved down after the deposition of each layer, allowing the overlapping of sections. The printing process provides for two extruders to be used: one is used for extruding and depositing the bounded metal powder material, the other extrudes a ceramic material that is interposed between the supports and the piece. Subsequently the printing process, pieces are subjected to a solvent bath that dissolves the binder between the metal particles.

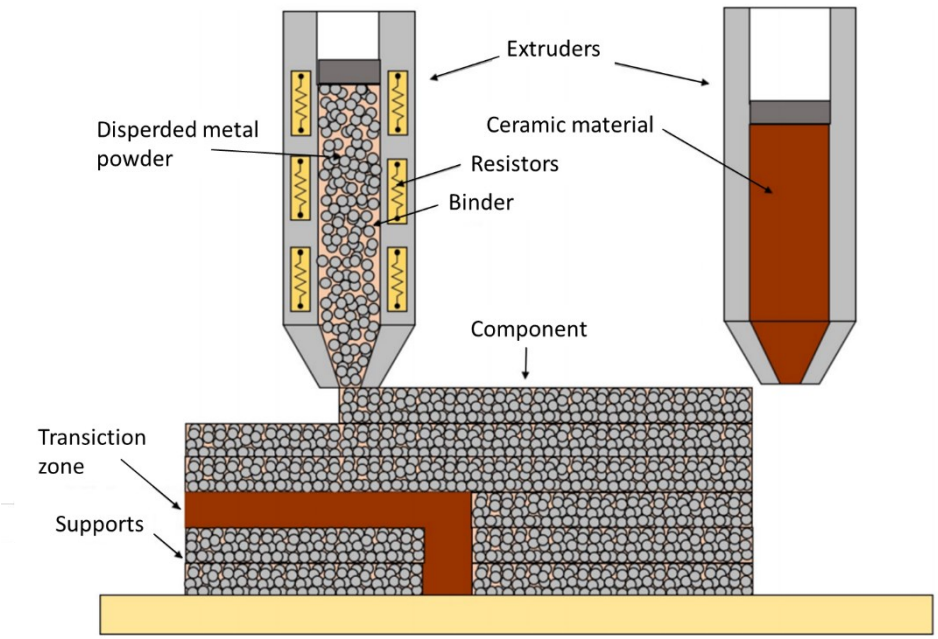

Figure 1.9: Sscheme of the BMD processes

Parts are then placed in a furnace where, in controlled atmosphere, high temperatures are reached for metal sintering to take place, similar to that described for Binder Jetting technology for metallic materials. During the sintering phase, the ceramic material, instead of bonding with the metal, is reduced to powder and facilitates the removal of the supports during post-processing. Note that the design of support structures and transition zones must be such that they can be removed, i.e. disassembled by supported blocks. The latter can also be easily separated manually, without resorting to cutting systems that are necessary for other metal 3D printing systems. During sintering, components produced by BMD undergo an important volumetric variation (between 17% and 22%). This can also lead to strong internal tensions and consequent distortions of the component. The BMD process is theoretically applicable to all sinterable materials that can be joined with a thermoplastic matrix.
Below is a list of materials that can be processed with this technology currently on the market, even if they can be used with dedicated printers:

- Stainless steel 17-4 PH: martensitic steel used when high mechanical strength and corrosion resistance are required;
- Stainless steel 316L: austenitic molybdenum steel used for its resistance to corrosion even at high temperatures;
- H13: tool steel with chromium and molybdenum characterized by high hardness, abrasion resistance, and stability to high temperatures;
- 4140: low-alloy steel with chromium, molybdenum and manganese. It is suitable for various industrial applications due to its resistance to fatigue, impact and abrasion;
- Copper: Characterized by high thermal and electrical conductivity; It is used for electronic applications and where good heat exchange is required.

There is a variant of this process in which the metallic material is dispersed within a polymer filament that is deposited with techniques similar to the BMD process. In this case we speak of Atomic Diffusion Additive Manufacturing (ADAM).

In the scientific literature there are many works that deal with AM technologies for the realization of metal parts starting from powders, such as those mentioned above, while scientific works on BMD technology are limited [3–6]. In fact, among these it can be mentioned the researchers Watson et al. who in their work [7] started the characterization analysis of 17-4 PH stainless steel demonstrating that the mechanical properties are in line with those related to as-sintered metal injection molded (MIM) 17-4 PH. Bjørheim et al. [8], instead, they focused on printing metal parts with various printing orientations in order to investigate the directional dependence on the mechanical properties. They found that the material exhibits

anisotropic behavior, and have a mesh of crack like defects, related to the printing orientation.

To better understand how the additive manufacturing process can influence the mechanical properties of the products made with these techniques, a description of the main printing parameters of the Material Extrusion technology is provided. Some of the parameters are shown in Figure 1.10 and later described in the following paragraph.

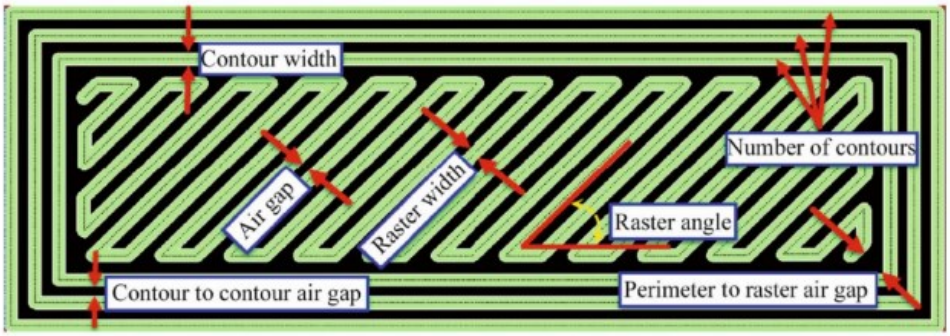

Figure 1.10: Examples of parameters of the Additive Manufacturing process [9]

Filament width

The width of the deposited filament, raster width, depends on the size of the extruder head, in particular the diameter of the hole through which the material is extruded, and the number of passes required to complete the process. This parameter does not have a particular influence on the mechanical properties of the object, but on the aesthetic quality and process times. In fact, thinner filaments lead to a better surface quality of the object and longer construction times because, with the same covered surface, the nozzle will have to make more passes.

Filament deposition orientation

In the BMD printing process, the first areas where the resin is deposited are those that make up the edge of the piece in the deposition plane (Figure 1.11a), in order to avoid any leakage of the material deposited inside it. Once the edge is completed, we proceed with the filling of the section according to the user-defined architecture (Figure 1.11b) and finally proceed with the realization of the next layer, as shown in

Figure 1.11c. The orientation of the deposited filament, raster angle, represents the angle that the extruded wire forms with respect to a reference axis and can take values between 0° and 90°. Generally, the workpiece is produced with a regular architecture, for example by alternating layers at +45°/-45°.

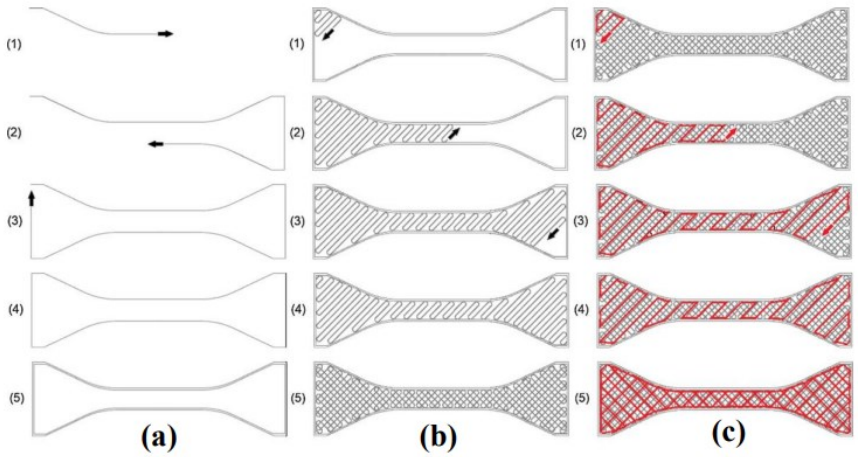

Figure 1.11: Representation of the essential steps of deposition during the printing process: boundary deposition (a), first layer filling (b) and subsequent layer deposition (c) [10]

This parameter influences the tensile strength of the object, as the directionality of the deposition and growth process typical of this technology does nothing but cause anisotropy in the mechanical properties of the printed product. Figure 1.12 shows the main orientations typically used for filament deposition.

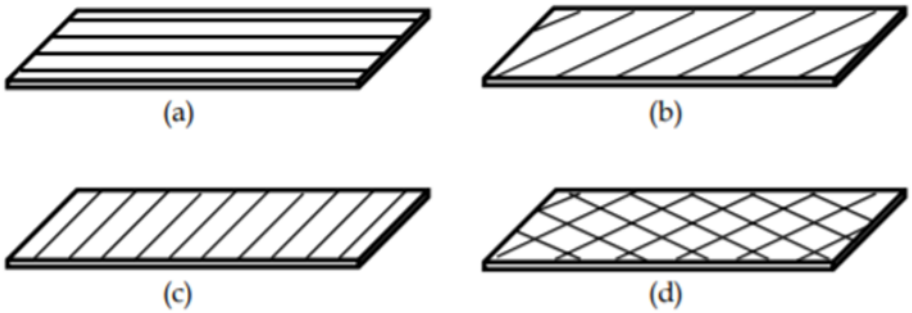

Figure 1.12: Illustration of the raster angle parameter: a) 0° orientation; (b) 45° orientation; (c) 90° orientation; (d) orientation of +45°/-45° [11]

In fact, the direction of the external load relative to the direction of molding particularly affects the strength of the material in that direction. In particular, in most cases, there are higher resistance values when the deposition takes place at an angle of 0° with respect to the direction of the load. The explanation derives from the fact that the filament fibers, when they are subjected for example to a tensile test, are subjected to an external action in the longitudinal direction that ensures that there is no modification of the internal bonds between the different layers, i.e. there is no detachment action; the situation corresponding to an orientation of 90° with respect to the direction of the external load, on the other hand, represents the worst condition as it favors the breaking of the bonds between the individual layers, thus generating worse mechanical properties. The above considerations can be deduced from the analysis in Figure 1.13. In practice, it is often preferred to adopt the orientation +45°/-45° to ensure that the behavior of the material in operation is as isotropic as possible, as in addition to mechanical strength, other parameters such as fatigue strength, wear resistance and impact resistance must also be considered.

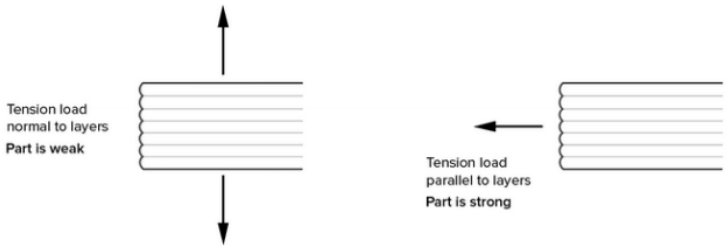

Figure 1.13: Directions of the external load relative to the orientation of the layers [11]

In Figure 1.14 several solutions regarding layer orientation architecture are shown.

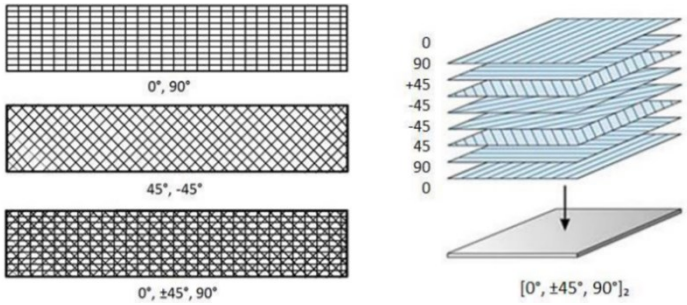

Figure 1.14: Different filling architectures alternating layers with different raster angle values [12]

Finally, it should be noted that the choice of raster angle also has an influence on the type of fracture surface of the component, which will occur along the interface between one section and another of the piece, or by breaking of the filaments themselves. Examples of typical breaks are shown in Figure 1.15 1.14.

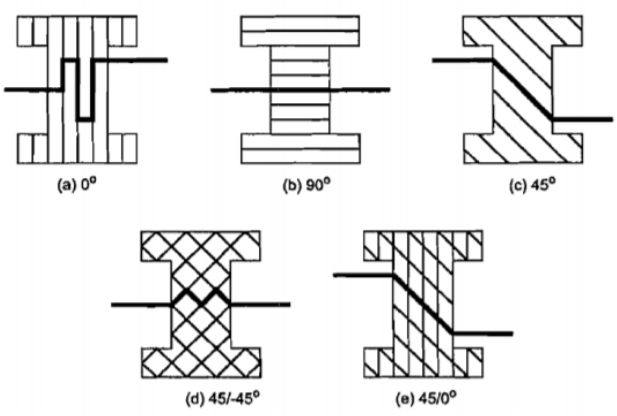

Figure 1.15: Fracture types based on fill architecture and raster angle values [13]

Direction of growth of specimens in the plan

In a technique like BMD that makes pieces through the deposition of a filament, the ways in which it is possible to build the same piece are many, so the final result in terms of mechanical performance, surface quality and other characteristics can be very different. It is therefore important to keep in mind, in addition to the contribution of raster angle, also that of building orientation and very often these two parameters are considered simultaneously.

Building orientation means how the piece is positioned on the platform during the process and therefore the way in which it is built in reference to the three axes X, Y, Z, as shown in Figure 1.16. Usually, to distinguish the different combinations with which the same piece can be built, a pair of letters is used between X, Y, Z. For the manufacture of tensile test specimens, the first letter identifies the direction parallel to the axis of the specimen.

In second place is the axis of the Cartesian reference which, together with the first character, form the plane in which the specimen is contained.

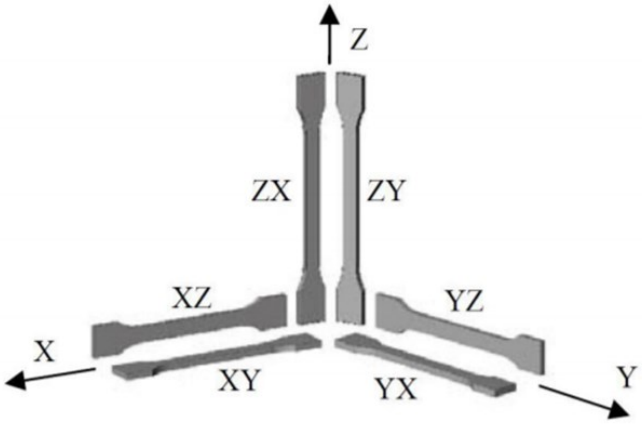

Figure 1.16: Arrangement of specimens in space according to the orientation of the specimen axis with respect to the direction of growth

Finally, in Figure 1.17, all the possible combinations are reported taking into account both the raster angle and the building orientation.

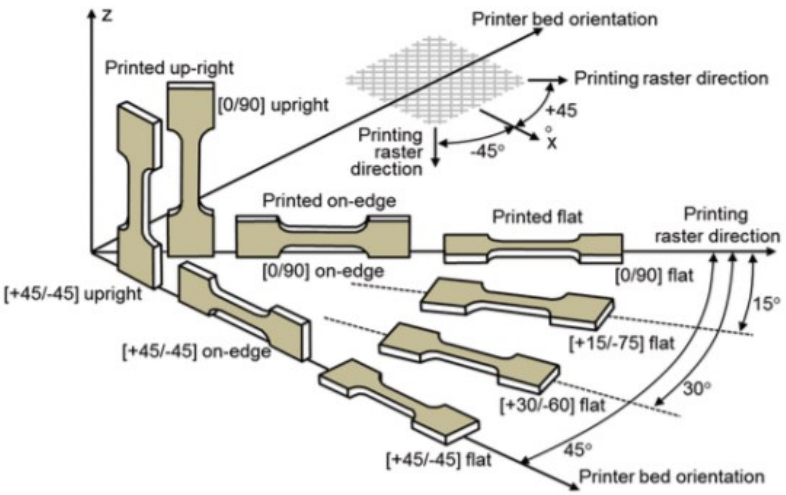

Figure 1.17: Representation of growth orientations (flat, on edge, up-right) [14].

Layer thickness

The thickness of the layers is mainly responsible for the aesthetic quality and surface roughness of the piece. It depends first on all the size of the extruder head and partly on the type of material but can be partially controlled by setting the displacement in the Z direction of the deposition bed.

The smaller the thickness of the single layer, the more homogeneous the lateral surface of the piece is, limiting the staircase effect represented in Figure 1.18. In other words, for smaller layer heights, the surface is able to better reproduce the CAD drawing, while for larger heights the surface is discontinuous and stepped. On the other hand, a smaller thickness leads to an increase in construction times (building time), which are therefore proportionally higher.

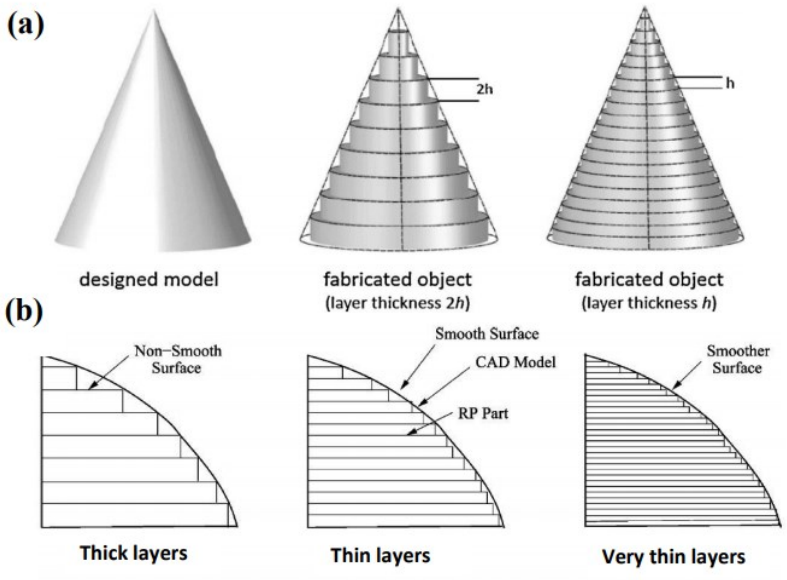

Figure 1.18: Effect of the number of deposited layers and the layer thickness on the reproducibility of flat (b) and curved [15] *(a) surfaces* [16]

In the case of geometries more complex than planar ones, a fair compromise to avoid these defects and have acceptable building times is to adopt an approach defined as adaptive slicing. It consists in the use of variable thickness layers with curvature

(usually thinner layers are used in the most curved areas and vice versa thicker for the more planar ones). These considerations allow us to understand how the optimization of process parameters requires a fair compromise of the variables involved, in this case between building time and quality of the piece. However, the effect of the staircase can also occur during the process of converting the CAD file to STL and then during the tessellation operation (meshing during the creation of the STL file). The approximation of the CAD model during tessellation can lead to deviations of shape from the original model and to the staircase effect, which can only be compensated by correcting the layer thickness and orienting the object optimally during manufacture. The staircase effect could lead either to an excess of deposited material or to a quantity at a loss compared to the originally designed piece, as shown in Figure 1.19.

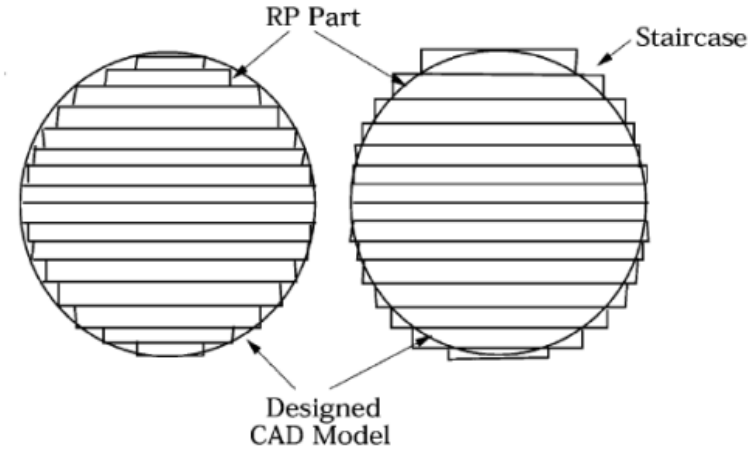

Figure 1.19: Staircase effect in deviation, in excess or in defect, from the original geometry [16]

In addition to aesthetic reasons, surface quality and roughness directly influence the wear properties of the object. Increasing layer thickness inevitably reduces wear resistance, not only because an increase in roughness is observed but also because fewer layers result in fewer reflow steps. When a layer is deposited, there is in fact a local remelting of the lower layer that favors a more solid and intimate union between the layers. The increase in the number of layers leads to the formation, along the direction of growth of the piece, of a greater number of solid interfacial bonds and favors the reduction of voids between one layer and another, allowing to obtain

a dense and cohesive piece. The result is a product with better mechanical properties and a harder, wear-resistant interface. As the thickness of the layers increases, the phenomena of thermal distortion are accentuated to the detriment of the phenomena described above, with a greater tendency to the presence of voids, weak interfacial bonds and therefore to lower wear resistance. All the above considerations allow us to conclude that thinner layers lead to obtaining better mechanical properties thanks to the decrease in the number of porosities.

Air gap

The air gap, i.e. the distance between two adjacent filaments in the same layer, is the parameter that most affects the internal porosity and mechanical properties of the piece. It can be controlled to obtain a denser structure at the expense of production speed.

The air gap, together with the raster angle and the layer thickness, has effects on the mechanical properties and on the wear rate of the printed product, these considerations are reported in Figure 1.20.

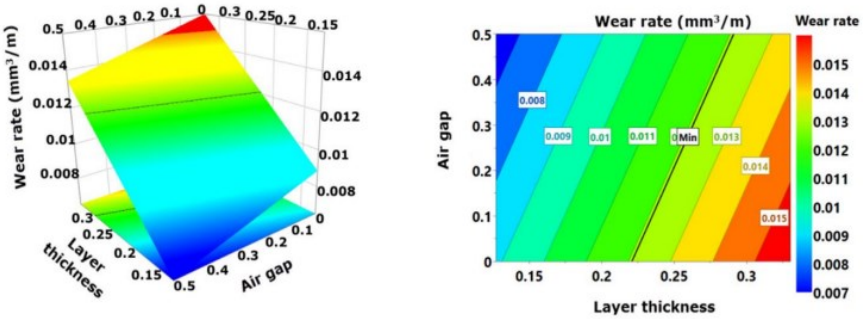

Figure 1.20: Dependence of wear rate on layer thickness and air gap [17]

The air gap is however a parameter that depends directly on other aspects such as the model and the filling density. The percentage and shape of the filling will be chosen according to several aspects: total weight of the piece, material used, strength to be achieved and decorations (where applicable). In general, the higher the filling percentage, the greater the mechanical strength of the piece, but the longer the

printing time. Figure 1.21 shows, by way of example, some models of tensile specimens with different filling percentage molded with FDM technology of plastic material, a method similar to the BMD technique.

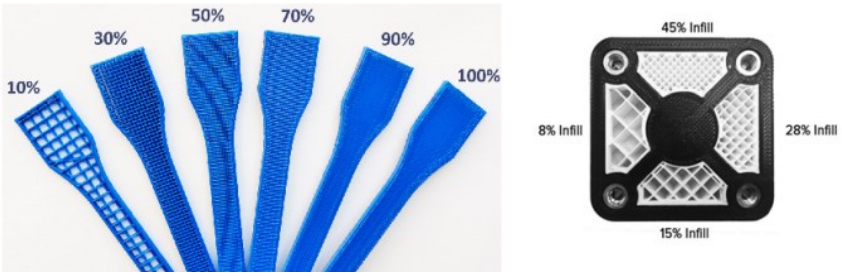

Figure 1.21: Different fill percentages [18]

In Figure 1.22 instead, there are several filling models used as filling shapes of the internal parts of the product. Among the most used is the honeycomb filling, which guarantees at the same time lightness and excellent resistance, especially to compression loads in the direction orthogonal to the plane. As the percentage of filling (infill) increases, the printed part becomes denser and more resistant, but printing times grow accordingly.

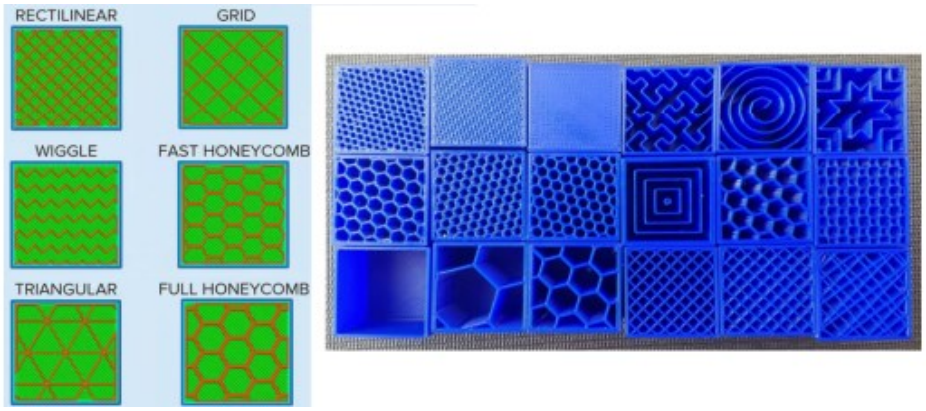

Figure 1.22: Different filling patterns [18]

Additional process parameters

In a 3D printing process, the parameters involved are many. Surely the printing parameters mentioned in the previous sections are those that most influence the properties of the artifacts obtained but there are also other parameters that, despite having a marginal importance on mechanical properties, deserve to be mentioned. Figure 1.23 shows all the printing parameters and their influence, in percentage terms, on the quality of the piece obtained. As for the printing speed, the extrusion temperature and the temperature of the deposition bed, their variation depends on the type of material used.

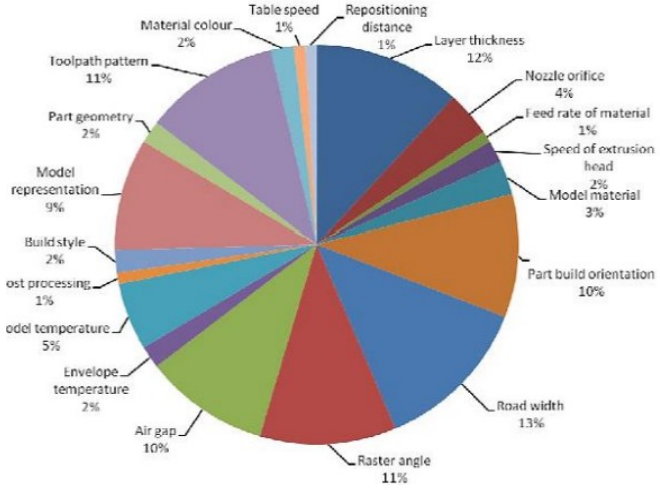

Figure 1.23: Printing parameters and percentages of their influence on the product obtained [19]

For example, with regard to the FFF 3D printing technique, very similar to BMD that is used for polymeric materials such as acrylonitrile butadiene styrene (ABS), it is reported in Figure 1.24 how the variability of these process parameters has a very small influence, compared for example to another parameter such as the thickness of the layers, on the mechanical properties of the piece obtained.

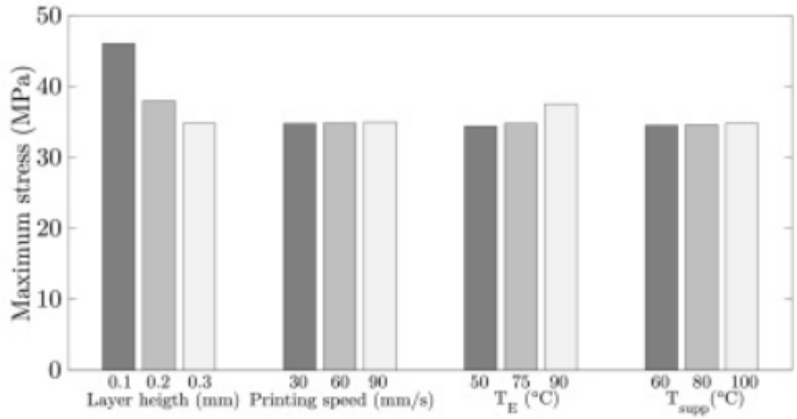

Figure 1.24: Influence of some process parameters on the mechanical properties of a part made of ABS using FFF [19]

1.4.3 Powder Bed Technologies

Additive processes for the consolidation of material from a powder tank are usually classified as Powder Bed Technologies. In this family, in fact, a predominant role is played by those processes that use a laser source as an energy source for melting the material, while other technologies of this category, even starting from a bed of powder, consolidate the material by depositing on the powder a binder that aggregates the grains of material which, also in this case, can be polymeric or metallic. In fact, within this category, an important distinction is made between processes that transform polymeric or metallic powders. The profound differences in physical and chemical properties between these two classes of materials lead to very different measures in the design and implementation of these processes.

Selective Laser Sintering (SLS)

It is an additive manufacturing technique that starts from polymer powder and uses, as a thermal source to selectively melt the particles, a laser. Although the name is misleading, as its translation is selective laser sintering, in reality there is no sintering, but the polymer powders are melted by the laser. The process, shown in Figure 1.25, consists of a fixed laser that is focused by a system of mirrors and selectively melts the layer of powder, previously deposited and leveled by a doctor

blade or roller. At the end of the section creation, the elevator descends along the z-axis and the hopper deposits the new layer of dust, so that the process can start again.

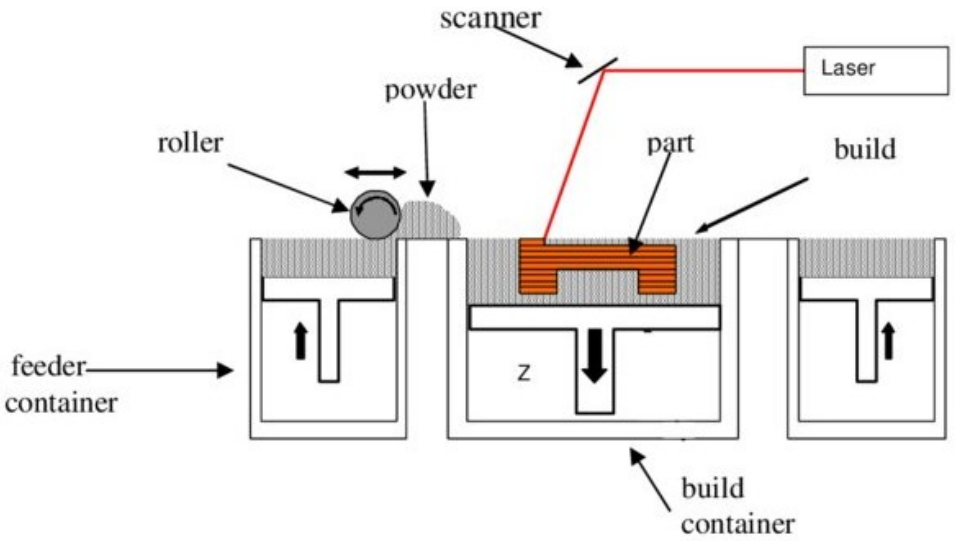

Figure 1.25: Scheme showing how the SLS machine works

For this technology it is not necessary to use support because the powder bed is quite compact, both because of the preheating to which the working chamber is subjected, and because of the roller; moreover, since the density between dust and solid does not change much, the solidified component does not sink, and the powder can support it. Inside the working chamber nitrogen is blown and the preheating temperature is close to that of melting the polymer, this determines two advantages:

- The laser has a low installed power, being necessary a ΔT = 20-30 ° C to get to fusion;
- Poorly controlled solidification shrinkages are avoided, in fact in polymers the shrinkage is a function of the thermal gradient, which here remains quite low.

In the case of metallic materials, which have very high melting temperatures, the preheating of the chamber is not sufficient to guarantee reduced temperature gradients, which is why the shrinkage will be greater with consequent need for supports, which will also have the function of avoiding the deformation of the section

created. The disadvantage is that, at the end of the construction process, you will have a compact block that will be at the preheating temperature of the chamber, which cannot be immediately cooled to start the cleaning phase, otherwise you would incur the deformation of the component. For this reason, it is necessary a natural cooling of the entire block, but it is removed from the machine, so that a new printing process can be carried out while waiting for cooling. The nitrogen coating is essential to ensure that the polymer does not oxidize; in fact, remember that the temperatures are close to that of fusion, so the powder will react with oxygen becoming the typical yellow color.

It is important to underline that the powder treated at high temperature can be recycled, not entirely, but in part, and then used again in combination with the virgin powder. The applications of this technology concern:

- Direct production of final parts;
- Functional prototyping;
- Production of sacrificial models for lost wax casting.

The first two applications include 85% in particular areas such as fashion, interior design, as well as aerospace, racing and medicine, while the remaining 15% concerns use in foundries. The thermoplastic polymers available are:

- Polystyrene (PS) mainly in foundry applications;
- Polyetheretherketone (PEEK), a technopolymer with interesting mechanical properties;
- nylon or polyamide (PA12) which can be pure or loaded with different types of particles that allow to modify the mechanical characteristics, already good compared to photopolymers. The particles of the charge are mixed before being loaded into the machine with the PA12 powders and must have a grain size compatible with the latter. Fillers, for example, can help increase the elastic modulus, making the component more rigid, but they do not change the thermal performance, which is constrained by the matrix, i.e. nylon. The particles that are most commonly added are: glass spheres, aluminum particles, short carbon fibers or additives that make the material self-extinguishing.

Powder Bed Fusion (PBF)

PBF processes allow the construction of three-dimensional objects by selectively melting in sequence layers of powder. The process begins with the distribution of a

thin layer of powder over the print area. The cross-sections are then selectively fused one layer at a time via a thermal energy source. After melting and solidifying a layer, the distribution system lays a new layer of powder. A PBF production process scheme is show in Figure 1.26. The 3D body is made as an overlap of layers of molten and solidified material.

All PBF processes share some basic elements:

- thermal energy source needed to melt the powder (lasers, electron beams or intense infrared lamps);
- system to control the melting zones of each layer;
- mechanism for distributing the powder on layers.

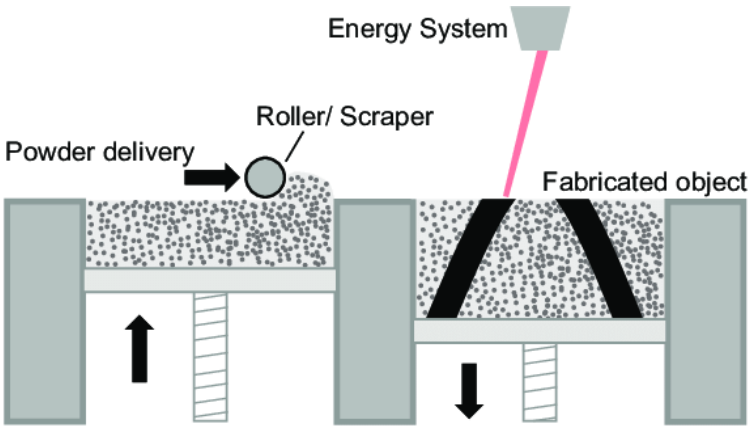

Figure 1.26: Diagram of the powder bed melting process

Lasers are the most widely used energy source for powder bed fusion processes. In the case of printing polymeric materials, the technology is called selective laser sintering (SLS). This involves the creation of an object construction chamber that can be heated to a temperature higher than the glass transition temperature of the polymer. This allows to minimize the forces and temperature variations encountered during the printing process, and consequently to obtain parts with low residual stress and reduced tendency to deform. Due to this heating, the powder around the part under construction is partially solidified (caked powder) and provides support to the part itself, without the need to build support structures, as shown in Figure 1.27.

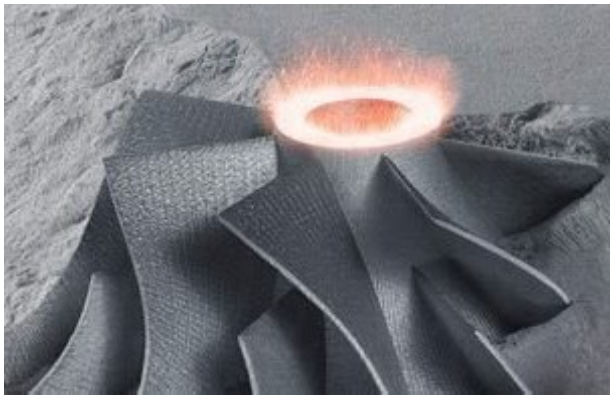

Figure 1.27: PBF process of a component 3D realization

The absence of supports greatly simplifies post-processing and the dense packaging of components within the production volume is facilitated. Agglomerated powder around the workpiece can be removed by air jets.

In this process, among the materials that can be used for this technology there are metals, including steel, aluminum alloys and titanium, but also semi-crystalline thermoplastics, which have a well-defined melting temperature and greater recyclability of non-solidified powder than amorphous thermoplastics. Among the most commonly used materials in SLS are Nylon (PA12, PA11) and PEEK (Figure 1.28). To improve the mechanical properties of the components, a fraction of short fibers (e.g., carbon or glass fibers) can be added to the powder. The dimensions of the molded parts vary from a few cubic millimeters, with printable details of up to 0.5 millimeters, up to maximum values of 0.5-1 m^3. PBF techniques are also suitable for the production of components in metallic materials. In the case of 3D printers equipped with thermal energy modulus supplied by lasers, the technologies are called Selective Laser Melting (SLM) and Direct Metal Laser Sintering (DMLS). In the case of metallic materials, reinforcement structures are necessary to help heat dissipation from the part and to reduce thermal stresses. In addition, to reduce residual stress and affect the microstructure and properties of the parts, a bed heating system can be introduced. The latter, however, increases the complexity of the machine and can cause the unmelted metal powder to be sintered, limiting its recyclability.

Figure 1.28: Example of components realized by powder bed fusion using a polymer material

SLM machines typically have multiple lasers, each independently controlled with a mirror scan. This allows to considerably reduce production times, increasing the productivity of this technology.

PBF processes can be divided into two categories based on the thermal energy source used for powder welding. The first is the Laser Powder Bed Fusion, which uses the energy of a laser beam to quickly melt the powder deposited on the different layers.

For the metallic material 3D printing, fiber optic lasers or Nd:YAG lasers are used. They use optical fibers doped with rare earths (e.g. Erbium, Neodymium, Holmium etc.) and work at a wavelength of about 1.08 μm. The latter use a crystal of yttrium aluminum garnet (YAG) as an active laser medium and work at a wavelength of 1.06 μm [20]. The spot size of the laser beam varies, depending on the process, between 30 μm and 600 μm. Varying the size of the laser dot serves to change the energy density of the laser, accuracy and production speed. During the process, chemical and physical processes take place that can be a source of defects within the components. The laser causes rapid melting of the powder and consequent thermal cooling gradients that lead to residual stresses in the parts. Going to act on overlapping layers, during a scan, the laser also melts or heats part of the previously solidified layers, modifying their structure. This results in different crystallography's between the first deposited layers and the last. The powder around the "melt pool" is affected by heating and can partially melt and agglomerate. A recall pressure is

generated around the pool; the laser-powder interaction creates a depression, attracting and re-emitting the surrounding powder. Metal condensation and impurities are created on the rest of the powder and on the walls of the machine, including the area where the laser is emitted, and this causes a reduction in intensity during the process. Figure 1.29 shows the laser-powder interaction.

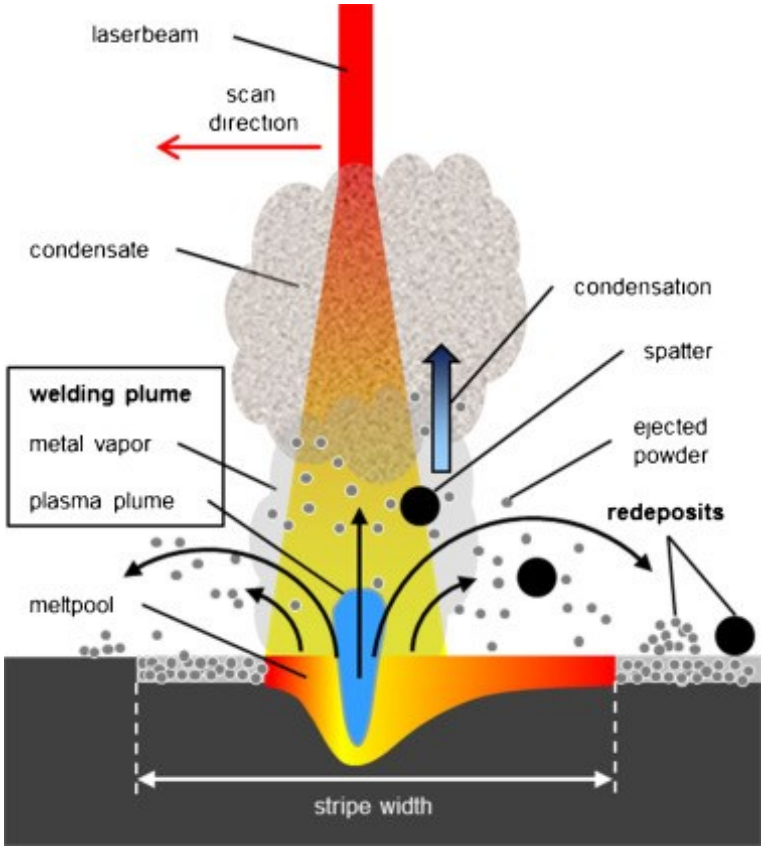

Figure 1.29: Laser powder interaction

Electron beam Melting (EBM)

EBM differs from the PBF mainly for the use of an electron beam as a source of thermal energy instead of laser. This technology has been marketed since 1997 by ARCAM, a company later acquired by the General Electric group. The electron

beam is generated by a tungsten filament heated by the Joule effect and emits electron beams directed at the powder bed at high speed. When the beam impacts the powder bed, its kinetic energy is converted into heat, causing the metallic material to melt locally. The scheme of the Electron Beam Melting process is shown in Figure 1.30. The average free path of the electrons is very reduced in air and without special precautions it would be almost impossible to use the electron beam to bring the powder to fusion; for the process success the vacuum must be created inside the construction chamber in such a way as to avoid collisions of the beam with the air particles. For the direction of the electrons, it is not possible to use galvanometric mirrors, as was the case for the laser process, but windings with current passage are necessary.

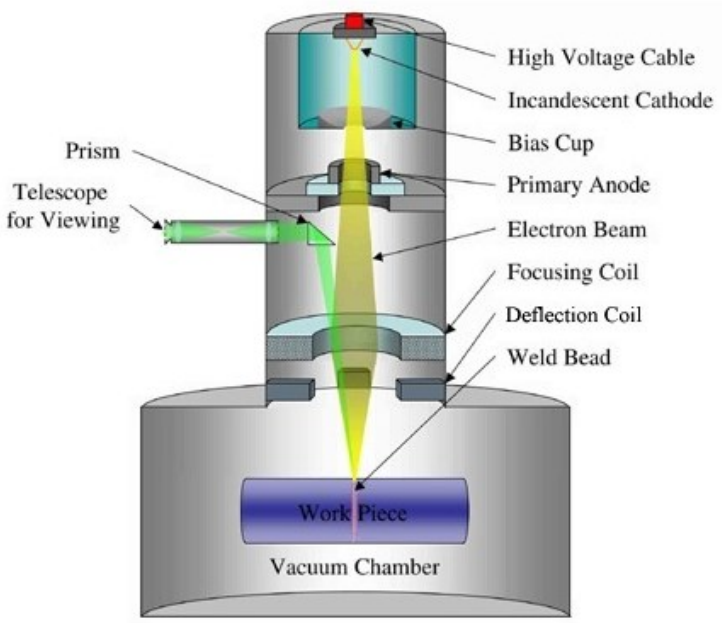

Figure 1.30: Electron Beam Melting Process

These generate magnetic fields capable of interacting with the beam and directing and focusing it on precise points of the bed. The single beam can also be divided into multiple beams that act simultaneously to heat multiple points of the powder bed. This allows a high production speed.

Each layer of the powder bed is scanned in two steps in succession. The first is the preheating phase, in which a high-current, high-speed beam preheats the bed powder to 40-60% of the powder melting temperature.

Figure 1.31: EBM acetabular hip replacement cup

The next step is the one that leads to fusion with a beam of electrons at low scanning speed the section of the piece defined by the virtual model. The preheating reduces the stresses induced in the workpiece and it is also possible to heat treat the solidified metal directly during the printing process, heating it without reaching the melting temperature. While in Laser-PBF systems two pistons are used to move the powder to be used and the workpiece under construction, in EBM machines a single handling system is required for the workpiece. The powder to be used is taken from special tanks (powder hooper) placed above the construction chamber. Figure 1.31 shows a typical application of the EBM process ARCAM EBM systems use 3000 W high-power electron beams. The thickness of the powder layers is typically between 50 μm and 200 μm. Other relevant parameters are the diameter of the electron beam, the current, and the preheating temperature of the powder.

The whole construction chamber is preheated (not just the building floor). This greatly reduces the residual stresses that are generated inside the molded parts, thus also reducing the need for support structures. This also allows parts to be stacked on top of each other in the build chamber, increasing the number of printable parts per print cycle and consequently the productivity of the technology.

Binder Jetting

It was developed in the early 90s at the Massachusetts Institute of Technology (MIT) and its original name was Three-Dimensional Printing (3DP). It is based on the inkjet deposition of a liquid binder on a powder bed to define successive sections of an object to be printed. It is a technology that combines the basic principles of the subsequent described technology of Powder Bed Fusion (in which, however, the bed of powder deposited is melted by an energy source) and the Material Jetting technique. Figure 1.32 shows a typical scheme of a binder jet 3D printer.

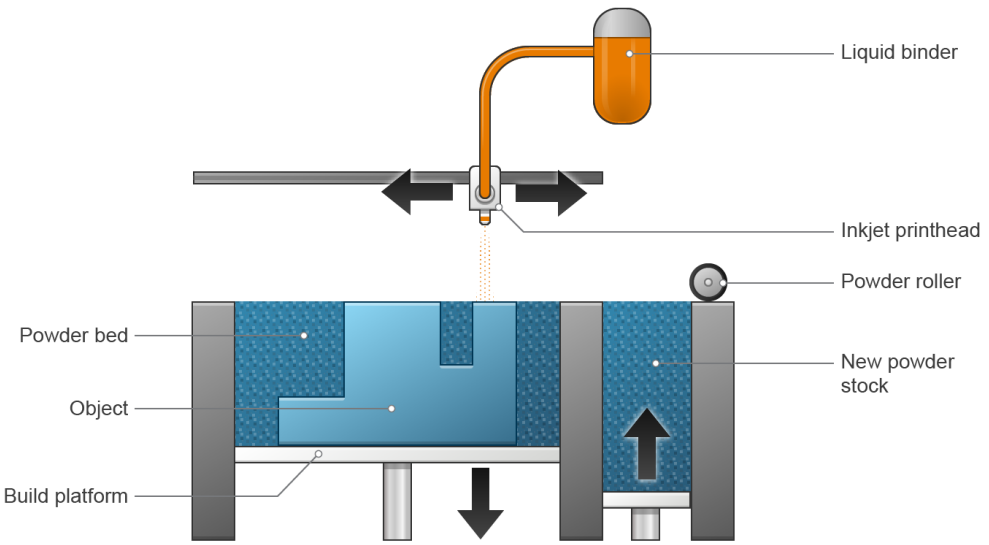

Figure 1.32: Scheme of a binder jet machine

In particular, the following components are represented:

- Print head: emits drops of liquid binder. It is connected to the binder tank and is moved by a planar mechanism. It could be made up by several hundreds of nozzles as shown in Figure 1.33;
- Powder distribution system: similar to the PBF one;
- Unused powder: it is positioned on a mobile plate that moves upwards to always provide new powder to the system;
- Part under construction;
- Powder of material not impregnated with the binder (caking): the powder around the piece and the absence of thermal gradients (the powder material is not brought to fusion) allow, in some cases, to carry out the printing process without the use of support structures;
- Print plate: moves downwards to allow the binder to be applied to successive sections of the workpiece under construction

With this technology it is possible producing components in different materials (polymeric, ceramic and metallic). In addition, some Binder Jetting 3D printer contain ink extruders that allow to realize parts with different colors.

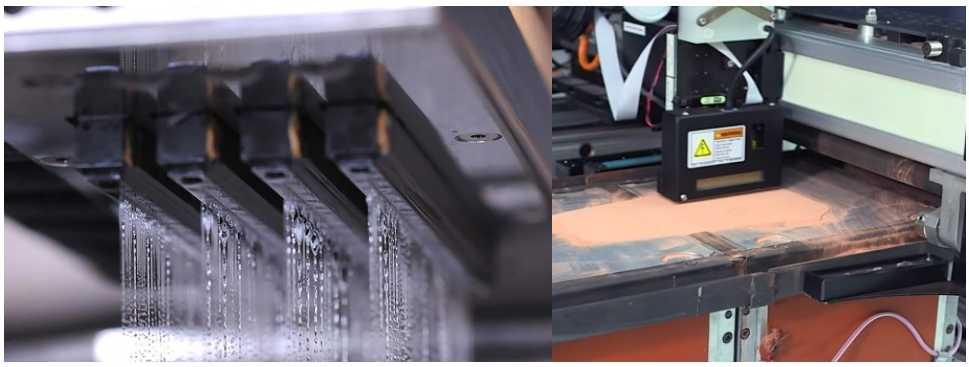

Figure 1.33: Drops released by several hundreds of nozzles by the printing head and a typical binder deposition on a powder bed during a printing process

For the production of polymeric materials, powders of thermoplastic resins and light-curing liquid resins are used as binders. The liquid resin settles on the powder and occupies the cavities between the different particles. A light source is passed over the powder in order to cure the thermosetting resin. Due to the volumetric shrinkage of the resin during solidification, microporosities may form in the final part, resulting in a reduction in its mechanical properties. Post-processing operations are necessary

to eliminate supports (if any), to eliminate incrusting through sandblasting, tumbling or using compressed air jets and to make heat treatments. The latter are particularly useful in the case in which hygroscopic resins are printed with a high tendency to absorb moisture. The permanence in oven at elevate temperature eliminates the moisture present in the finished products, increasing their mechanical properties [21].

As far as metals are concerned, Binder Jetting has much higher construction speeds than laser Powder Bed Fusion (SLM) methods. The metal powder is not melted during the process but assumes stiffness thanks to the use of a liquid binder. The output of the printing phase is a part that needs further processing to achieve optimal characteristics. After the printing phase, a powder consolidation process is necessarily carried out. After an optional infiltration phase of a second metal material, the sintering phase takes place. This compacts the piece and reduces its porosity, increasing its mechanical resistance, removing the binder by evaporating it. Binder Jetting (BJG) is suitable for molding different types of metals such as, for example, aluminum, copper, iron, nickel and cobalt alloys and, more generally, any sinterable material that can be found in the form of powder. It uses two materials: the one that constitutes the powder bed, which will form the final part, and a liquid polymer binder. The first phase of the BJG process for metals is the production of the green part according to the methods already described. After the powder has been distributed to form a layer, drops of bound (inkjet) are distributed into the areas corresponding to the desired cross-section of the part. The binder can be cured in situ by using an infrared heat source on the powder bed immediately before and after binder deposition. Print speeds are fast because inkjet heads can deposit millions of drops per second. The impact and diffusion of binder drops inside the bed have a strong influence on the success of the process. The powder-binder interaction gives the initial mechanical strength of the part and determines the final geometry of the part. If the binder is well dosed, when deposited on the powder, the balance between capillary and viscous forces determines the sharp edges of the piece. The binder dose, measured against the volume of empty space between the powder particles in the layer to be bound, is kept below 100%, to avoid material loss and edge definition. When the ligand diffuses into the small gaps between the particles, it reaches a steady state mediated by asymmetry in the forward and retreating contact angles.

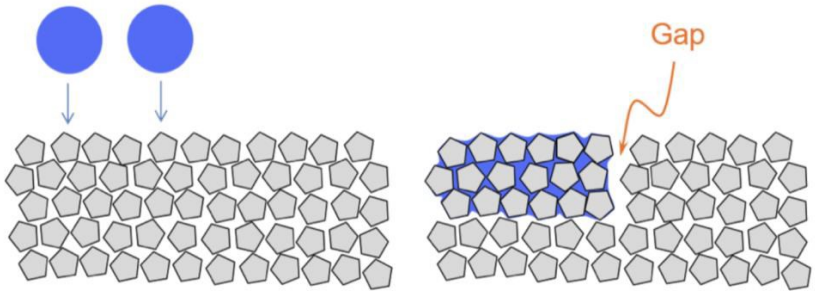

Figure 1.34: Gap created between printed and non-printed powder bed regions due to legacy recession

Recession of the binder due to capillary forces can create a small gap between the printed and unprinted regions of the powder bed (Figure 1.34). When the binder solvent evaporates, the remaining solid part of the binder concentrates on the necks between the powder particles [22].

The post-processing phases have the objectives of eliminating excess powder, eliminating all the binder from the green part and to obtain the desired density. The green part is an apparently spongy semi-finished product, consisting of 25-50% by volume of binder and air. It has low mechanical strength and cannot be used without additional preparation processes. After the printing phase, the whole powder bed is placed in the oven for about two hours to evaporate the water and binder compounds and to completely cure the binder to increase its resistance. In some cases, this step is carried out directly inside the printing press. The parts are then pulled out of the bed and the part of the powder that has not been contaminated by the binder is recycled. Parts subject to warping during the sintering phase must be properly supported. There are 3 possible strategies:

- The supports are printed together with the part and are removed after the sintering phase. Supports increase process waste material but are usually the most efficient choice for low production volumes;
- The supports are produced separately from the ceramic workpiece; they are expensive and time-consuming to build but are reusable so only the best solution for higher production volumes;
- Supports are not necessary but considering the distortion of the geometry at the design stage it can be needed to modify the drawing accordingly. There is software being developed to do this. It is not a solution suitable for all geometries.

The pieces are placed on a support structure and placed in an oven with controlled atmosphere. The furnace carries out a de-binding cycle that eliminates the polymer component from the pieces. It is important to eliminate binder completely because carbon residues could affect the sintering process and compromise the mechanical properties of the products. De-binding is a slow process because the binder must evaporate through the small pores of the material structure; This phase can also take days for parts with large thicknesses. After this process, the piece is called the "brown part".

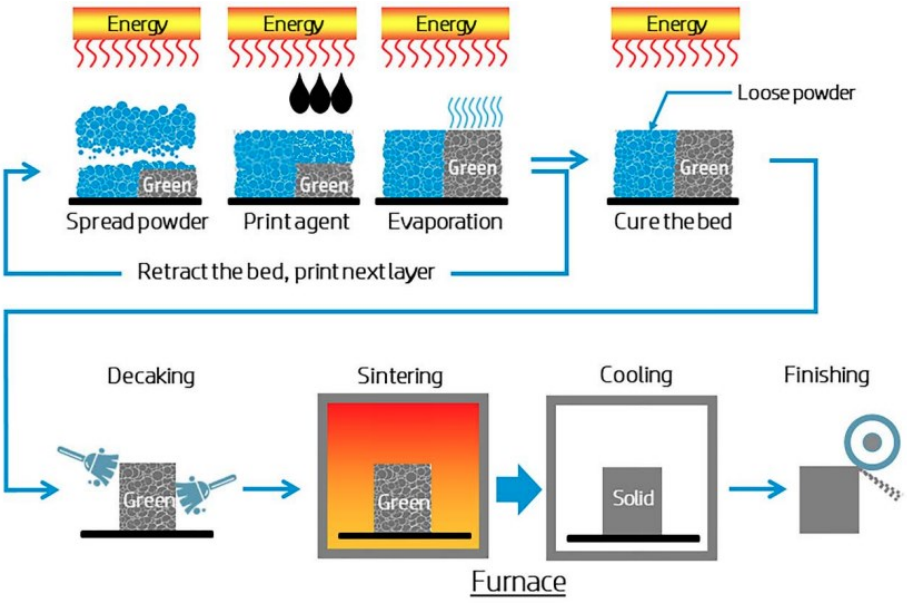

Figure 1.35: Molding for Binder Jetting and related post-processing

The furnace carries out a second heating cycle at about 80% of the melting temperature of the stamped metal (e.g., 1200-1400° for stainless steel). This is the sintering step, in which the workpiece shrinks and increases its density to 93-99% of the nominal value of the material (Figure 1.35). A successful sintering is essential for the production of high-density metal materials with good mechanical properties. The driving force for densification is the reduction of surface energy that is obtained with the growth of necks at the particle-to-particle contact points and with the elimination of the grain boundary area through grain growth. Sintering can be considered divided into three phases (Figure 1.36) [23]:

1. Initial phase: necks begin to form between the powder particles and minimal densification is observed;
2. Intermediate phase: in this phase most of the densification occurs. The grains grow and the space around the particles is similar to a channel surrounding solid particles;
3. Final phase: the growth of the grains continues and the pores, previously similar to channels, become closed voids inside the part. This makes it difficult to eliminate the last 0.1-1% porosity

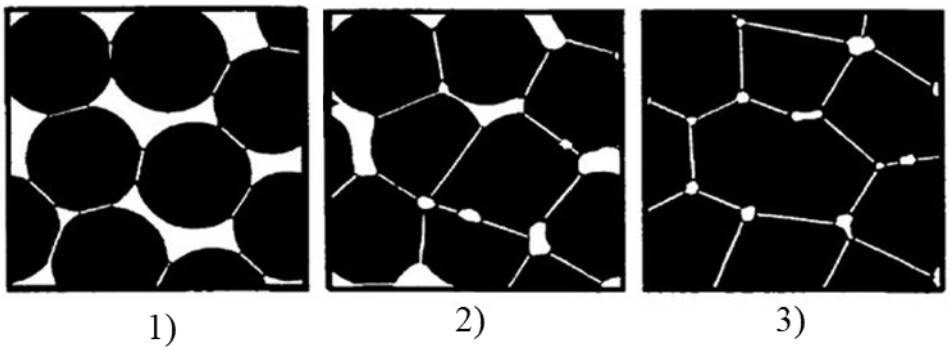

Figure 1.36: Densification of particles during the sintering phase [24]

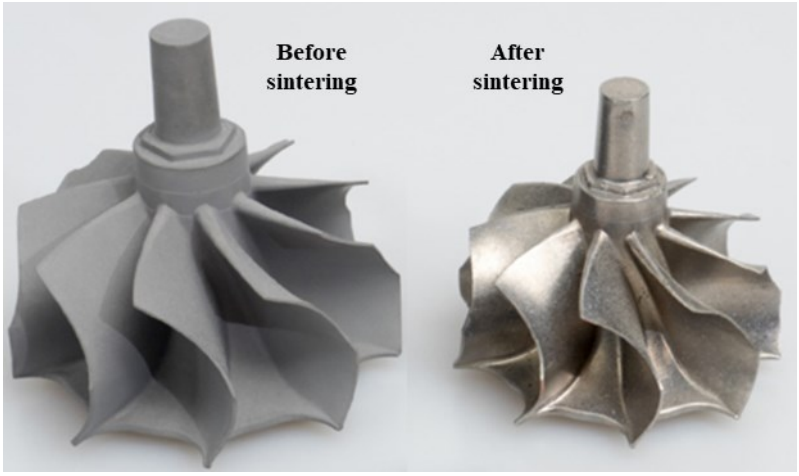

Figure 1.37: Printed object for Binder Jetting before and after the sintering process

In some cases, a second metal can also infiltrate the unsintered structure to achieve an almost complete density. During sintering, there are strong shrinkages of the workpiece (30-40% volumetric and 15-20% linear reductions) as shown in Figure 1.37. In the case of small pieces with uniform thicknesses, shrinkage is easily predictable. For parts of greater dimensions and variable thicknesses, sintering can cause important variations in the surveyor; this limits the number of possible applications of Binder Jetting. As a general indication, the BJG is suitable for small components with thicknesses of less than 10 mm and a maximum weight of 200 g. After the sintering and cooling of the part, parts can be subjected to post processing (e.g. surface finishing) to obtain the tolerances required by the project.

Complex geometries can be obtained but must be optimized for de-binding and sintering; uniform thicknesses are preferred. The good resolution of the process makes it suitable for creating small details, such as latex structures.

The properties of the components are influenced by many variables and process parameters, which must be considered and chosen carefully in order to avoid non-compliant parts:

- Specifications and characteristics of the powder
- Scanning strategy
- Layer thickness
- Laser parameters
- Material and thickness of the construction plate
- Temperature of the constriction plate
- Inert gas flow conduction
- Type of inert gas used
- Oxygen level during the process
- Position and orientation of parts
- Recoater blade material

The main variables and parameters of Powder Bed processes are described below.

Metal Powders

In the production of metal components through PB technologies, the type and quality of the powder used are of fundamental importance for the final properties of the parts. The following paragraphs contain information on the possible materials used, their characteristics, production systems and powder characterization systems.

The metal powder used in AM processes has a strong influence on the success of the production process. Its characteristics, such as shape, size, density, thermal properties, and smoothness, affect the material-laser/electron beam or other energy sources interaction, determining the properties of the finished product. Powder characteristics are important to ensure the repeatability of production processes. Commercially used alloys can be pre-alloyed, therefore already containing the stoichiometric proportion of binders, or pure, such as copper or precious metals powders. The PBF process is based on the rapid melting and solidification of metal powders, reaching a solidification speed of 106 k/s (depending on process settings). This can lead to inadequate microstructures with large grains, periodic cracks and poorly distributed alloying elements [25]. For this reason, not all metals, that can be processed with traditional techniques (machining by chip removal and plastic deformation), can be printed using AM technologies. Only few alloys have characteristics suitable for AM processes. Table 1.1 shows some of the most widely used alloys for PBF processes. Among the most used alloys they can be found the Ti6Al4V alloy, some stainless steels and Nickel and Aluminum alloys.

Table 1.1: Typical commonly used metal alloys in PBF process

Alloys	**Metal Powder**
Cobalt Based Powders	CoCr (ASTM F75)
	CoCr28Mo6 (ASTM F799)
Nickel Based Powders	Inconel 625
	Inconel 713
	Inconel 718
	Inconel 738
	Inconel 939
	Hastelloy X 276
	Haynes* 230
Aluminium Based Powders	AlSi7Mg
	AlSi10Mg
	AlSi12
	AlSi9Cu3
	Scalmalloy (Airbus Grou)
Iron Based Powders	Stainless Stell 304L (1.4306)
	Stainless Stell 316L (1.4404)
	Stainless Stell 17-4PH (1.4542)

	Stainless Stell 15-5PH (1.4545)
	Mould Steel (1.2344)
	Maraging Steel (1.2709)
	CORRAX Precipitation Hardening SS
Titanium Based Powder	Titanium Grade 2
	Titanium Ti6Al4V
	Titanium Ti6Al7Nb
Other Alloys	Invar (1.3912)
	Nitinol 55
	Bronze

Metal powder has a strong economic relevance. It can contribute about a third to the total production costs of components and must be easily reusable so as to reduce the consumption of virgin powder. It must then have certain technical specifications that make it suitable for Additive Manufacturing processes. Especially:

- The properties of the powder must be consistent and must be kept constant on the different layers of the piece;
- The stoichiometric composition of the powder is the same as that will be obtained in the printed component; its chemical composition, therefore, must comply with the required specifications;
- There must be no impurities such as particulate matter, oxides and moisture;
- It must have the right particle size fraction. For processes that use lasers as an energy source (LPBF, SLM) it is typically between 15 μm and 45 μm, while for processes that use an electron beam to melt the powder, the particle size fraction is between 45 μm and 106 μm;
- It must have the right smoothness (fluidity), i.e. the ability to be evenly distributed on the construction platform. This property is influenced, for example, by the presence of moisture that causes groupings of particles and makes it more difficult to create uniform powder layers. To obtain a good fluidity, a powder must be spherical, with particles of different sizes, with a low surface roughness, incompressible, hard, rigid, and with a low coefficient of friction between the various particles;
- Packing density: the higher the packing density, the higher the density of the parts and, consequently, better mechanical properties will be obtained for the final product;
- Particle shape.

Powders can have different shapes and sizes. Figure 1.38 shows two examples of powders that tend to be tetrahedral (Sx) or spherical (Dx). The latter is the most used because it guarantees a good packing density and good fluidity. To further improve packaging, spherical powders with particles of different sizes are used so that smaller ones fill the interstices between the larger particles.

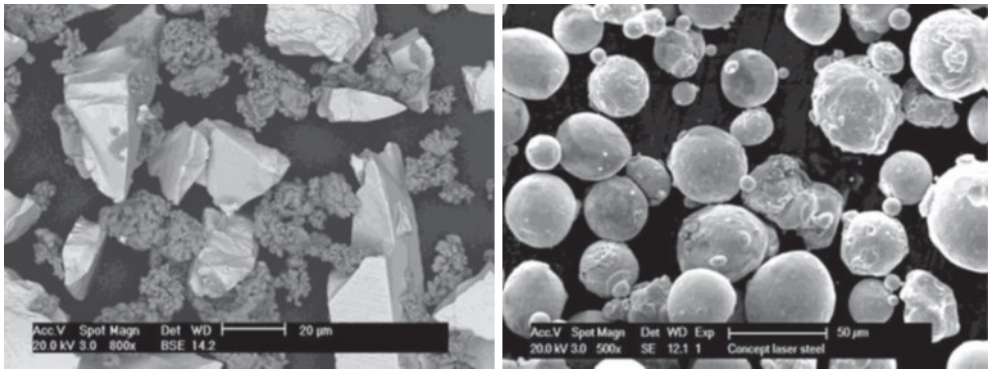

Figure 1.38: Powders with particles of different shapes. Sx) tetrahedral tungsten carbide powder with irregularly shaped cobalt; Rx) Stainless steel spherical powder [26]

There are many metal powder production systems that differ in technology used, cost, and size and quality of the powder. Some of the methods used at industrial level are described below.

- Gas atomization
- Plasma atomization
- Plasma rotating electrode processes (PREPs)

Other examples of atomization processes are the Armstrong process and the Hydride-dehydride (HDH) process, recently implemented and still scarcely used.

The properties of metal powder have a strong relevance on the quality of the objects produced for Powder Bed Fusion. A good characterization of the powder is therefore essential to determine whether it is suitable for AM manufacturing processes. A series of properties can be investigated such as shape, size, density, electrostatic charge, cohesion, hygroscopy, surface area, porosity, presence of interstitials, smoothness and chemical composition. Table 1.2 shows some methods for the

characterization of metal powders reports some analysis systems for metal powders [27].

Table 1.2: Some methods for the characterization of metal powders

Measure	**Metrology Method**
Density of particles	Helium Pycnometry
Particle Size Distribution	Laser Diffraction
Particle Size and Morphology	X-Ray Computed Tomography
Particle Crystalline Phases	X-Ray Diffraction
Particle Morphology	Scanning Electron Microscopy
Particle Elemental Composition	Energy Dispersive Elemental Analysis
Particle Surface Molecular/Chemical Composition	X-Ray Photospectroscopy

Volumetric Energy Density (VED)

The volumetric energy density is defined by equation (1):

$$VED = \frac{p}{v \cdot h \cdot t} \qquad (1)$$

Where:

- VED is the volumetric energy density;
- p is the laser power;
- v is the scanning speed;
- t is the thickness of the powder layer;
- h is hatch spacing.

This is a key factor influencing the properties of as-built parts made using PBF. The laser power is the most used parameter to control the printing process. Depending on the process, the laser power can vary from 50 W to 400 W. Through control systems, the laser power can be varied automatically; For example, if the width of the melting pool is insufficient, the laser power is increased. The scanning speed indicates the speed at which the laser beam is moved on the powder bed. With high scanning speeds, the energy density of the laser is lowered, and the laser-powder interaction time may not be sufficient for a complete melting of the powder. Typical scanning speed values range from 0.1 mm s-1 to 15 m s-1. High scanning rates lead

to longer, thinner melting pools that have a higher chance of breaking into more smaller pools due to Rayleigh instability. The thickness of the powder layer is defined during the slicing phase of the CAD model; the greater the thickness of the powder layer, the higher the production speed of the part but its precision is reduced. With lower layer thicknesses, costs and lead times increase but the required energy density is reduced and parts with better surface finish, tighter tolerances and lower volumetric shrinkage phenomena are obtained. To maximize production speed, without losing precision at the most important points, different thicknesses of layers can be used within the same piece, decreasing their thickness where necessary. Spacing is the distance between the centers of two successive rays; as the spacing increases, the time for scanning each layer decreases but a larger spot laser is necessary and therefore a greater laser power, otherwise gaps would remain between successive beams, with a porous finished product. To avoid these problems, there are overlaps between the areas hit by rays in succession; these are also necessary considering that the power of the laser beams has a Gaussian distribution, maximum in the center and reduced at the ends, which could result in an incomplete fusion of the ends of the beam. You can also define the degree of overlap of tracks as:

$$\phi = \frac{w - h_d}{w} \quad (2)$$

With Φ, the degree of overlap, w the width of the individual laser scanning tracks and h_d hatch spacing. If Φ is greater than 20% there is the complete superposition, if it is between 0% and 20% the superposition is partial, while if it is less than 0% the superposition is absent. Figure 1.39 shows a diagram of a PBF process where the 4 parameters that influence VED are highlighted.

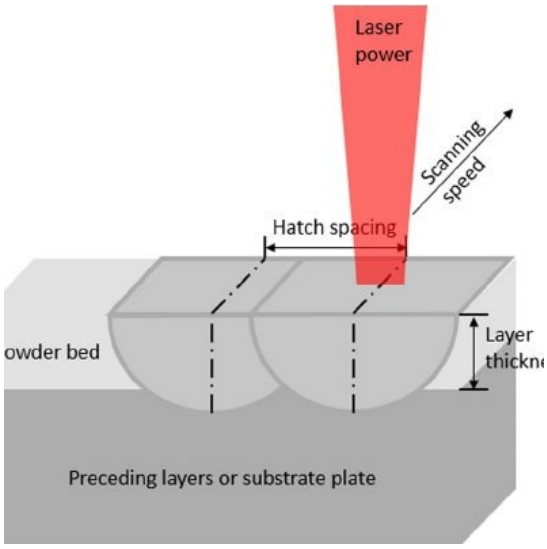

Figure 1.39: Diagram with parameters that influence volumetric energy density

Stress mitigation

There are certain processes and strategies necessary for the reduction of residual stresses in the workpiece. This is the case of the sacrificial support structures that must be defined during the preparation phase of the STL files. They prevent the piece under construction from deforming or breaking during printing and are generally necessary in the case of complicated shapes or large surfaces. They act as an anchor to avoid distortions of the piece under construction; They reduce residual tension phenomena and dissipate heat, avoiding breakage of the piece. Support structures must be eliminated at the end of the printing process; In some cases, this operation can be carried out manually but typically it is necessary to resort to cutting operations such as EDM.

Internal tensions can also be reduced with stress relief heat treatments or with appropriate laser scanning strategies. The latter also help to optimize the processing time, structure and morphology of the grain and to obtain parts without distortion, warp and porosity. Scanning is usually done in two stages: creating the outer edges of the section and filling. Creating small zones and scan lines reduces the problem of distortion for volumetric shrinkage. Short scan lines with rotated orientation between one layer and the next are preferred, in order to avoid the growth of columnar grains and trying to obtain isotropic properties of the piece. Figure 1.40

shows some scanning strategies: a) without rotation between one layer and the next; (b) 90° rotation; (c) 45° rotation; Optimized rotation of 67°.

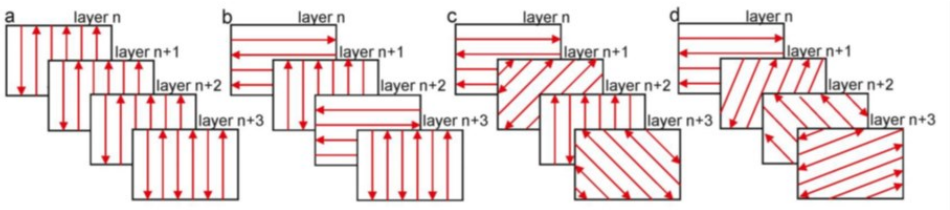

Figure 1.40: Schematic of some scanning strategies

Positioning of parts

During the preparation phase of the print, the positioning of the parts on the construction plate is also defined. The orientation, position, and arrangement of the part on the build platform can have an impact on the stability and speed of the process and, consequently, on the properties of the components. Of particular importance is the orientation of the parts in relation to the blade of the powder redistribution system. When the blade approaches the solidified zone of the workpiece, if the contact is extended for a large area, the force applied by the blade could lead to delamination of the workpiece or stalling of the blade motor. By tilting the piece with respect to the direction of dust deposition, the first contact area between the recoater and the workpiece is reduced, and any defects generated would have very small dimensions. The correct orientation of the parts also reduces the number of surfaces that need to be subjected to finishing treatments at the MU after printing. The best solution would be to make the surfaces that need greater finishes and precision coincide with those in contact with the support structures. The support surfaces, in fact, locally reduce the dimensional and surface quality of the piece, making further post-processing operations necessary to remove them. They should be avoided for elements that are too thin and could break during the removal of the support.

In the case of printing processes of several components, it is advisable to minimize the obstacles encountered simultaneously by the recoater, decreasing the impact of the blade with the solidified geometries. A few mm of deviation between one piece and another with respect to the direction of blade movement are sufficient. Always considering multiple prints, it is necessary to avoid positioning the parts one behind

the other according to the direction of distribution of the powder because collisions and damage in one part result in a deterioration of the dust bed in the area behind the collision area. Finally, considering a possible protrusion of the pieces under construction, it is necessary to ensure that it is not facing the covering blade during the powder redistribution phase (Figure 1.41).

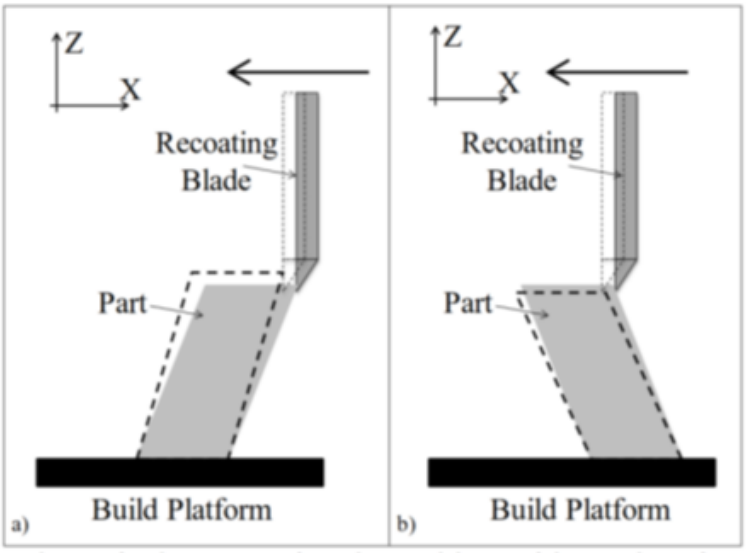

Figure 1.41: Overhang angle with respect to recoater blade

Recoater blade

The blade that distributes the powder layers (recoater) can be made of different materials with different stiffness.

The higher rigidity blades (hard recoater) are made of super-fast steels (HSS high speed steel) or ceramic materials and guarantee advantages in terms of part quality and repeatability. The hard blade compacts the powder during recoating, increasing the density of the powder bed, and removes any spatters emitted by the melt pool during the previous scan. It has a good resistance to wear and is therefore also suitable for processes that require high times. It is the most adopted solution when high process reproducibility, good mechanical properties and dimensional accuracy are required.

Soft recoaters are made of silicone or nbr rubber and are used to reduce the force exerted on the workpiece during powder distribution. They are economical and suitable for parts characterized by high fragility and high Aspect Ratio (vertical proportions). With soft blades, the chances of interruptions in the printing processes due to collisions between the distribution system and the component are reduced. It is a solution adopted when the optimal mechanical properties are not sought in the pieces made but economy and speed are preferred. Rapid blade wear can cause lack of uniformity in parts with long molding cycles.

The brush recoater consists of short carbon fibers mounted on a support. It has a higher cost compared to the alternative in polymeric material; In case of contact with the workpiece under construction, the chances of it breaking are limited because the fibers can bend sideways. It is a good solution for printing fragile parts because, even in the case of contact, this only happens with a certain fraction of fibers.

Laser-powder bed interaction effects during fusion

We can identify 4 different phenomena of laser/powder interaction that can lead to defects in the part:

- Rayleigh-Plateau instability
- Flow of shags
- Balling
- Denudation

Raileigh instability, or capillary instability, is a fluid dynamic phenomenon due to the action of surface tension that destabilizes a fluid system (in the case of PBF, the melting pool) and creates one of equal volume but smaller surface. It is the same phenomenon that causes a jet of liquid to break into small droplets. Figure 1.42 shows experimental tests of single scanning traces carried out with variable speed and power where, for some combination of parameters, Raileigh instability phenomena are visible [28].

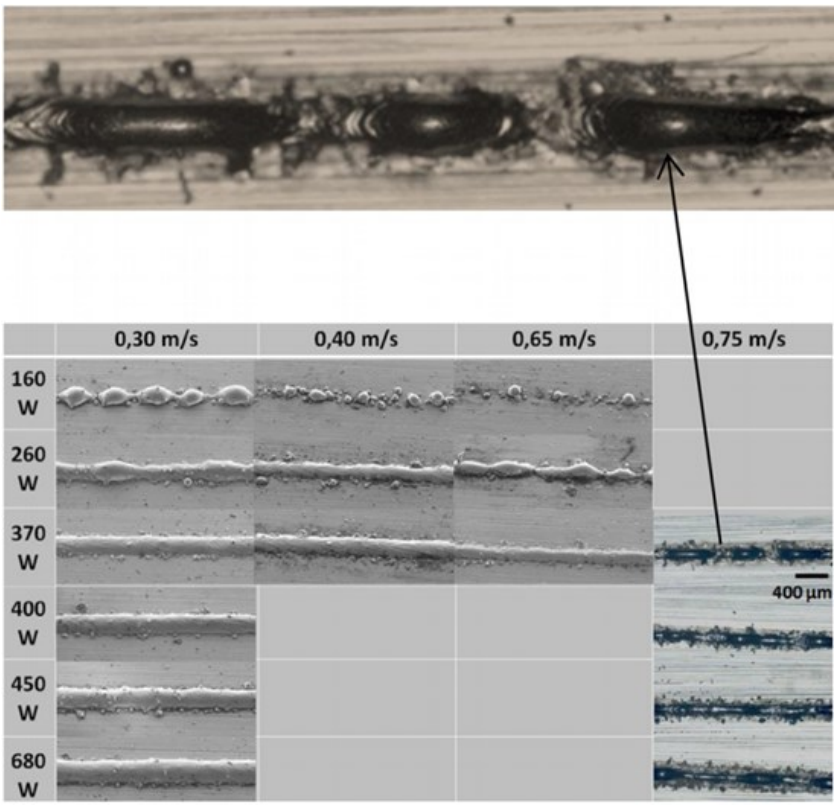

Figure 1.42: Single scanning traces of a 316L stainless steel powder made with variable scanning power and speed [29]

Marangoni flow is a mass transfer that occurs along an interface between two fluids due to a surface tension gradient between the two. The stress gradient can be caused by gradients of temperature or chemical composition on an interface. In Laser Powder Bed Fusion processes, the phenomenon occurs due to the temperature gradient in the laser spot area due to the Gaussian distribution of energy in the beam. In the liquid-solid interface and within the melt area, surface tension gradients are generated due to differences in concentration and temperature, causing shags to flow.

The phenomenon of balling is linked to Raleigh instability and occurs as a result of printing processes with suboptimal parameters. It consists of breaking the trace of the liquid during LPBF, with a formation of discontinuous traces and spherical bulges on the surface of the trace. In the piece this results in high surface roughness.

The denudation effect occurs due to the interaction between the rapidly formed melt bath and the powder bed. The pressure difference between the melt pool and the powder bed generates a stream of particles that are repelled and attracted by the melting zone, creating zones of denudation. The laser as the scan continues, it may encounter areas with less dust, causing strong porosity in the part produced [30].

1.4.4 Other AM technologies

Direct Energy Deposition (DED)

The DED process uses a stream of powder or metal wire that is melted locally via a high-intensity energy source such as laser, electric arc or electron beam. The fusion of the material takes place on the deposition head that moves following the indications of a virtual model. No longer having the limitations of the powder bed, large structures can be realized, with the only constraint of the positioning of the deposition head. For optimal positioning of the deposition head, 5-axis handling systems are used. DED systems can be classified according to the type of material used (powder or wire) or according to the type of energy source used for melting the

Figure 1.43 shows the deposition head of a DED system with laser and powder that uses powder as raw material and laser as an energy source. In the case of using a laser as an energy source, this is concentrated on a point of the build platform and at the same time the metal powder is injected into the focal path of the laser. The energy supplied by the laser is sufficient to form a melt bath; the surrounding powder and gas stream are coordinated to capture as much powder flowing into the melt pool as possible. Molten metal has a strong reactivity with oxygen, so inert gases are needed to protect the molten metal pool. These, in addition to the role of protection from the external environment, help in directing the powder stream, reducing its dispersion. As in LPBF, sparks and powder are formed, and particles are re-emitted outside the melt pool.

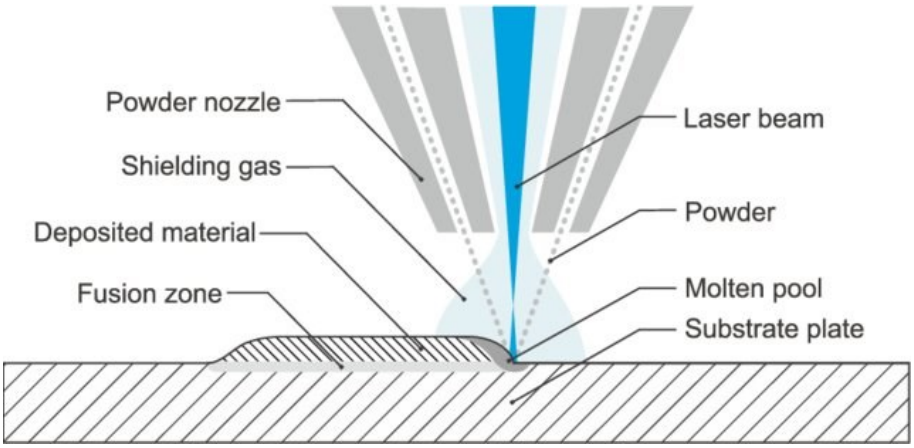

Figure 1.43: Direct energy deposition process of metal powder with lasers as an energy source

Compared to powder bed systems, less powder is used but it is more difficult to recover and reuse the powder which, following interaction with the laser, is re-emitted out of the melting zone. Powders with grain sizes between 45-106 µm and lasers with 2-3 mm spots are used. The cooling rate of the melting pool is about 105 k/s. No support is needed, and DED systems are typically not used for the construction of structures with complex geometries. Common uses are the repair and coating of mechanical components. The low surface quality that the processing confers makes post-processing operations necessary.

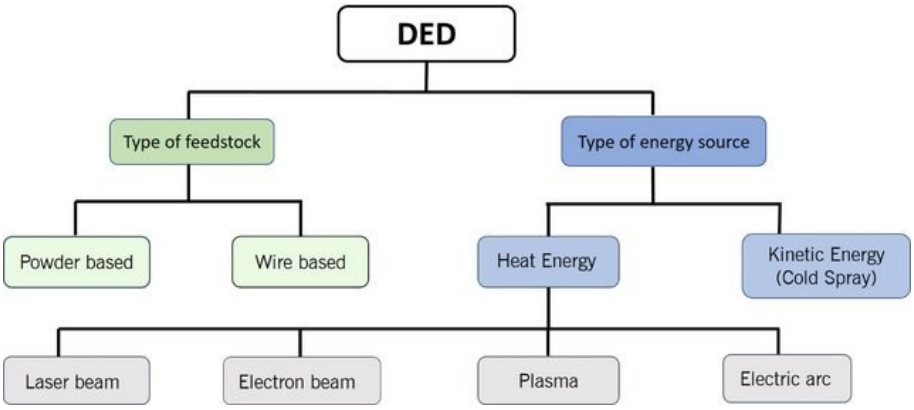

Figure 1.44: Classifications of direct deposition technologies

Direct deposition processes can be classified according to the energy source used and the type of input materials [31]. Figure 1.44 shows these classifications.

Although DED can be used for molding polymeric, ceramic and composite materials, its main use is associated with the molding of metal powders. These can be used for the production, repairing and the deposition of metal for the creation of coatings [32].

DED systems allow to produce, in a single molding cycle, components made of different materials. Different materials, contained inside tanks, can be mixed before being deposited; In this way, components with variable chemical compositions can be obtained. For example, the percentage of each material contained in the deposition mix can be varied after the deposition of each layer gradually. shows a scheme and application of this technology [33].

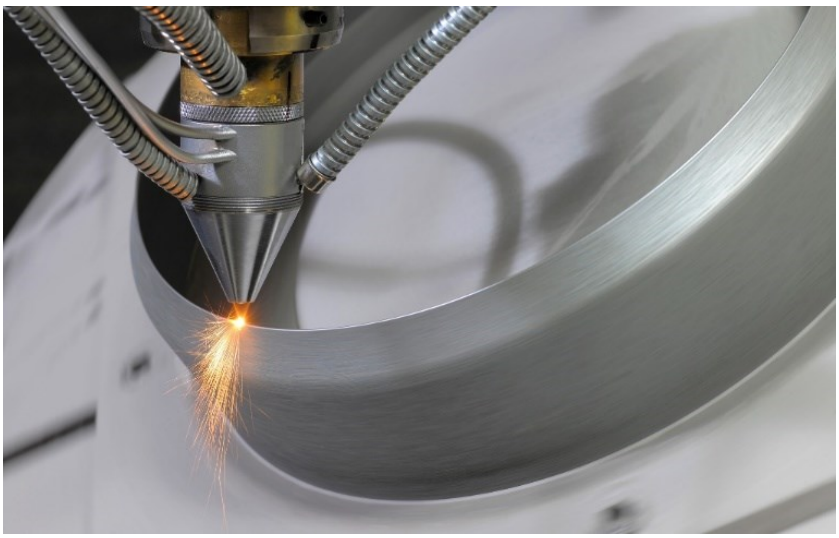

Figure 1.45: Typical DED process

Another type of processing by direct deposition involves the use of metal wires as starting material and electron beams as energy source. This system is characterized by a higher build speed than the powder-fed DED. In addition, metal wires often cost less than powder and are easier to handle. The use of the electron beam usually requires the creation of a vacuum. This kind of systems are currently used for the

production of metal fuel tanks for aircraft. The DED technology allows the realization of components with large dimensions but low surface finishes. It is therefore used to produce Near Net Shape parts, which require subsequent machining to obtain the desired finishes and tolerances. Figure 1.45 shows a typical DED process.

In recent years, hybrid systems have also been developed, able to combine the functions of traditional machine tools with direct deposition systems of Additive Manufacturing. These are robotic machines or arms equipped with chip removal systems that also have a direct energy deposition head for powder or metal wire. This allows to combine the two processes and to obtain extremely complex geometries and good surface finishes. The intermittent processing (with alternation of deposition and removal) allows to reach with the removal systems also the internal cavities that are enclosed in the final part. Their use requires some precautions, for example in the positioning of the piece, to prevent the chips produced from remaining inside the part even after the end of processing.

Cold Spray

Cold Spray is an alternative DED process originally developed as a coating technology in the 80s. Gases at high temperature and pressure (air, helium or nitrogen) are used as thrusters to accelerate metal powders to high speeds (over 300 m/s). The powders, therefore, are deposited following the impact with the construction plan. The formation of the deposited layer is not based on high temperatures as in other DED processes, but on the high kinetic energy of the particles before impact. When powder particles come into contact with the surface of the part, the high kinetic energy causes plastic deformation, creating mechanical interlocks and metallurgical bonds. Following the impact, heat is generated by conversion of kinetic energy into thermal energy, but this is not enough to melt the powder, which remains solid throughout the process. This completely eliminates problems encountered in high-temperature DED processes such as oxidation, residual stress, and phase changes [34]. The Cold Spray, or solid process, allows the processing of metals that tend to break during the rapid solidification typical of other AM systems for metals. In addition, it is a process that can also be carried out in the open air without major complications associated with oxidation.

Cold Spray processes can be divided into two categories: with high pressure systems (>1 Mpa) and with low pressure systems (<1Mpa). Figure 1.46 shows diagrams of Cold Spray systems. High-pressure systems use a gas that is divided into two

streams, one for heating and one for collecting powder, and which are joined before the extruder. It sprays powder at high speeds (800-1400 m/s) and allows the processing of heavy and low-ductile materials such as steel and titanium alloys. They can also work at the pressures typical of low pressure systems. Low pressure systems are used to treat light or ductile materials such as aluminum and copper. The compressed gas is replaced by a portable air compressor. They are low-cost systems also used in case of repairs because of their simplicity and transportability.

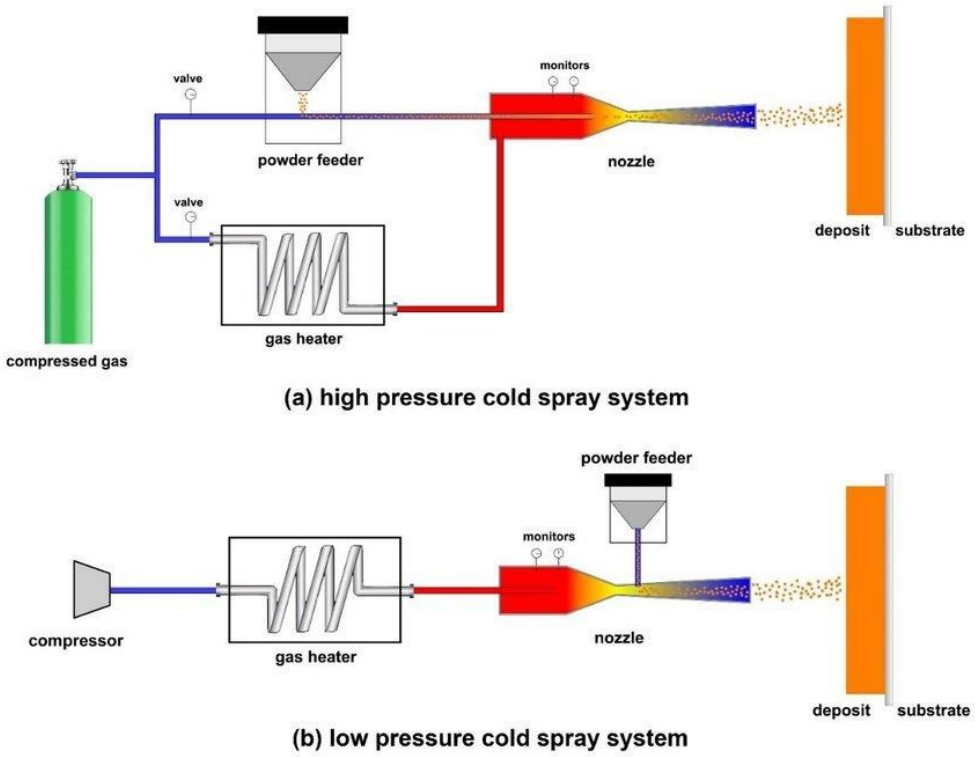

Figure 1.46: High- and Low-Pressure Cold Spray Systems

The Cold Spray is also suitable for large parts. Since an inert working environment is not required, the produced pieces dimensions are limited only by the handling system used. As with other DED systems, near-net-shape parts need additional

machining to meet design accuracy requirements; with printing, accuracies of ±1-3 mm are achieved, so any surface that requires a tighter tolerance must be reworked.

Sheet Lamination

Commonly known as LOM (Laminated Object Manufacturing), sheet lamination is a process by which consecutive layers of sheet material are joined and cut to form a 3D structure. It was one of the first AM techniques to be commercialized and initially involved the overlapping of layers of paper, each representing a layer of the virtual model, subsequently cut by means of a laser. Several sheet lamination systems were developed with difference type of material processed and cutting and joining strategies of the layers.

The workflow of the printing process with gluing involves a first phase of insertion of the sheets of material into a construction area. After that, an adhesive component is deposited on the surface of the sheets. Pressure is then applied to ensure adhesion of the layers. Next phase concerns the cutting of the piece and to a coloring phase (not always present). Figure 1.47 shows a diagram of the sheet lamination process.

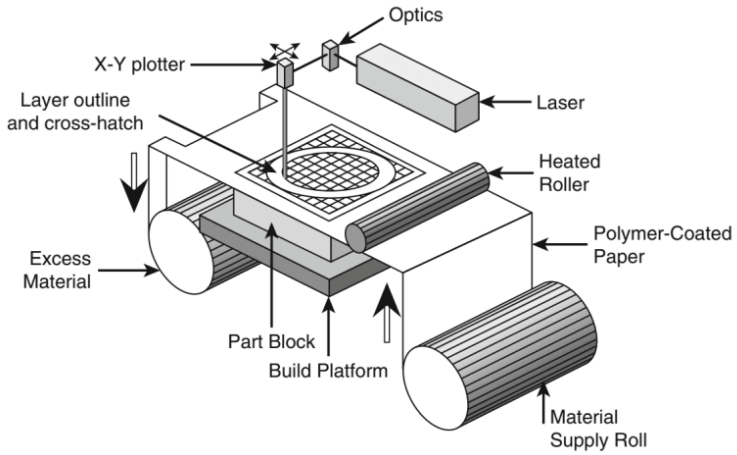

Figure 1.47: Sheet lamination process

Adhesion between layers of material can be ensured by several methods, which constitute a way of categorizing technologies. Adhesion strength is an important parameter to consider in part design and applications. In addition to bonding

adhesion there are the thermal bonding, the clamping and the ultrasonic welding. A brief description of the latter technique process is provided for his technological relevance.

Ultrasonic consolidation (UC) o Ultrasonic Additive Manufacturing (UAM) is a hybrid sheet lamination technique that combines ultrasonic welding with CNC machining. For the process an instrument, called sonotrode, capable of creating ultrasonic vibrations and applying this generated energy to gases, liquids or, in this case, solids is used. Specifically, metal sheets are typical material for this kind of process.

Figure 1.48: Machining Example for Ultrasonic Additive Manufacturing

Initially, a base plate is fixed in place on the anvil of the CNC machine. The metal foil, under the action of the sonotrode, which applies pressure by normal force and oscillations, is attached to the base plate. The process is repeated, overlapping metal sheets and consolidating them with ultrasound. The excess material is removed by means of a computerized CNC cutter in order to obtain the desired shape. The deposition and machining cycle is repeated until a height between 3 mm and 6 mm is obtained. At this point, a smaller finishing cutter is used to ensure the design tolerance and surface finish. This cycle is repeated until the finished object is obtained. The Figure 1.48 shows a typical machining example for the UAM process.

Sheet lamination technologies, based on the overlapping of several layers of metal sheet, are characterized by anisotropy. With a good design phase, parts made for LOM with composite or metallic materials are also suitable for structural applications. As for composite materials, LOM machines use advanced fiber laminates as raw material. These can be woven, non-woven or unidirectional and can have thermosetting and thermoplastic matrices. The application of sheet laminations for composite material is of interest because it allows the use of prepregs commonly used for the traditional production of laminate composites.

Chapter 2

2 Environmental impact analysis: life cycle assessment

2.1 Life Cycle Assessment: introduction

The increase in interest in environmental issues has led to the development of techniques to assess the impacts on the ecosystem of human activities and the production of goods. Since the 70s there have been studies to determine the effects on the environment of industrial activities, considering all phases of the life cycle of the product, from the extraction of underground materials to waste disposal (from cradle to grave). SETAC (The Society for Environmental Toxicology and Chemistry), in a publication of January 1991, responded to the need for a standardized method for conducting these studies by defining guidelines for Life Cycle Assessment (LCA). Today we follow international standards defined by the UNI EN ISO 14040 and 14044 standards that describe the principles and the reference framework for these analyzes. These define LCA as "a process of assessing the environmental aspects associated with a product or service" that "considers environmental impacts over the life cycle of the product (from cradle to grave)" (ISO UNIEN, 2011) (ISO UNIEN, 2010). LCA has several possible uses:

- helps to improve the environmental performance of products in the various stages of the life cycle, identifying critical issues and possibilities for efficiency;
- provides information to those in governmental and non-governmental organizations who need to make decisions such as strategic planning, prioritization, and product and process redesign;
- supports the choice of environmental performance indicators and measurement techniques;
- it can add perceived value to the finished product thanks to marketing policies that show the eco-sustainability of the processes and the company.

The LCA process is a systematic and gradual approach that is divided into four phases, as shown in Figure 2.1:

1. Definition of objectives: define and describe the product, process or activity analyzed. Establish the context in which the assessment is to be carried out and identify the boundaries and environmental effects to be considered for the assessment. Life Cycle Inventory (LCI): identify and quantify energy, water and material use and emissions into the environment (such as air emissions, solid waste disposal, wastewater discharges) during all phases considered within the boundaries of the system.
2. Life Cycle Impact Assessment (LCIA): assess the potential human and ecological effects of energy, water and material use and the environmental emissions identified in the inventory analysis using the environmental indicators chosen in step 1.
3. Interpretation of results: Evaluate the results of the LCI and LCIA and interpret them according to the objective and application of the study. Possibilities for process improvement are then identified to reduce the overall environmental impact.

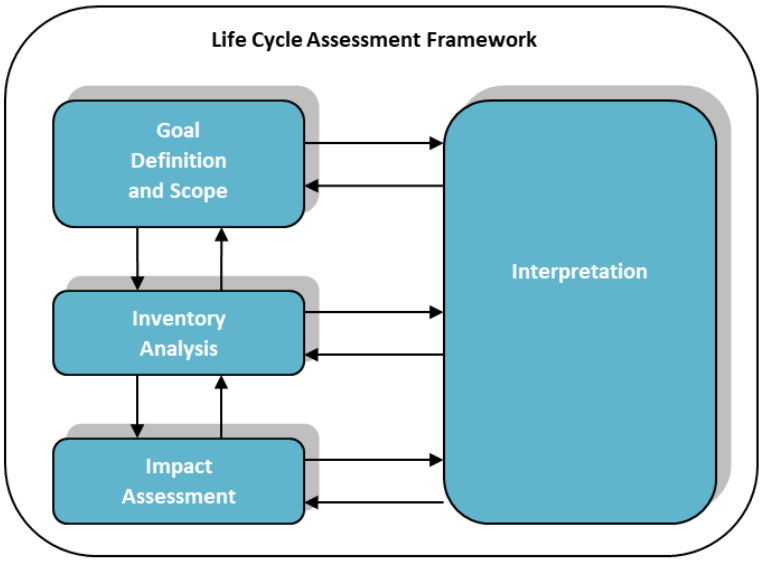

Figure 2.1: Steps of an LCA analysis

2.2 Goal and scope definition

Goal definition is the stage of the LCA process that defines the purpose and method for including life-cycle environmental impacts in the decision-making process. When defining the objectives of an LCA analysis, it is necessary to clearly describe the intended application and the reasons for the study, such as, for example, the assessment of CO2 emissions or the creation of guidelines to improve production processes. The public to whom the results of the study will be disclosed shall also be identified and any comparative assertions intended for disclosure shall be defined. Below are descriptions of some elements of the first phase of LCA analysis.

- Definition of the objective
  Concrete goals and interest in understanding LCA must be set in the goal-setting process. In addition, customers and target groups must be indicated. If necessary, it should be indicated what role LCA plays in decision-making and whether it is linked to further investigations (e.g. economic, technological, social issues). When communicating results, it must be made clear for which objectives LCA is suitable and for which it is not.

- Determination of the System Boundary (Figure 2.2)
  The boundary of the system must be determined according to the objectives defined by the LCA.

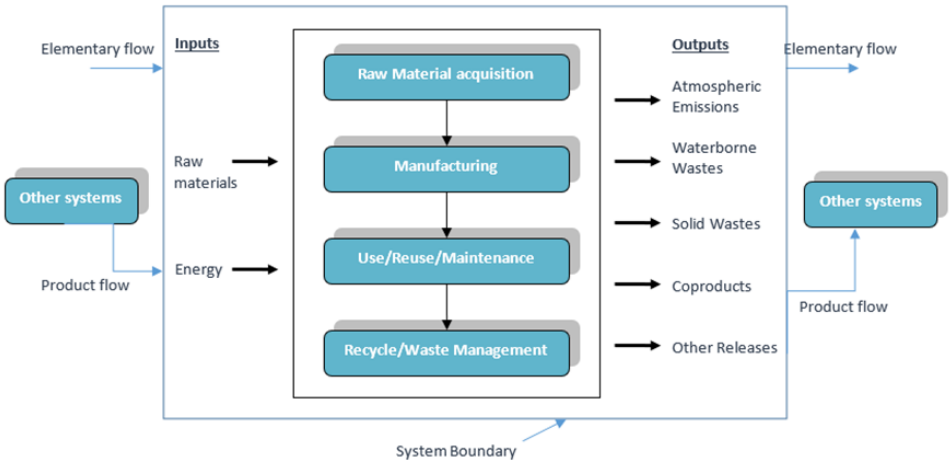

Figure 2.2: System boundaries

The means available, the time frame and the availability of the necessary data must be taken into account. In particular, the temporal, spatial and technical spheres of data recording shall be determined. The boundary of the system marks the interface between environment and other production systems. They also define which procedures are included or excluded from the investigation. With regard to data acquisition, the scale, type (specific, average) and quality of the data required shall be determined. Two problems arise when establishing the system boundary. First, separation criteria and product allocation procedures must be defined for the individual processes considered in the budget. Secondly, the functions of the systems examined and of the functional unit must be determined. The differences and possible restrictions of the systems to be compared shall be documented.

- Separation criteria
  In order to reduce the scope and complexity of the survey framework, the system boundary is limited to a scale of inquiry that adequately responds to the functional unit. With the help of sensitivity analyses and performance criteria, it is determined whether a material flow can be interrupted. Mass criteria and energy criteria can be taken into account, for example.

- Allocation procedure
  If multiple productions occur in the system of the product under consideration, allocations must be applied. Multiple productions are production processes that, together with the planned product production, generate additional products that can be used in other processes. The environmental effects caused by this process must be added proportionally to all the products of the process according to a given procedure. Waste is not considered in this case. If allocations cannot be avoided, system inputs and outputs should be allocated to different products to reflect the basic physical relationships. The distribution is not necessarily based on the mass criterion but additional physical criteria are applicable. If physical relationships are not applicable or are not sufficient, allocation may be based on other relationships, such as economic values. If more than one allocation procedure is eligible, a sensitivity analysis shall be carried out.

- Functional unit
  The functional units of the systems examined must be clearly defined. The functional unit serves as the reference unit for all incoming and outgoing flows and potential environmental effects. When comparing different products or

procedures, it is of particular importance that the criterion of functional equivalence (properties and function of similar products, e.g. total weight in kilograms of footwear consumed in Italy in one year) satisfies the systems considered.

2.3 Life Cycle Inventory (LCI)

Life cycle inventory analysis is a process of quantifying energy needs, raw materials, atmospheric emissions, water emissions, solid waste and other emissions for the entire life cycle of a product, process or activity. The level of accuracy and detail of the data collected is important throughout the rest of the LCA process. Lifecycle inventory analyses can be used in a variety of ways. They can help an organization compare products or processes and consider environmental factors when selecting materials. In addition, inventory analyses can be used in decision-making, helping decision-makers develop regulations on resource use and environmental emissions.

The 1993 EPA document, entitled "Life-Cycle Assessment: Inventory Guidelines and Principles", and the 1995 document, "Guidelines for Assessing the Quality of Life Cycle Inventory Analysis", provide the framework for carrying out an inventory analysis and assessing the quality of the data used and the results. The two documents define the following four phases of a life cycle inventory.

- Development of a flowchart of evaluated processes: a flowchart is a tool for mapping inputs and outputs in a process or system. The more complex the flowchart, the greater the accuracy and usefulness of the results. The increase in complexity also means more time and resources to devote to this phase, as well as to data collection and analysis.

- Develop a data collection plan: when selecting data sources to complete lifecycle inventory, an LCI data collection plan ensures that data quality and accuracy meet decision makers' expectations. The key elements of a data collection plan are as follows: defining data quality objectives, identifying data sources and types, identifying data quality indicators, and developing a data collection worksheet and checklist.

- Data collection: data collection activities involve a combination of research, site visits and direct contact with experts, which generate large amounts of data.

Alternatively, it may be more cost-effective to purchase a commercially available LCA software package. All industrial processes have multiple input streams and can generate multiple output streams. Usually only one of the results is interesting for the ongoing life cycle assessment study, so the analyst needs to determine the amount of energy and materials required and the environmental emissions associated with the process. For example, steam turbine systems can sell both electricity and low-pressure steam as useful products. Where co-products are present, the operator shall determine to what extent the charges associated with the management and supply of the multi-output process should be attributed to each co-product. The analyst must also decide how to allocate the environmental burden among co-products when one is a waste stream that can be sold for other uses. Guidance provided by the International Organization for Standardization (ISO) recognises the variety of approaches that can be used to address the issue of allocation and, therefore, call for a step-by-step approach.

- Evaluate and report results: when preparing a report to present the final results of the life cycle inventory, it is important to describe in detail the methodology used in the analysis. The report should explicitly define the systems analyzed and the boundaries that have been defined. All assumptions made when carrying out the inventory must be clearly explained. The basis for comparison between systems should be provided and all equivalence ratios used explained.

2.4 Life cycle impact assessment

The Life Cycle Impact Assessment (LCIA) phase is the assessment of the potential impacts on human health and the environment of resources and environmental emissions associated with the considered system. These effects, quantified through appropriate indicators, are calculated from the system inputs and outputs identified during the LCI. The results of an LCIA show relative differences in potential environmental impacts for each option. For example, an LCIA could determine which product/process causes the greatest global warming potential.

The LCIA consists of three mandatory elements:

- selection of impact categories, indicators and characterization models;
- classification, i.e., the assignment of LCI results of the chosen impact categories;

– characterization, the calculation of category indicator results.

And three optional elements:

– normalization: to better understand the relative magnitude of each result by comparing it with the reference information;
– grouping: sorting and possible hierarchical classification of impact categories;
– weighting: conversion and possible aggregation of the results of the different categories, while maintaining the data prior to this analysis.

All these elements are represented in the diagram in Figure 3.3.

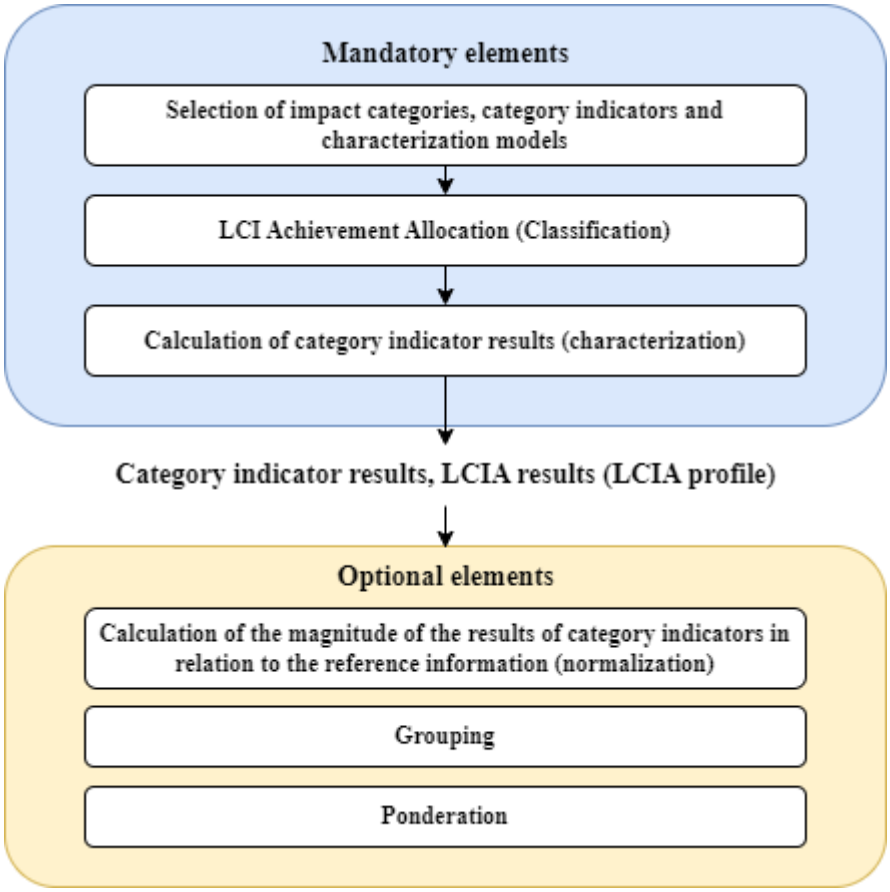

Figure 2.3: LCIA elements

Finally, a data quality analysis could be performed to guide the iterative process of LCA, identify negligible LCI results, and understand the significance, uncertainty, and sensitivity of the results.

The goal of LCIA is to achieve results that are relevant, clear and easy to manage and communicate. For this reason, the choice of categories and the method used is fundamental. Below are some methods for conducting LCIA, each of which is suitable to represent certain types of impact. Different approaches can also be used within the same study, so you have a complete view of a product's impacts.

- Cumulative energy demand (CED) or primary energy consumption: the cumulative energy demand quantifies, thanks to characterization factors, all the energy, direct and indirect, used by a product throughout its life cycle, also including the extraction, production and disposal phases. It is expressed in MJ and consists of the sum of the demand for fossil, nuclear, wind, hydroelectric and solar energy. Although it is a method used since the 70s there is still no standardization and unification and today there are several possible approaches. Among these is the "energy harvested approach" (Frischknecht et al., 2015) which focuses on how much a product or process contributes to the protection of energy resources available to man.
- Global Warming Potential (GWP): it is used to quantify greenhouse gas emissions (GHGs) into the atmosphere and their effect on global warming and climate change. One of the methods for calculating GPM has been proposed by the IPCC (Intergovernmental Panel on Climate Change) and considers the effects of greenhouse gases by comparing them with those of CO2 and evaluating their effects over a time horizon of 100 years.
- ReCiPe: the ReCiPe is a method developed in 2008 with the aim of expressing the long list of information of an LCI, in a series of indicators representing different categories of impact, divided into midpoints and endpoints. There are 18 midpoint categories, and they focus on specific environmental problems, such as soil acidification or water consumption. The assessment of all these types of impacts guarantees a complete view of the effect on the environment of a product or process.

The endpoints bring together the previous categories into three types of impact: damage to human health, damage to the ecosystem, and damage to resource availability. Aggregating indicators makes it easier to interpret the results but increases the uncertainty of the results (Figure 2.4) [35].

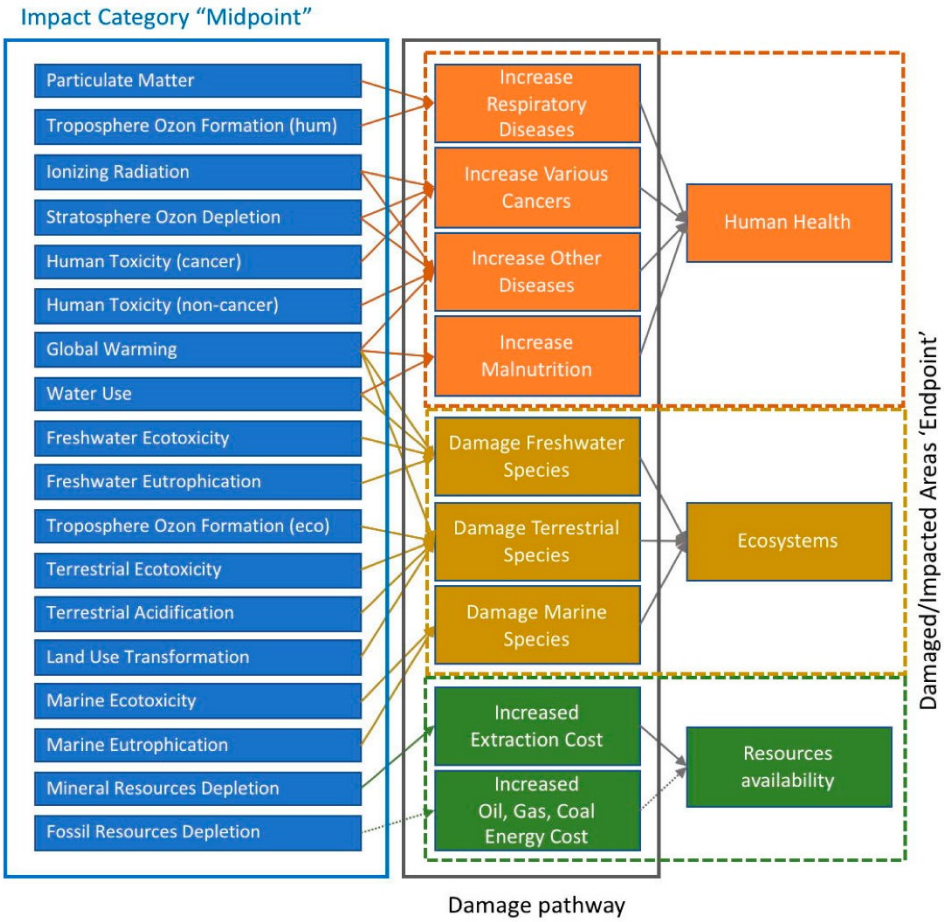

Figure 2.4: Midpoint and endpoint categories of the ReCiPe methodology

2.5 Life cycle interpretation

Life cycle interpretation is a systematic technique for identifying, quantifying, controlling, and evaluating information from LCI and LCIA results and communicating it effectively.

At this stage, the results of the impact assessment are interpreted, and conclusions are drawn to guide the decision-making process. Environmental criticalities are defined and the significance of the relative contribution of some components or

processes of the product to the environmental load is recognized. Depending on the need of the study, the verification of the results can be carried out considering 3 different aspects:

- Completeness verification: verify the completeness of the study, so that the significant environmental issues previously identified represent the information of the different phases of the LCA in an appropriate manner according to the objective and the defined scope.
- Sensitivity analysis: verify whether the final results and conclusions are influenced by uncertainties in the selected data or evaluation methods. The purpose of sensitivity control is therefore to establish the degree of confidence obtained in the results of the study with respect to the general objective. This control is mainly used to test the assumptions made during the study. The sensitivity analysis can be carried out by making a sort of hypothetical scenario, in which the value of the different input parameters is systematically modified. This can also be done using simulations (e.g. Monte Carlo simulations).
- Consistency check: assess the consistency of the methods, procedures and data processing used during the study and verify their consistency with the objective and scope of the study. The items that can be subject to the consistency check are: data source, data accuracy, geographical representation, system boundaries and assumptions.

2.6 Life Cycle Costing

The analysis of environmental impacts can be associated with a cost analysis called Life Cycle Costing (LCC). As in the case of LCA, LCC allows you to evaluate the entire life cycle of the product, from production to disposal. The purpose is to evaluate all the items that contribute to the cost of a product or service in order to optimize activities and minimize economic impacts. Therefore, environmental sustainability is associated with economic sustainability.

The operating modes of the LCC are similar to those of the LCA; Referring to the functional unit and the system previously defined in the impact analysis, we proceed with the definition of all the phases that have a non-negligible contribution to the total cost and an analysis of the inventory is carried out. The total costs are then evaluated, and the results are analyzed, identifying the best possible choices from an economic point of view.

Chapter 3

3 Materials and experimental procedures

3.1 Materials

The material used in the present work is a Type 630 stainless steel (commonly known as 17-4 PH stainless steel), composed of about 15-17.5% chromium, 3–5% nickel and 3–5% copper. This material is a martensitic precipitation-hardening stainless steel characterized by high strength, good corrosion resistance and good mechanical properties at temperatures up to 320°C. Table 3.1 reports the main mechanical properties of 17-4 PH stainless steel according to the MPIF Standard 35. These properties make this alloy suitable for many industrial applications such as oil field valve equipment, pumpshafts, gears, chemical process equipment, and aircraft components. The material investigated in the present research was supplied by the manufacturer of the 3D printer Desktop Metal in form of bound metal rods, 6 mm in diameter, realized by metal powder held together by wax and polymer binder (Figure 3.1). Such feedstocks are contained in media cartridges to avoid breakage during handling.

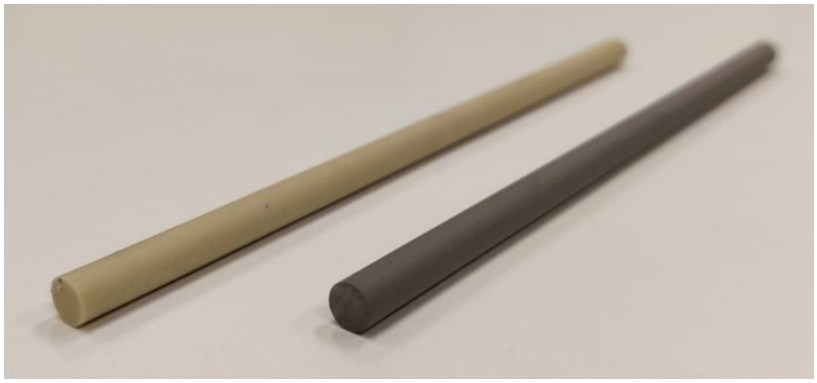

Figure 3.1: Ceramic and bound metal powder rods used for 3D printing process

Table 3.1: Tensile properties of 17-4 PH according to MPIF Standard 35

Tensile Properties - TYPICAL VALUES - 17-4 PH (MPIF Standard 35)	
Yield strength (MPa)	650
Ultimate tensile strength (MPa)	790
Elongation at break (%)	4
Young's Modulus (GPa)	196
Hardness (HRC)	27
Density (g/cm^3)	7.5

3.2 3D Printing system

The "Studio System" 3D printing apparatus used for this work was developed by Desktop Metal, an American company founded in 2015 that deals with the design and manufacture of 3D printing systems. The new technology was created with the aim of creating a simple and economical system for printing metallic materials, also suitable for office applications. The system consists of three units:

– The 3D printer
– The de-binder
– The sintering fournace

The 3D printer of the "Studio System" uses a material extrusion system similar to that of FDM printers of plastic materials. For printing operations, bound metal rods are used as starting materials. As with 3D printing of plastic materials, the system heats and extrudes the material layer by layer following the geometries of a virtual model. The construction plate is moved down after the deposition of each layer, allowing the overlapping of sections. Depending on the deposition head used, the thickness of the deposited layer can be varied from 35 μm to 100/220 μm, allowing the management of construction quality and printing time. The construction chamber has dimensions of 30x20x20 cm. Thanks to the metal rods, the use of powders, melting beds and high-intensity energy sources, such as lasers or plasma torches, is avoided. These features make the printing system safe and also suitable for office use. The machine has been designed to allow rapid change of materials without

interruption of printing processes and without risk of contamination through interchangeable cartridges. This is a significant improvement over laser-based systems that require a lot of time and demanding safety requirements to perform the material change; In addition, in powder bed systems, the use of different materials on the same machine is often not recommended. The printer is equipped with two extruders: one is used for molding the metal material, the other extrudes a ceramic material that is interposed between the supports and the piece. During the sintering phase, the ceramic material, instead of bonding with the metal, is reduced to powder and facilitates the removal of the supports during post-processing. The latter can also be easily separated manually, without resorting to cutting systems (e.g. EDM) that are necessary for other metal 3D printing systems.

Figure 3.2: Studio System apparatus supplied from Desktop Metal

Figure 3.2 shows the BMD Studio System printer. From the image it can be seen the two extruders (one for metal and one for ceramic materials) and the movement system of the extruders and the construction plate. Table 3.2 shows the technical specifications of the printer.

Table 3.2: Studio System Printer Technical Specifications

3D printer Studio System equipped with BMD extrusion-based technology	
Max build rate	16 cm3
Layer height	35 μm (high resolution printhead) 100/220 μm (standard resolution printhead)
Build envelope	300 x 200 x 200 mm
Dimensions (H x W x D)	94.8 x 82.3 x 52.9 cm
Weight	97 kg

As with Binder Jetting, at the end of the printing process a part is obtained that needs further processing to acquire good mechanical characteristics. The second phase of production is that of debinding which consists in eliminating the binder from the printed part. The process takes place in a special machine in which the molded parts are positioned; the machine is filled with a solvent that submerges the workpiece, penetrates inside the porosities and dissolves the polymer binder. The solvent is then removed from the machine automatically and a heating cycle is carried out up to 200-600 ° C to dry the part and eliminate the residual polymer. The time required for this phase varies depending on the geometry and size of the parts and is usually between 9 and 72 hours. At the end of the process, a completely metallic porous structure is obtained (unless residual traces of binder). A complete removal of the binder is important to ensure good metallurgical properties to the piece; In addition, an incorrect debinding process can lead to defects and crack formation.

The third machine used in the process is a furnace that allows the sintering of the part. The sintering process is the same as described in the previous paragraph, with a heated chamber and an inert gas under pressure. Thanks to metallurgical phenomena, the part increases in density up to 96-99% and porosity is reduced with an increase in the mechanical properties of the molded piece. The sintering cycle lasts about 40 hours; The times are automatically modified by the system according to the parts introduced. In the case of large objects and complex geometries, sintering can take up to 49 hours. With the sintering process, a near-net shape part is obtained from which the supports must be removed, and any post-processing carried out.

3.3 Printing, debinding and sintering

The first phase for the realization of tensile specimens is characterized by several steps starting from the design of the actual printing process. As with any AM process, the beginning phase is always the design of the CAD model (in this case the geometry of a tensile specimen according to ASTM E8 – Standard Test Methods for Tension Testing of Metallic Materials). For this aim, the commercial CAD software Rinocheros 7 is used. The three-dimensional file is then transformed into a mesh model of the type .STL then described as a set of closed surfaces to form the three-dimensional model. At this point, the file can be used as input to be sent through a cloud to the print job management software provided by Desktop Metal. This step is used to convert the .STL file in a .gcode file. Once all the desired values for the printing parameters have been setted, the software translates the three-dimensional geometry into a set of machine instructions that can be executed by the 3D printer.

3D Printing

For this project it was decided to keep some of the main settings of the 3D printing process constant, in order to investigate only some of the parameters described above, which will be varied within specific ranges of values for the realization of the specimens, in order to evaluate how they can influence the tensile mechanical properties of the 17-4 PH stainless steel. The values of the printing parameters kept constant, shown in Table 3.3, are chosen in order to guarantee the better quality for the printed parts. In this way, layer height, extruder and bet temperature was chosen of 0.1 mm, 175° C and 65° C values respectively for the best compromise between realization speed and print quality. The percentage of infill, on the other hand, is maintained equal to 100% for all the specimens with the aim to test the 17-4 PH material according to different printing conditions, following ASTM E8 standard, and not to analyze the effect of specific geometries on the products thus realized. The parameters chosen for this analysis, with their respective ranges, are summarized in Table 3.4. The parameters that can mainly influence the tensile mechanical characteristics of 17-4 PH stainless steel obtained by BMD technology have been chosen. In particular, the growth orientation angle was chosen to evaluate how the deposition in the 3 different conditions investigated (0°, 45° and 90°) could affect both the quality of the product obtained and its mechanical performances. With the same objective, 3 different conditions were chosen regarding the direction of the infill pattern during the printing of the specimens (Linear 0°, ±45° and 0°-90°). The

influence of the diameter of the nozzle on print quality and mechanical performances was also investigated because, together with the 3D printer in question, two types of extruder were supplied: one with a nozzle with a hole size 0.4 mm and one with a hole size 0.25 mm. This has been deepened with the aim of better understanding if, using a smaller nozzle, a higher quality of the part realized, also corresponds to mechanical properties superior or at least corresponding to those obtained with the other type of extruder. As far as printing speed is concerned, a specific study was considered appropriate to understand in the best way if higher printing speeds (45 mm/s and 60 mm/s) or lower printing speed (15 mm/s) than the one considered standard (30 mm/s) can increase or worsen both the mechanical properties of the products in 17-4 PH, and the quality of construction, with the aim, therefore, of studying the productivity of this innovative technology.

Table 3.3: Constant 3D printing process parameters chosen for this research

Parameter	**Value**
Layer height	0.1 mm
Infill percentage	100%
Extrusion temperature	175° C
Printing bed temperature	65° C

Table 3.4: 3D printing process parameters chosen for this research and ranges to be varied in

Parameter	**Range value**
Growth orientation angle in respect of XY plane	0° 45° 90°
Infill pattern	Linear (0°) ±45° 0°-90°
Nozzle diameter	0.25 mm 0.4 mm
Printing speed	15 mm/s 30 mm/s 45 mm/s 60 mm/s

The growth orientation angle parameter is explained in the Figure 3.3 where specimens are rotated in respect the XY plane that is considered the plane parallel to the building plate, where layers will be deposited along the Z direction. The deposition plane that represents every single layer is explained in the Figure 3.4.

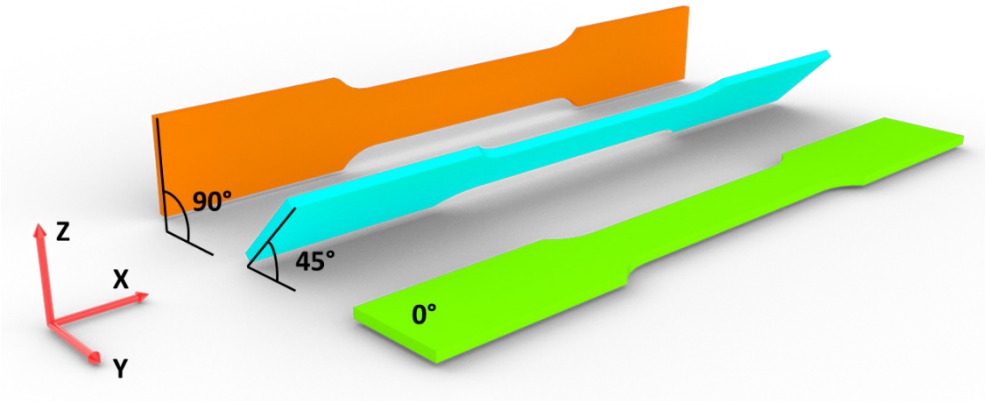

Figure 3.3: Growth orientation angle parameter

Once the .gcode is sent to the printer through the cloud, it is placed in the print queue. On board the machine, the specific job can be selected, and the actual printing process can begin. Once carried out the various checks concerning the loading of the material and the leveling of the printing bed, the printing heads begin to extrude the material and to generate the model layer by layer.

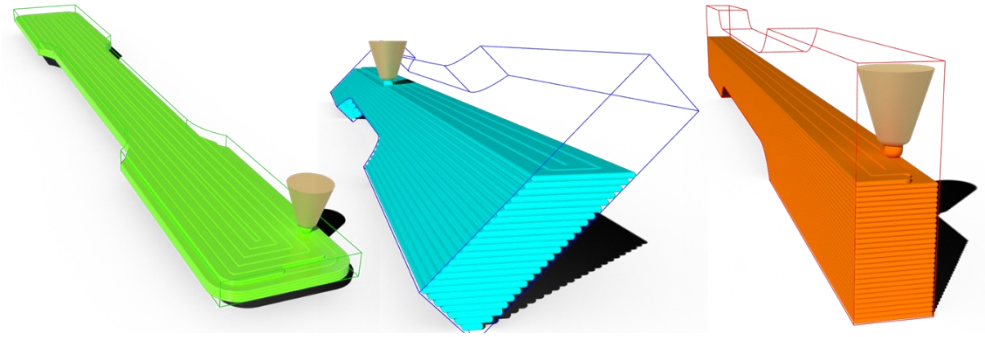

Figure 3.4: 3D reconstruction of the linear deposition for the tensile extensions in the 3 different growth orientations with respect to the plane

An example of two tensile specimen printed with BMD technology with linear infill and 0° of growth orientation angle are shown in Figure 3.5. Between the actual specimen and the print bed there is a solid base larger than the piece, but of the same material that acts as a support. This part will be necessary for the drying phase of the

debinding, which takes place at temperatures close to 600 °C, may induce deformations due to shrinkage stresses during cooling.

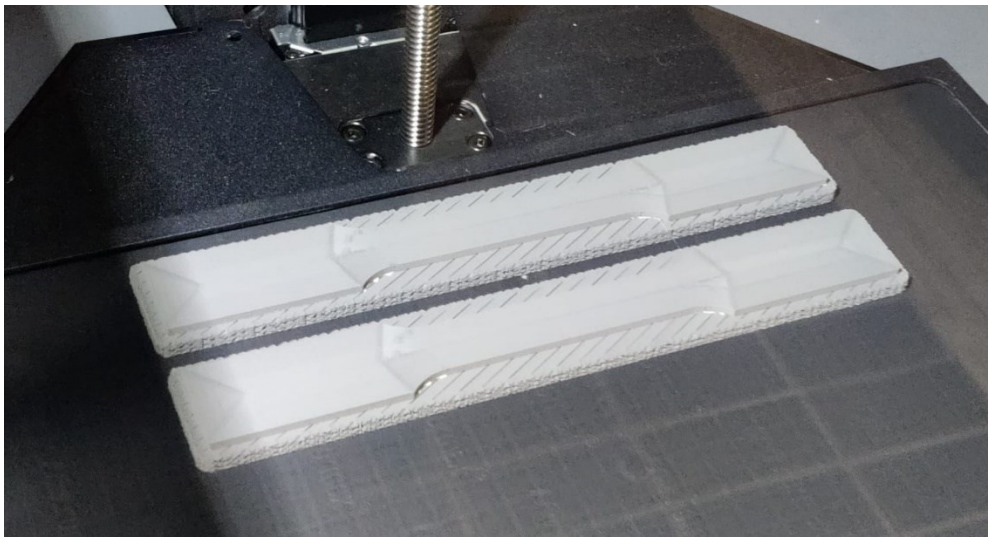

Figure 3.5: Examples of tensile specimens printed with BMD technology

In particular, at least 5 specimens per condition were printed with BMD technology to ensure good repeatability of the results. The conditions studied in this work provided that only one parameter was analyzed at a time. In this way it was possible to compare the data deriving from tests, and based on the results, define how the single parameter influences the tensile properties. Subsequent tables describe the specific parameters for each condition that were carried out for this study. The Table 3.5 describe printed conditions with a nozzle diameter of 0.4 mm and a printing speed of 30 mm/s.

Table 3.5: 3d printed specimens condition with realized with nozzle diameter of 0.4 mm and a printing speed of 30 mm/s

Parameter	Values	Growth orientation angle in respect of XY plane		
		0°	45°	90°
Infill pattern	Linear (0°)	X	X	X
	±45°	X	X	X
	0°-90°	X		X

The Table 3.6 describe printed conditions with a nozzle diameter of 0.4 mm and an orientation angle of the filament deposition of the linear type (0°).

Table 3.6: 3d printed specimens condition with realized with nozzle diameter of 0.4 mm and a linear orientation angle of the filament deposition (0°)

Parameter	Values	Growth orientation angle in respect of XY plane		
		0°	45°	90°
Printing speed	15 mm/s	X		
	30 mm/s	X	X	X
	45 mm/s	X		
	60 mm/s	X	X	

The Table 3.7 describe printed conditions with a printing speed of 30 mm/s and a linear orientation angle of the filament deposition (0°).

Table 3.7: 3d printed specimens condition with realized with a printing speed of 30 mm/s and a linear orientation angle of the filament deposition (0°)

Parameter	Values	Growth orientation angle in respect of XY plane		
		0°	45°	90°
Nozzle diameter	0.25 mm	X	X	X
	0.4 mm	X	X	X

Debinding

Once the printing was completed and the specimens were removed from the machine, they were cleaned up on the surface in order to make the surfaces as uniform as possible, i.e. eliminating the imprint generated by the deposited filament. This operation is carried out at this stage because the metal powder is not yet sintered and can be easily removed by smoothing the binder on the surfaces, which is quite complex once the material has undergone the last phase of the process. This operation can be carried out either through the use of a sandblasting machine or abrasive paper with different weights depending on the result to be obtained. At this point it was possible to house the specimens on the shelves of a special basket that is inserted inside the debinder and hermetically closed. Inside, the main chamber is filled with a particular fluid with the aim of dissolving the binder that keeps the powders aggregated, in order to remove as much as possible, the resin component and leave only the metal powder.

The debinding process lasts from 20 to 28 hours depending on the amount of material that is inserted into it. In fact, the basket allows you to load more parts at a time, many more than the printer can make at the same time. The debinding cycle, in fact, was carried out only once for all the tensile specimens that instead were made in different printing cycles, which is due to the difference in process parameters set for the different specimens that do not allow a single printing phase.

Sintering

Once the debinding process is over, the pieces that come out are particularly delicate for the reasons mentioned in the previous paragraph and must be handled with great care. The debinderized specimens, in fact, once the debinding was completed, were carefully removed from the basket and placed on overlapping carbon shelves and

inserted into the sintering furnace. This phase involves the consolidation of metal powders through the sintering process that takes place at a temperature of about 1400° C for a duration of about 40 hours (the actual time depends on the number of pieces that are placed inside it, calculation that is always carried out through the cloud software that manages all the processes). Once the oven is closed, taking care that the different shelves are not in contact with the resistances, the vacuum is generated inside the chamber as the sintering must take place in a controlled environment. To do this, an inert gas, in this case 97% Argon, is circulated between the different shelves. The sintering furnace is shown in (Figure 3.6) where it can be seen the carbon box where metal parts are positioned for the sintering phase.

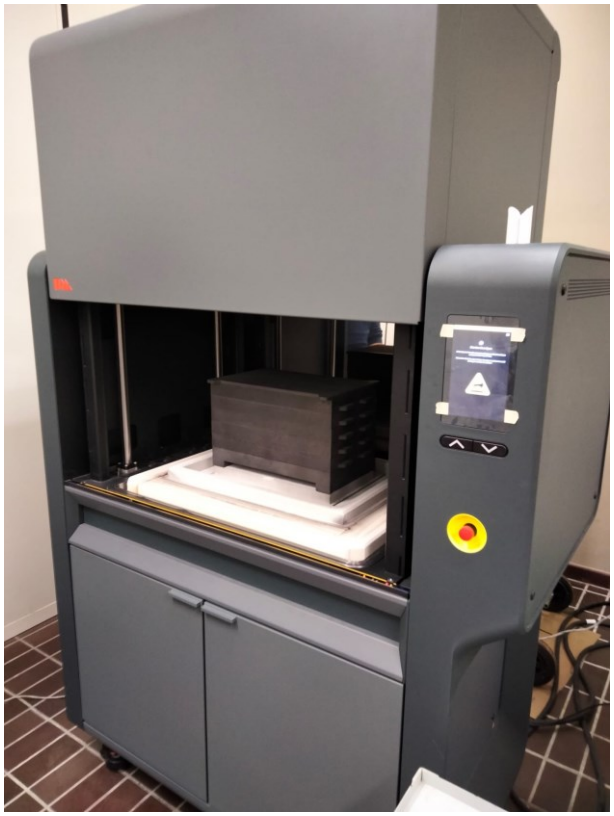

Figure 3.6: Sintering furnace

At the end of the sintering, the specimens are removed from the furnace, and they are separated from the support that had been generated during printing, a phase simplified by the prior deposition of a layer of ceramic material between model and support in order to facilitate the detachment between the two sections at the end of sintering.

3.4 Heat treatment

Specimens were tested right afterwards the sintering cycle (as sintered) or subjected to a heat treatment in order to improve their mechanical properties (aged). In particular, an aging treatment was carried out in accordance with the ASTM B883 standard; the tensile specimens were heated up to 482 °C, kept constant for 1 hour and then air-cooled (H900 aging process). The treatment was carried out through the muffle furnace FM 13 by FALC Instruments. Only few conditions were subjected to aging.

In particular, the specimens subjected to H900 heat treatment were printed with the three growth orientation angles (0°, 45° and 90°), with same nozzle diameters (0.4 mm), with same liner infill pattern (0°) and with the same printing speed (30 mm/s).

3.5 Tensile tests

The specimens, made according to the conditions described in the previous chapters, were subjected to the tensile test (Figure 3.7). With the aid of an MTS 810 universal testing machine, whose test conditions are always in accordance with the ASTM E8 standard, once numbered and measured the samples were properly positioned between the jaws of the machine setting a crosshead travel speed of 0.1 mm/s. The data acquisition took place through both an LVDT with which the machine is equipped, and with a single-axis strain gauge positioned directly on the specimen.

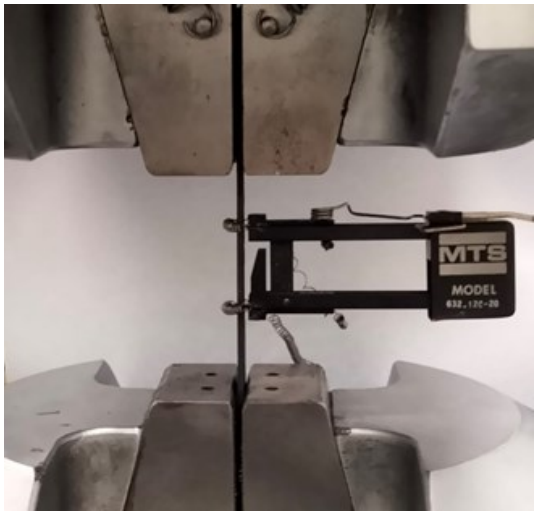

Figure 3.7: Clamped specimen for the tensile test with the single-axis extensometer

The acquired data were then processed to be able to make the different comparisons and evaluate which configuration guarantees the best results in terms of mechanical resistance.

3.6 Scanning Electron Microscope (SEM) and Energy-Dispersive X-ray (EDX) spectroscopy

The specimens in 17-4 PH were observed using the ZEISS Supra 40 scanning electron microscopes. Specifically, sections parallel to the external surfaces of the specimens made in the three different growth orientations angles (0°, 45° and 90°) were analysed. In addition, in order to get information on the constituent elements, Energy Dispersive X-ray (EDX) analysis was carried out on some particular areas by the same scanning electron microscope coupled with a Bruker Quantax serie 5000L N2-free XFlash.

3.7 Spectrophotometry and optical microscope investigation

A spectrophotometry analysis was carried out using the Spark Analyzer Spectrolab tool in order to evaluate the constituent elements of 17-4 PH material once sintering phase has taken place. In order to observe the fracture surfaces of specimens deformed under tension loads, a Leica EZ 4D stereomicroscope was used at different magnification levels.

3.8 Life Cycle Assessment

The environmental evaluation of the samples was conducted following the standardized methodology of Life Cycle Assessment. LCA is composed of four iterative phases:

1. Goal and scope definition, in which the objectives, the Functional Unit (FU) and the system boundaries are clearly defined;
2. Life Cycle Inventory (LCI), consists in the collection of data regarding all inputs and outputs of the system boundaries;
3. Life Cycle Impact Assessment (LCIA), in which LCI data are converted into possible environmental damages in terms of different impact categories;
4. Result interpretation, in which the results are critically reviewed, consistency check is made and final recommendation are proposed.

The LCIA was carried out using SimaPro 9.1.0.11 software and the Ecoinvent 3.1 commercial database. 3.1. Goal and Scope definition.

3.8.1 Goal and Scope definition

The objective of this LCA is to evaluate and compare the environmental impacts related to the production and postprocessing of tensile specimens using the BMD technology. Two possible scenarios were considered:

- Scenario 1: sample as sintered

- Scenario 2: heat-treated sample (aged)

The functional unit can be defined as “the production of a 17-4 PH stainless steel tensile specimen by means of the BMD technology with dimensions defined by the ASTM E8 standard and a final weight of 40.6 g”.

The present work is defined as a “cradle to grave” analysis as impacts from the extraction of raw materials to the final disposal of the printed samples are considered within the system boundaries. More specifically, the following processes were included in the analysis:

- Input materials: includes the atomization of the metal powder, the production of the binder and the ceramic interface material, the extrusion of the rods.
- 3D printing considers the energy consumption of the printer and the production of the building plate (raw material and plastic sheet extrusion).
- Debinding: takes into account the electrical energy consumption and the organic solvent production.
- Sintering: includes the furnace energy consumption and inert gas production.
- Heat treatment (only for Scenario 2): considers the energy consumption of the muffle furnace used for aging. This phase represents the only difference in terms of environmental impacts between the two scenarios.
- End of Life (EoL) of the specimens considering steel recycling and of the solvent considering incineration.

Steel recycling is credited as an avoided burden related to pig iron production. Transport via road or ship has been considered for each material input. Impacts related to the machines production (i.e. printer, debinder, furnace and muffle furnace) were not included within the system boundaries as they would have been negligible with respect to the others production phases, as proved in previous literature studies [36].

3.8.2 Life Cycle Inventory

Inventory data were retrieved from direct measurements, scientific literature research and the Ecoinvent commercial database. A cut off mass of 2 g has been applied. reports all the relevant inventory data used in the LCA analysis.

Table 3.8: Inventory data

Input Materials		**Quantity**
Specimen finale weight		40.6 g
Bound metal rods		106.3g
Stainless steel		102.1 g
Ceramic interface		1.54 g
Binder		4.2 g
Organic solvent		14.6 g
Inert gas		250 g
Building plate		45 g
Electric energy consumption (per part)		
Gas atomisation		0.08 kWh
Printing		4.48 kWh
Debinding		0.14 kWh
Sintering		3.57 kWh
Heat treatment		0.45 kWh
Transportation		
Raw materials	Transoceanic	11000 km
	Truck 16 – 35 ton	150 km
Input	**Ecoinvent dataset**	
Organic solvent	Solvent, organic	
Steel powder	Steel, chromium steel 18/8	
Inert gas	Argon, liquid	
Binder	Polyethylene, high density, granulate	
Building plate	Polypropylene, granulate	

More in detail:

- Environmental impacts related to raw materials (steel, inert gasses, polymers and chemicals) have been retrieved from the Ecoinvent 3.1 database.
- The energy consumption of the steel atomization process was estimated on the basis [37].
- The exact quantity of each material used during the printing process (metal rods and ceramic interface) was automatically calculated by the software used for the 3d printing job preparation. The percentage of binder in the metal rods was calculated considering the weight loss of the component during the debinding and sintering phases.
- All electric energy consumptions were directly measured by means of a power analyser. The use phase impacts of each machine were divided by the number of specimens processed simultaneously.
- The building plate is made of ITW Formex®, a flame-resistant polypropylene. Its weight was directly measured. It was considered that up to 10 specimens can be printed using the same plate.
- The consumption of inert gas was directly measured.
- The organic solvent consumption was estimated on the basis of a study by Raoufi et al [38] evaluates the environmental impacts of a Metal Injection moulding production process. The spent solvent was considered to be incinerated; the Ecoinvent process for spent solvent mixture incineration was utilized.
- Transport distance of raw materials was estimated considering the geographic location of the suppliers; impacts related to trucks and ships transport were obtained from the Ecoinvent database.

3.8.3 Life Cycle Impact Assessment

The environmental effects of the two scenarios were quantified using three different impact assessment methods chosen among the most relevant ones employed in literature research [39–41]. Cumulative Energy Demand (CED), Global Warming Potential (GWP) and ReCipe Midpoint impact indicators were considered. CED quantifies all the energy consumptions (both renewable and non-renewable) associated with each scenario and it is expressed in MJ. GWP provides an assessment of the possible effects on climate change of each production system, and it is expressed in kg CO2eq. The methodology proposed by the IPCC (International Panel

on Climate Change) was used considering a time horizon of 100 years. The ReCiPe method provides a comprehensive view of the environmental impacts of a system in terms of 18 midpoint categories representing specific effects (i.e. ozone depletion and human carcinogenic toxicity).

Chapter 4

4 Results and discussion

The mechanical behaviour of 3D printed specimens in 17-4 PH stainless steel was investigated by means of uniaxial tensile tests, according to ASTM E8/E8M and BS EN 895. Figure 4.1 shows typical tensile samples, printed at a build-up orientation angle of 0°, after the sintering phase.

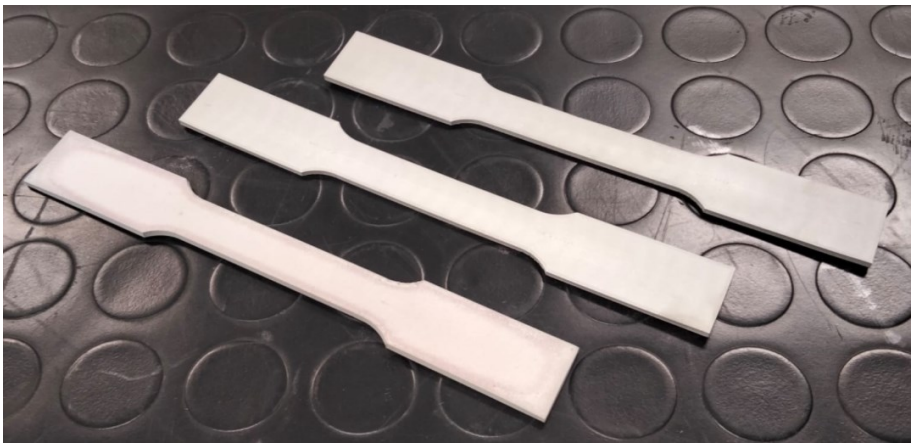

Figure 4.1: Typical tensile sample obtained using the BMD process after the sintering phase

The spectrometry analysis shown in Table 3 shows the percentage composition of the elements present within the 17-4 PH after the sintering phase.

All the percentage values of 17-4 PH BMD specimens are in the range of given reference values reported in Desktop Metal technical datasheet, except for copper which is below the reported threshold. Despite silicon concentration is not reported in reference values, it was found significantly higher in the BMD than in a wrought 17-4 PH [42]. Since it has high mobility and a greater affinity to oxygen among the other alloying elements, higher concentrations of silicon are typical for stainless

steels powders to prevent the formation of other more detrimental oxides during the water atomization process.

Table 4.1: Chemical composition of 17-4 PH BMD compared to Desktop Metal reference values

	% C	% Si	% Mn	% Cr	% Ni	% Al	% Cu	% Nb+Ta
17-4 PH BMD	0.03	2.09	0.45	16.9	4.62	0.01	1.71	//
Desktop Metal reference values	0.07 (max)	// [1]	< 1.0	15.5 - 17.5	3 - 5	// [1]	3 - 5	0.15 – 0.45

[1] Not reported

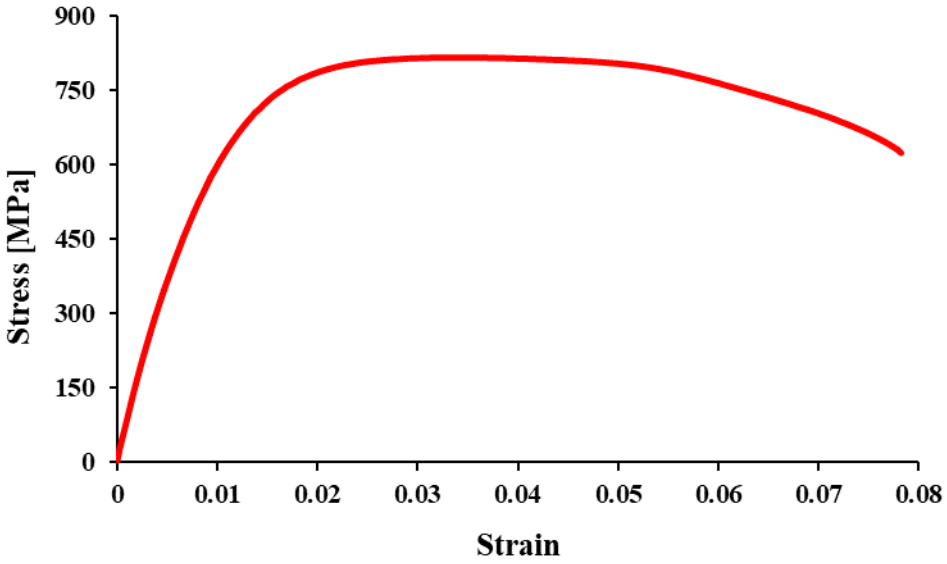

Figure 4.2: Typical tensile stress vs. tensile strain curve of tensile specimen realized with BMD technology in 17-4 PH with 0° orientation angle, 0.4 mm nozzle diameter, printing speed of 30 mm/s and a linear infill pattern

Figure 4.2 shows typical tensile stress vs. tensile strain curves of the 3D printed samples in 17-4 PH as a function of the build-up orientation angle. Irrespective of the build-up orientation angle, in the elastic region, the tensile stress linearly rises with strain until yielding; then, the stress value increases with a non-linear behaviour up to a peak value corresponding to the onset of necking. The samples exhibit a significant post-necking deformation, denoting a good deformability in the necking region. Finally, after necking, the stress exhibits an appreciable decrease with a further increase in strain until failure.

Effect of the growth orientation angle

In Figure 4.3 main stress vs. strain curves of tensile specimens realized with different growth orientation angles (0°, 45°, 90°), same nozzle diameter of 0.4 mm, same printing speed of 30 mm/s and same linear (0°) infill pattern are reported.

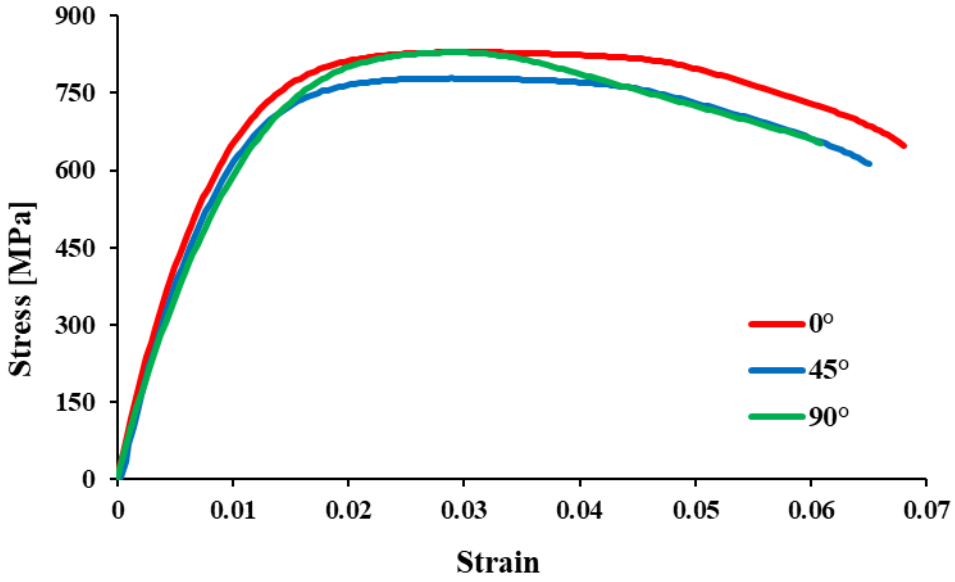

Figure 4.3: Mean tensile stress vs. tensile strain curves comparison of tensile specimens realized with different growth orientation angles (0°, 45°, 90°), nozzle diameter of 0.4 mm, printing speed of 30 mm/s and a linear (0°) infill pattern

Table 4.2: Main tensile properties of 17-4 PH realized with different growth orientation angles, linear infill pattern (0°), nozzle diameter of 0.4 mm and a printing speed of 30 mm/s

Linear infill pattern **Nozzle diameter 0.4 mm** **Printing speed of 30 mm/s**		Ultimate tensile strength [MPa]	Elongation at break	Young's Modulus [GPa]	Yeld Strength [MPa]
Growth orientation angles	0°	828.9 ± 4.2	0.068 ± 0.0005	181.3 ± 3.9	668.1 ± 10.4
	45°	778.4 ± 8.0	0.065 ± 0.006	162.1 ± 1.6	611.3 ± 5.0
	90°	828.7 ± 1.9	0.061 ± 0.0004	177.0 ± 1.3	655.4 ± 1.8

Table 4.2 summarizes the mean values of yield strength, ultimate tensile strength, ultimate elongation to failure, and Young's modulus obtained by means of tensile tests performed on samples at different build-up orientation angles. It can be observed that the samples printed using the build-up orientation angle of 0 and 90° are characterized by mechanical properties in agreement with those reported in the MPIF Standard 35 (Table 3.1). On the other hand, the configuration at 45° does not exhibit values similar to those reported in the standard. In fact, it can be observed that samples printed at a build-up orientation angle of 0° and 90° are characterized by similar values of Young's Modulus, yield strength, and ultimate tensile strength, even though the sample printed at 90° exhibits a lower ductility than the one obtained at 0°, with a reduction in ultimate elongation of about 10.5%. The samples printed at the build-up orientation growth angle of 45° are characterized by the lowest mechanical properties, with a decrease in ultimate tensile strength and Young's modulus values of about 7.3%, and in ultimate elongation of about 4.3% with respect the configuration at 0°.

Effect of the infill pattern

The same considerations can also be made for specimens realized with the infill pattern at ±45°, keeping constant nozzle diameter at 0.4 mm and printing speed of 30 mm/s.

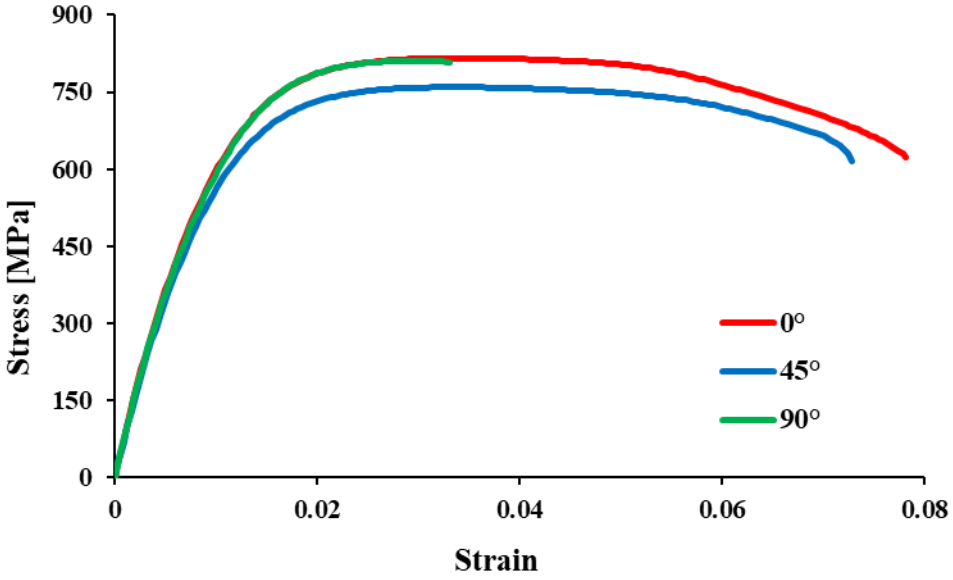

Figure 4.4: Mean tensile stress vs. tensile strain curves of tensile specimens realized at different growth orientation angles, with infill pattern of ±45°, nozzle diameter of 0.4 mm and printing speed of 30 mm/s

In fact, as shown in Figure 4.4 and confirmed by the Table 4.3, also in this case the growth orientation angles of 0° and 90° exhibit the ultimate tensile strength higher than that of 45° of 7.3% and 6.7% respectively.

Table 4.3: Main tensile properties of 17-4 PH realized with different growth orientation angles with an infill pattern of ±45°, nozzle diameter of 0.4 mm and printing speed of 30 mm/s

Infill pattern ±45° **Nozzle diameter 0.4 mm** **Printing speed of 30 mm/s**		Ultimate tensile strength [MPa]	Elongation at break	Young's Modulus [GPa]	Yeld Strength [MPa]
Growth orientation angles	0°	815.8 ± 2.5	0.078 ± 0.003	163.6 ± 4.5	635.6 ± 6.5
	45°	759.2 ± 3.0	0.073 ± 0.005	143.3 ± 2.7	604.8 ± 9.4
	90°	810.6 ± 4.5	0.033 ± 0.006	170.1 ± 4.4	652.7 ± 14.6

The same is true for the value of Young's modulus, which is greater for the growth orientation angles of 0° and 90° by 14.1% and 18.6% respectively, and the yield strength which is greater of 5.1% and 7.5% respectively. The only consideration that should be mentioned is the elongation at break for 90° which reaches values that are not even half of those relating to 0° and 45°. As can be seen from the table, in fact, the elongation at break values are of the order of 3.5%, while the other growth orientation angles reach values even close to 8%.

If specimens realized with an infill pattern of 0°-90° are taken into account, they shown the same behavior on the elongation at break as those realized of the specimens with growth orientation angle of 90° with infill pattern of ±45°. In fact, as mean tensile stress vs. tensile strain curves reported in Figure 4.5 show, the deformation at break is much lower than the specimens made with a growth orientation angle of 0°.

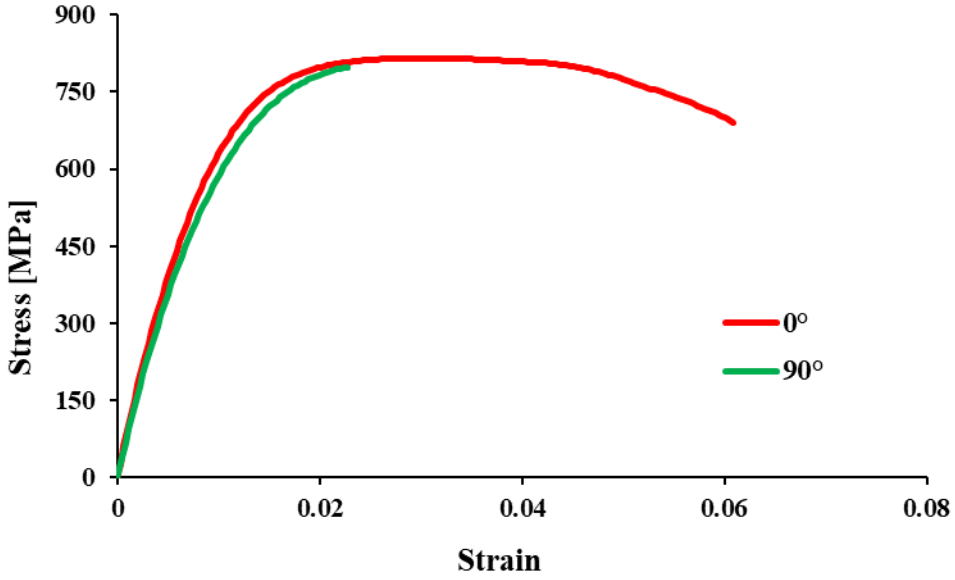

Figure 4.5: Mean tensile stress vs. tensile strain curves of tensile specimens realized at different growth orientation angles, with infill pattern of 0°-90°, nozzle diameter of 0.4 mm and printing speed of 30 mm/s

The values are shown in theTable 4.4, where it can be seen that the elongation at break has a considerably lower value that corresponds to about a third of its equivalent at 0°.

Table 4.4: Main tensile properties of 17-4 PH realized with different growth orientation angles with an infill pattern of 0°-90°, nozzle diameter of 0.4 mm and printing speed of 30 mm/s

Infill pattern 0°-90° **Nozzle diameter 0.4 mm** **Printing speed of 30 mm/s**		Ultimate tensile strength [MPa]	Elongation at break	Young's Modulus [GPa]	Yeld Strength [MPa]
Growth orientation angles	0°	815.0 ± 16.7	0.061 ± 0.002	160.3 ± 1.6	655.7 ± 8.6
	90°	797.9 ± 15.8	0.023 ± 0.003	147.2 ± 4.6	608.6 ± 6.9

A different consideration must be done for other tensile mechanical properties which, although lower for growth orientation angle of 90° parameter, do not show such a marked difference. In fact, the values for UTS, Young's modulus and Yield strength are respectively 2.1%, 8.2% and 7.2% lower. In order to compare how the infill pattern affects the tensile mechanical properties, Figure 4.6, Figure 4.7 and Figure 4.8, in which mean curves related to the three types of infill pattern studied are reported, show the differences in respect of the same growth orientation angles.

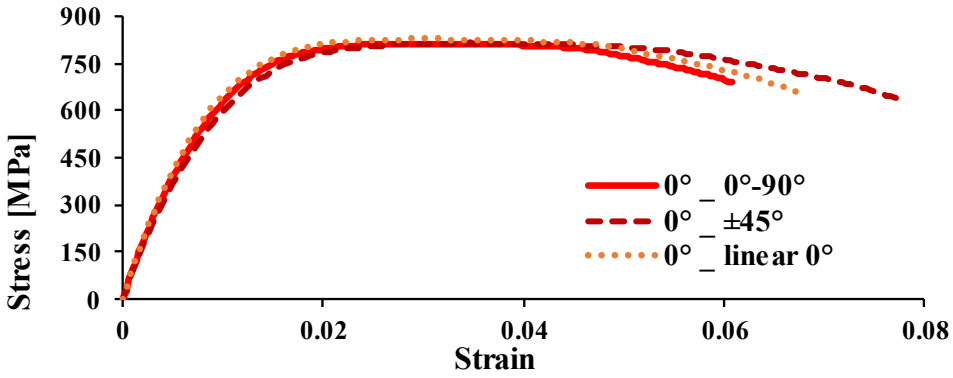

Figure 4.6: mean stress vs. strain curves of specimens realized with different infill pattern, with growth orientation angle of 0°, nozzle diameter of 0.4 mm and printing speed of 30 mm/s

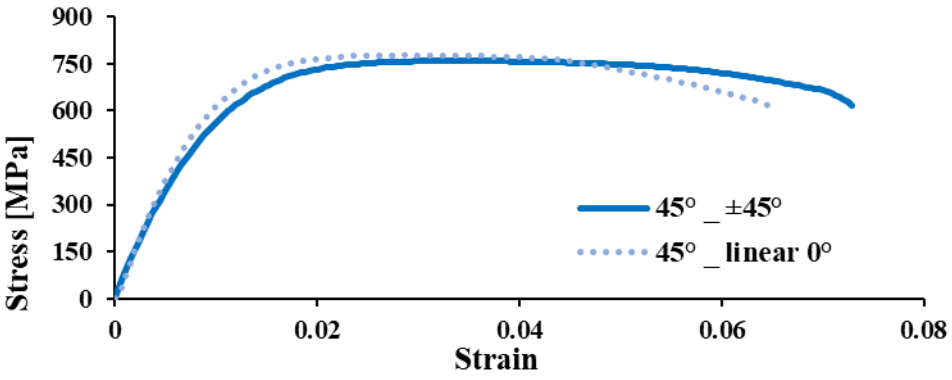

Figure 4.7: mean stress vs. strain curves of specimens realized with different infill pattern, with growth orientation angle of 0°, nozzle diameter of 0.4 mm and printing speed of 30 mm/s

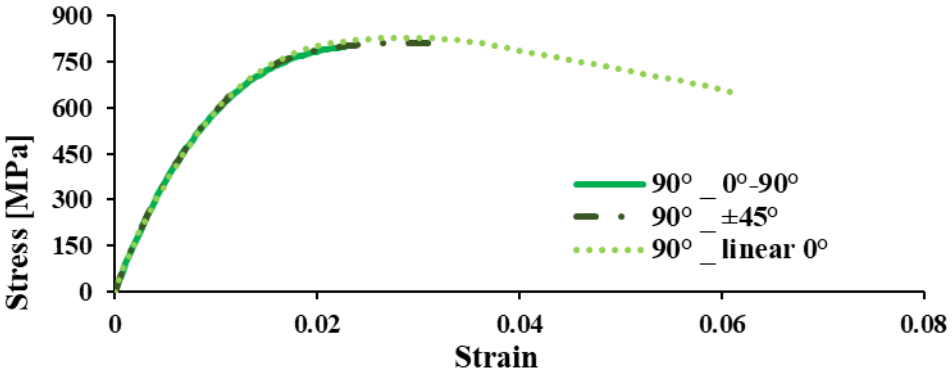

Figure 4.8: mean stress vs. strain curves of specimens realized with different infill pattern, with growth orientation angle of 0°, nozzle diameter of 0.4 mm and printing speed of 30 mm/s

The considerations to be made for all three growth orientation angles mainly concern the fact that, although minimal, there is a slight decrease in ultimate tensile strength and yield strength for configurations with infill patterns of ±45° and 0°-90° compared to the linear one at 0°, while is a little more evident the decrease in Young's modulus. For the elongation at break, as already mentioned above, the reduction of ductility due to the infill pattern different from the linear one for specimens made with a growth orientation angle of 90° is remarkable. These results are in accordance with the research of by Dudescu et al. in [43] that reports the effects of raster orientation, infill rate and infill pattern on the mechanical properties of 3d printed

materials. In particular, they found that a linear (0°) infill pattern ensures better mechanical performance than patterns ±45° and 0°-90° for material extrusion 3D printing.

Effect of the printing speed

Below are presented the results of the tensile tests carried out on the specimens realized at different printing speeds, with the same growth orientation angle of 0° and 45°, the same nozzle diameter of 0.4 mm and the same type of linear infill pattern 0°. In the Figure 4.9 graph it is possible to observe the mean tensile stress vs. strain curves related to specimens realized at different printing speeds.

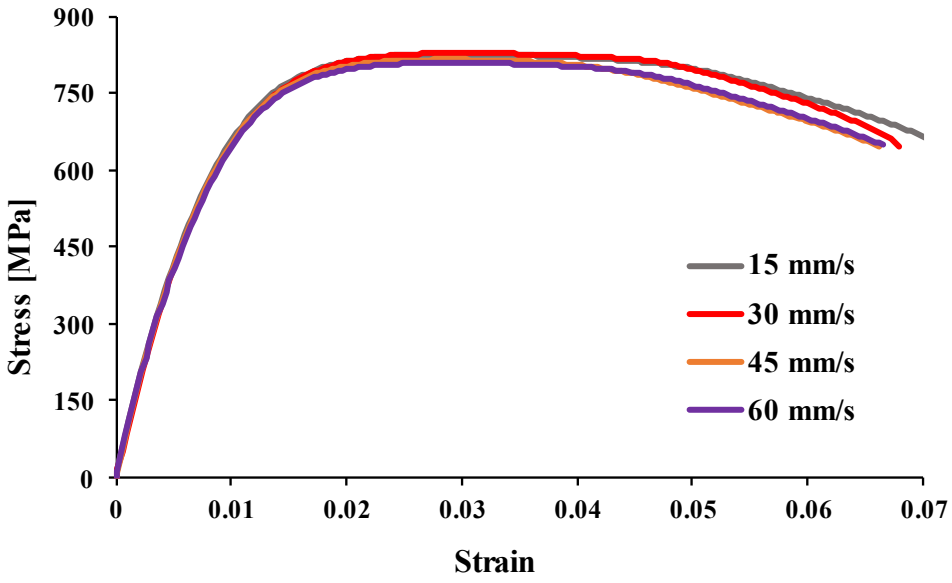

Figure 4.9: Mean tensile stress vs. strain curves of specimens realized at different printing speed, with a linear infill pattern of 0°, nozzle diameter of 0.4 mm and a growth orientation angle of 0°

It can be noted that the influence of the printing speed is minimal on the main tensile mechanical properties of the 17-4 PH. In fact, as reported in the Table 4.5, the values shown are very similar to each other for the different categories.

Table 4.5: Main tensile properties of 17-4 PH realized at different printing speed, with a linear infill pattern of 0°, nozzle diameter of 0.4 mm and a growth orientation angle of 0°

Linear infill pattern **Nozzle diameter 0.4 mm** **Growth orientation angle 0°**		Ultimate tensile strength [MPa]	Elongation at break	Young's Modulus [GPa]	Yeld Strength [MPa]
Printing speed	15 mm/s	826.9 ± 0.1	0.071 ± 0.009	179.9 ± 3.4	661.8 ± 0.6
	30 mm/s	825.8 ± 3.2	0.069 ± 0.002	181.3 ± 0.7	666.6 ± 4.3
	45 mm/s	816.1 ± 3.0	0.066 ± 0.003	172.3 ± 0.4	658.9 ± 6.0
	60 mm/s	810.1 ± 4.1	0.067 ± 0.001	172.6 ± 0.8	657.3 ± 4.1

The only observation that can be done is that there is a very slight tendency to decrease as the printing speed increases from 15 mm/s to 60 mm/s. In fact, it is a very small difference, which is estimated at around 1% for the UTS and for the Yield strength, while it is slightly more marked for the Young modulus (4%). The Figure 4.10 shows a magnification of the figure in the area of maximum tensile voltage and has been reported precisely to show this slight decreasing trend.

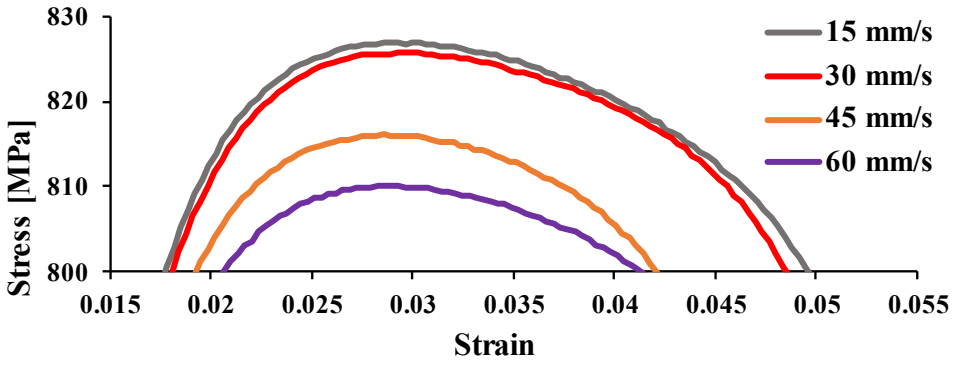

Figure 4.10: UTS differences between specimens realized with different printing speed

The confirmation of this observation can be found in the figure in which the average tensile stress vs. strain tensile curves of specimens made with speeds of 30 mm/s and 60 mm/s are depicted, keeping constant the growth orientation angle of 45°, the diameter of the nozzle of 0.4 mm and the linear infill pattern at 0°.

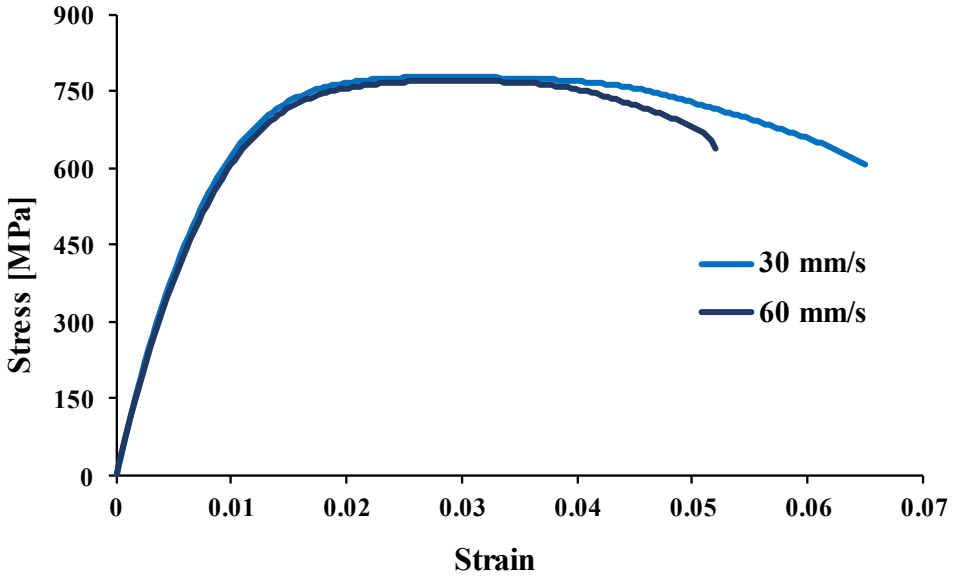

Figure 4.11: Mean tensile stress vs. strain curves of specimens realized at different printing speed, with a linear infill pattern of 0°, nozzle diameter of 0.4 mm and a growth orientation angle of 45°

As can also be seen from the Table 4.6, in fact, it appears that, even if the differences between the two curves are minimal, that relating to the printing speed of 30 mm/s is still higher than that relating to the speed of 60 mm/s.

Table 4.6: Main tensile properties of 17-4 PH realized at different printing speed, with a linear infill pattern of 0°, nozzle diameter of 0.4 mm and a growth orientation angle of 0°

Linear infill pattern **Nozzle diameter 0.4 mm** **Growth orientation angle 45°**		Ultimate tensile strength [MPa]	Elongation at break	Young's Modulus [GPa]	Yeld Strength [MPa]
Printing speed	30 mm/s	778.4 ± 4.7	0.0651 ± 0.006	162.1 ± 4.5	611.3 ± 5.0
	60 mm/s	770.8 ± 1.8	0.0521 ± 0.003	155.3 ± 6.1	619.8 ± 4.2

Assuming as a hypothesis that the minimum difference in mechanical performance presented by 17-4 PH to the variation of the printing speed is such as not to be appreciable, it was possible to evaluate the productivity of this technology in this way, considering the production of a finite number of tensile specimens. Considering that this type of technology is characterized by a time for generating parts proportional to the number of parts to be printed and knowing the actual times for printing in a single cycle of 1, 2 and 3 tensile specimens, it was possible to deduce the time needed to realize a greater number for each cycle. In the Table 4.7 printing times for the realization of 1, 2 and 3 specimens per printing session were reported.

Table 4.7: Printing time for the realization of specimens in 17-4 PH at different printing speed, with a linear infill pattern of 0°, nozzle diameter of 0.4 mm and a growth orientation angle of 0°

Linear infill pattern **Nozzle diameter 0.4 mm** **Growth orientation angle 45°**		Specimens printing time for every session [h]		
		1	2	3
Printing speed	15 mm/s	7.45	12.82	18.17
	30 mm/s	5.87	9.65	13.42
	45 mm/s	5.37	8.65	11.93
	60 mm/s	5.15	8.22	11.27

The graph in Figure 4.12 shows the print speed curves vs. the number of specimens obtained by keeping constant the parameters of the growth orientation angle of 0°, the linear infill pattern of 0°, and the nozzle diameter with different printing speed. Examining the graph, as the printing speed increases, printing times decrease proportionally and decrease proportionally even increasing the number of printed parts. Specifically, it can also be observed that to realize n° 3 tensile specimens at a speed of 15 mm/s the printing system takes about 17 hours, time that corresponds approximately to that needed for the realization of n° 5 tensile specimens at a speed of 60 mm/s, and the time needed to realize n° 2 specimens at 15 mm/s is the same for printing n° 3 specimens at 30 mm/s.

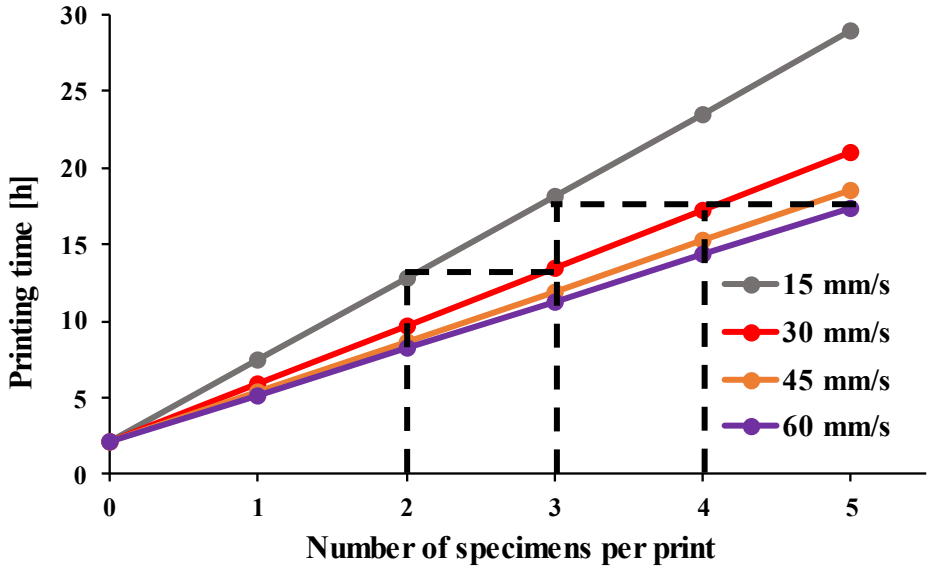

Figure 4.12: Printing time vs. number of printed pieces curves for each printing speed

If the evaluation of the mechanical performance did not reveal appreciable differences with the variation of the printing speed, the same cannot be said for the quality of the pieces made. In fact, observing the subsequent images, it is possible to notice how an increase in printing speed leads to a reduction in the quality of the parts, especially on the realization of aesthetic details that, at higher speeds, are much more evident than at low construction speeds. Figure 4.13 showing how the wabble effect is much more marked for specimens made at higher speeds.

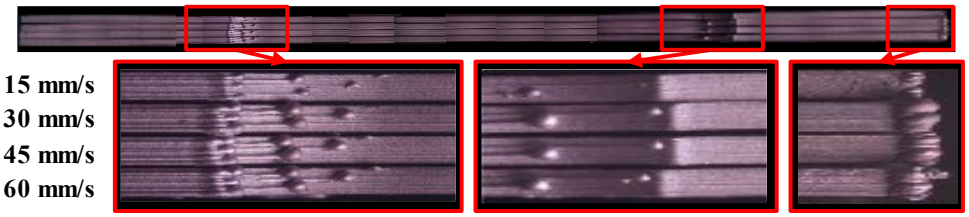

Figure 4.13: Lateral view of specimens realized at different printing speed

The Figure 4.14 instead represents the upper view of the same specimens shown in the previous figure. In this case, the points that most highlight the decrease in the aesthetic quality of the specimens are those in which the beginning and end of the deposition section takes place.

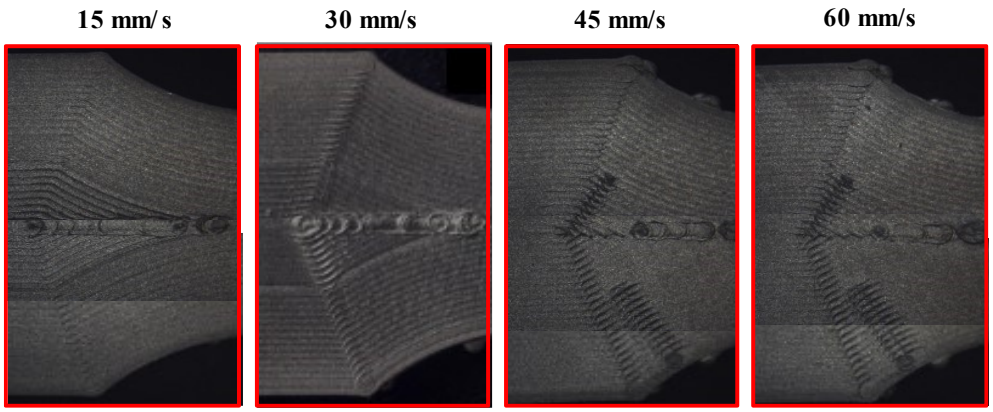

Figure 4.14: Front view of tensile specimens realized at different printing speed for the evaluation of the aesthetical printing quality

The reduced speed of 15 mm/s allows to obtain a quality of these points not even comparable with that obtained at greater speeds. For speeds of 45 mm/s and 60 mm/s, other signs of deposition also appear in the area near the fitting, which however contribute to reinforcing the concept that a higher printing speed certainly reduces production times, but also reduces the quality of printing.

Effect of the nozzle diameter

This study also made it possible to evaluate the effect of the diameter of the printing nozzle for the realization of the tensile specimens on mechanical performance. As done for the previously analyzed parameters, also in this case the mean tensile stress vs. strain tensile curves are reported, relative to tensile specimens realized through the use of a 0.25 mm diameter nozzle, keeping the other process parameters constant, namely growth orientation angle of 0°, linear infill pattern of 0° and printing speed of 30 mm/s.

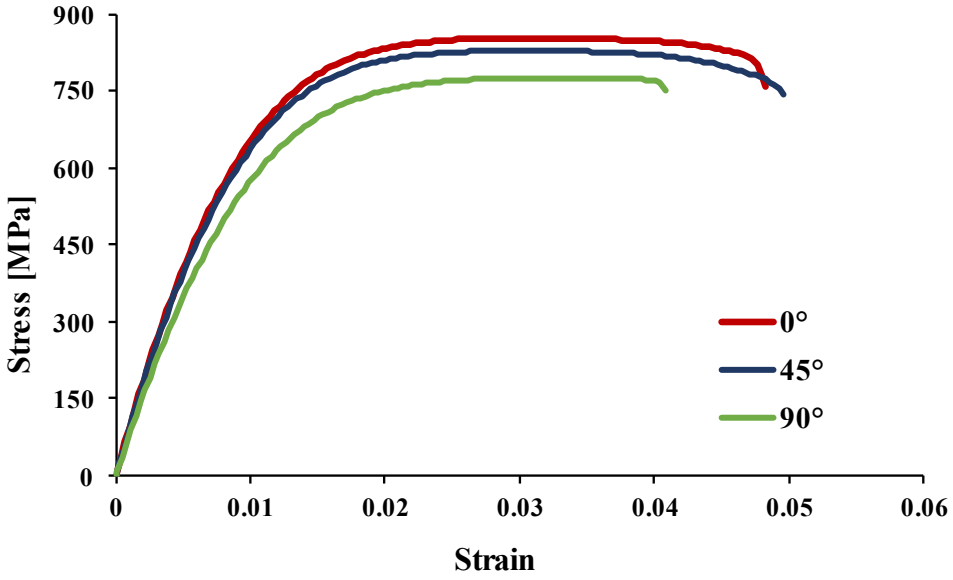

Figure 4.15: Mean tensile stress vs. tensile strain curves of specimens realized at different growth orientation angle, with a linear infill pattern of 0°, nozzle diameter of 0.25 mm and a printing speed of 30 mm/s

From the Figure 4.15 and from the Table 4.8 below, where the average values of the detected tensile mechanical properties are shown, it can be observed that the use of a nozzle with a diameter of 0.25 mm, instead of one of 0.4 mm, has left unchanged the results obtained for the tensile specimens with a growth orientation angle of 0°, while led to a reversal trend for specimens with a growth orientation angles of 45° and 90°. In fact, while in the case of the 0.4 mm nozzle, the specimens that had worse performance were those inclined by 45° compared to those at 90°, it is the opposite in this case. In particular, tensile specimens with a growth orientation angle of 45° showed performances close to 0° ones, with UTS, Young's modulus and Yield strength values only 2.9%, 7.3% and 7.1% lower respectively. This behavior can be attributed to the fact that, by decreasing the size of the nozzle, the level of quality of the material deposition increases, thus generating a better uniformity of the layer and consequently reducing the voids that are generated with a larger diameter nozzle. This favors a better adhesion of the powders during the sintering phase which allows to increase the density of the part made.

Table 4.8: Main tensile properties of 17-4 PH realized with different growth orientation angles with an infill pattern of 0°, nozzle diameter of 0.25 mm and printing speed of 30 mm/s

Infill pattern 0° **Nozzle diameter 0.25 mm** **Printing speed of 30 mm/s**		Ultimate tensile strength [MPa]	Elongation at break	Young's Modulus [GPa]	Yeld Strength [MPa]
Growth orientation angles	0°	854.4 ± 27.5	0.048 ± 0.002	184.4 ± 6.3	717.1 ± 28.7
	45°	829.6 ± 8.4	0.049 ± 0.001	171.1 ± 7.7	666.8 ± 9.1
	90°	773.4 ± 3.1	0.037 ± 0.002	184.8 ± 5.9	595.4 ± 7.3

As for the specimens made with growth orientation angle of 90°, they showed an average trend much lower than those oriented to 0° with regard to UTS and Yield strength (9.5% and 17% respectively), while the Young's modulus the same. This result is instead in agreement with several studies of the scientific literature such as those of Triyono et al. and Chacón et al. [44,45].

A further observation, however, must be made on the basis of the elongation at break. The Figure 4.16 compares the average curves of the specimens realized with nozzles of diameter 0.4 mm and 0.25 mm, with the same growth orientation angle of 0°, 45° and 90°, the same linear infill pattern and the same printing speed of 30 mm/s.

This is evident, even from the values shown in Table 4.8 that in all three cases there is a clear reduction in elongation at break, which denotes a substantial reduction in the ductility of the samples. In fact, it can be noted that for growth orientation angles of 0°, 45° and 90° the reduction of deformation at break is equal to 28.9%, 23.8% and 38.5%. This result is in agreement with what is reported by Chacón et al. [45], who report a graph in which it is evident that the reduction of the diameter of the nozzle involves a reduction of deformation at break, even if with values very close to a few tenths of a percent. In this case, however, the variation is much more marked, as it goes from strain values equal to 6.8%, 6.5% and 6.1% respectively to values 4.8%, 4.9% and 3.7%.

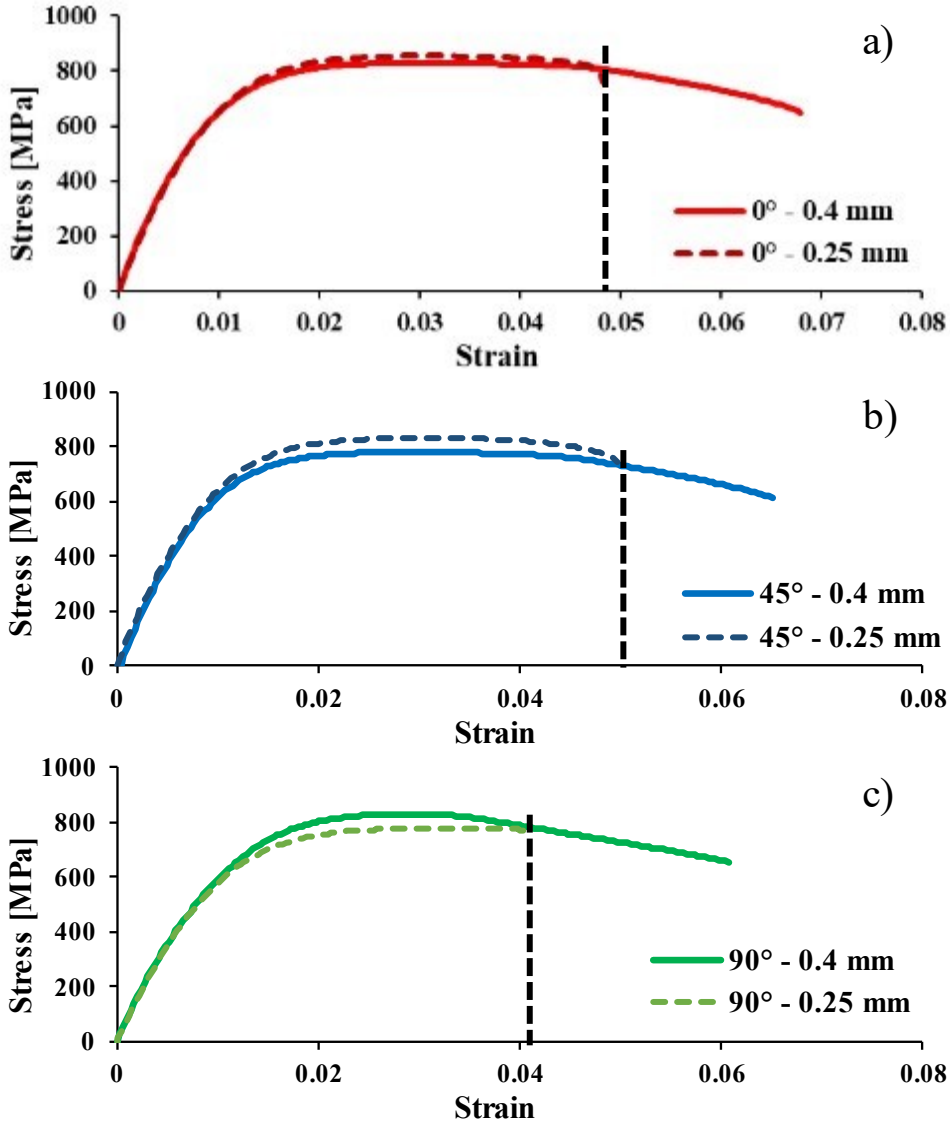

Figure 4.16: Mean tensile stress vs. tensile strain curves of specimens realized with printing speed of 30 mm/s, linear infill pattern of 0°, nozzle diameter of 0.25 and 0.4 mm and growth orientation angle of 0° (a), 45° (b) and 90° (c)

Effect of heat treatments

Specimens subjected to H900 heat treatment were printed with the three growth orientation angles (45° and 90°), with same liner infill pattern (0°) and with the same printing speed (30 mm/s). For the 0° oriented specimens' configuration both the 0.25 mm and 0.4 mm nozzle diameters used.

Table 4.9: Tensile properties of specimens H900 heat treated with different growth orientation angles, a linear infill pattern of 0°, nozzle diameter of 0.4 mm and printing speed of 30 mm/s

Infill pattern 0° **Nozzle diameter 0.4 mm** **Printing speed of 30 mm/s**		Ultimate tensile strength [MPa]	Elongation at break	Young's Modulus [GPa]	Yeld Strength [MPa]
H900 Growth orientation angles	0°	1129.0 ± 12.6	0.022 ± 0.004	188.2 ± 6.2	1019.5 ± 13.9
	45°	1103.2 ± 9.8	0.023 ± 0.003	140.7 ± 5.4	1004.8 ± 15.8
	90°	1163.5 ± 14.2	0.024 ± 0.003	186.7 ± 6.5	1055.6 ± 10.1

Table 4.9 reports tensile properties from which it can be deduces that this kind of heat treatment increase in a remarkable way the properties UTS and Yield Strength. The values of UTS and Yield strength reported, in fact, are considerably higher than those relating to the same category of specimens that have not undergone heat treatment as they are greater respectively by 36.2%, 41.7% and 40.4% for UTS and 52.6%, 64.4% and 61.1% for Yield strength. Different speech for the Young's modulus, that remains almost unchanged, and the elongation at break. In particular, comparing values from Table 4.9 and Table 4.2 regarding the elongation at break, the latter undergoes an important decrease, confirming a clear increase in the fragility of the material after heat treatment. The validation is also reported in the figures that show, for each growth orientation angles of 0°, 45°, and 90°, the average curves of the specimens as sintered and heat treated.

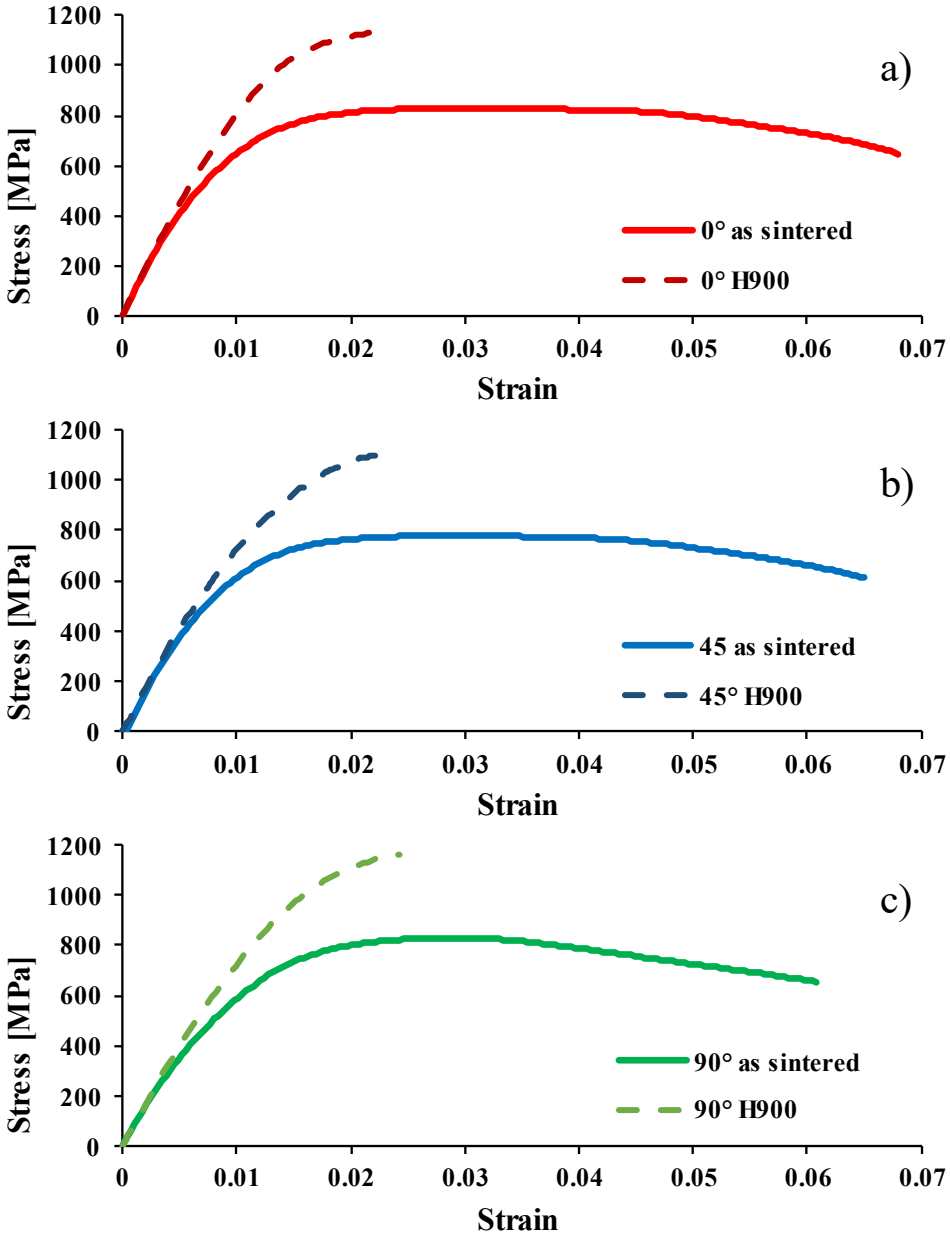

Figure 4.17: Mean tensile stress vs. tensile strain curves of as sintered and heat treated specimens realized with a linear infill pattern, nozzle diameter of 0.4 mm, a printing speed of 30 mm/s and at different growth orientation angle of 0°(a), 45° (b) and 90° (c)

Finally, the average curves relating to the as sintered and heat-treated specimens made with the 0.25 diameter nozzle are shown in the figure. The results of the tests in question were then used for the realization of an LCA analysis relating to the production of tensile specimens using BMD technology.

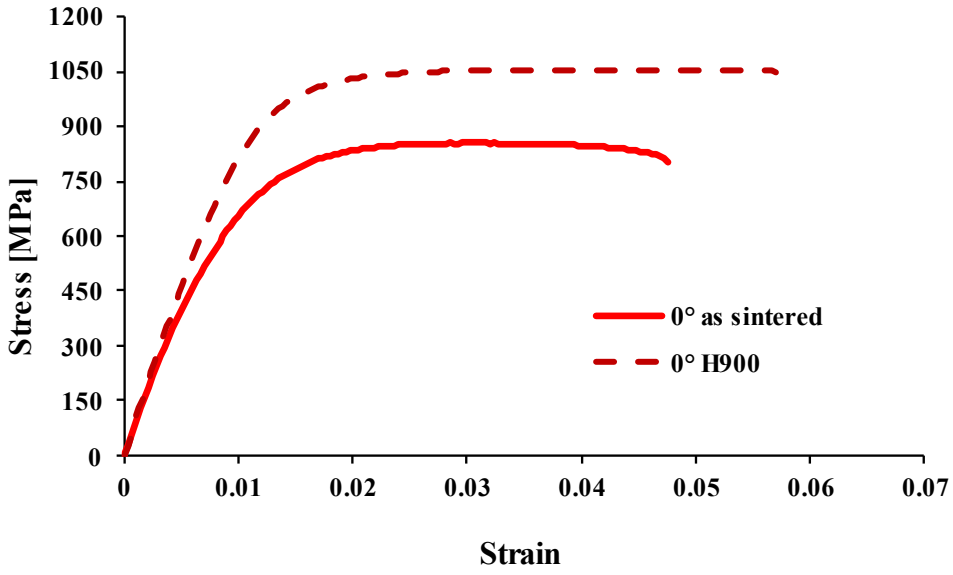

Figure 4.18: Mean stress vs. strain curves of as sintered and heat-treated specimen realized with linear infill pattern, nozzle diameter of 0.25 mm, printing sped of 30 mm/s and growth orientation angle of 0°

SEM, EDX and optical investigation analysis

In Table 4.10, the values of the atomic percentages of the elements that make up a second phase have been reported.

Table 4.10: Atomic percentage of the second-phase oxide

% Fe	% Cr	% Cu	% Ni	% Si	% O	% C
5.26	2.2	0.4	0.1	26.0	51.6	14.5

In fact, the EDX analysis carried out on the areas highlighted in red in Figure 4.19, showed the presence of second-phase oxide. From the stoichiometric ratio of silicon, present in 26%, and oxygen with about 52%, the presence of silicon oxides (SiO2) is therefore found. These oxides are dispersed throughout the material and represent internal inclusions that could cause a reduction in mechanical performances of the material.

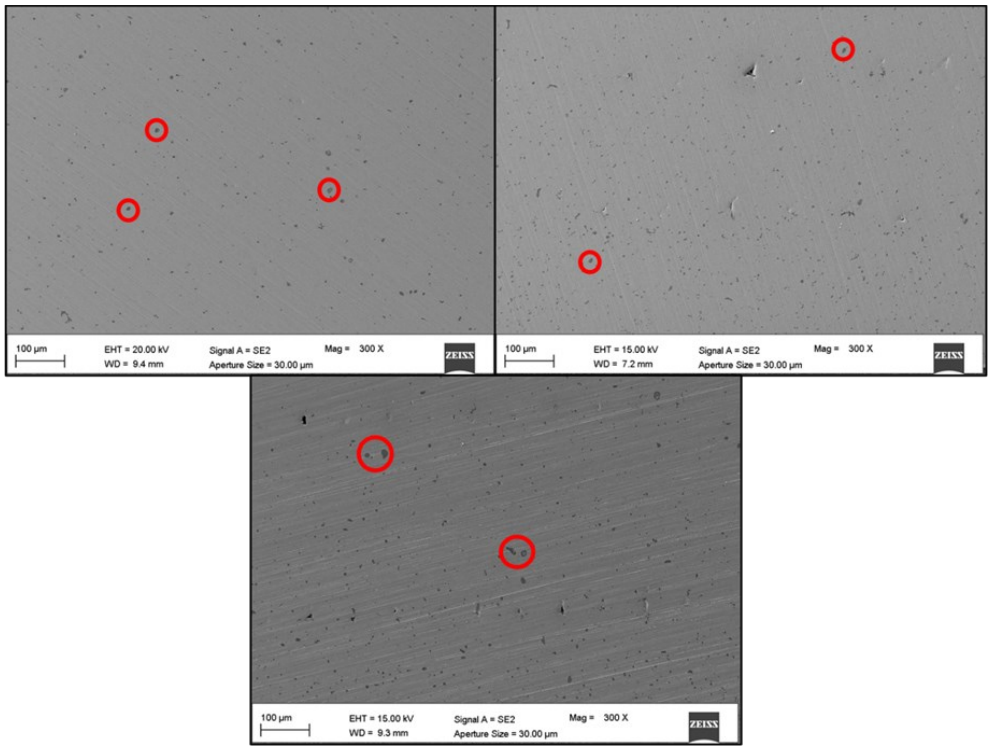

Figure 4.19: SEM observation at 300x magnitude for 0°, 45° and 90° growth orientation angle

Silica particles may form during both water atomization and sintering processes, indeed inclusions of SiO2 particles have been reported on the surface of metal powders as well as on sintered stainless steels. Their presence has been attributed to low dewpoint, or high residual water content in the sintering chamber, to low sintering or atomization process temperature, or to reoxidations processes which can occur for slow cooling rates of sintering or atomization. However, it is not possible to avoid

the formation of SiO2 inclusions due to the high oxygen affinity and its difficulty to reduction in the sintering furnace.

Optical investigations have shown fracture surfaces characterized by the presence of aligned voids due to deposition during 3D printing. Figure 4.20 shows the distribution of the voids which are visible only at the ends of the 45° fracture section of the 0° oriented specimen. The 3D reconstruction is an explanation of the voids formation during the material deposition.

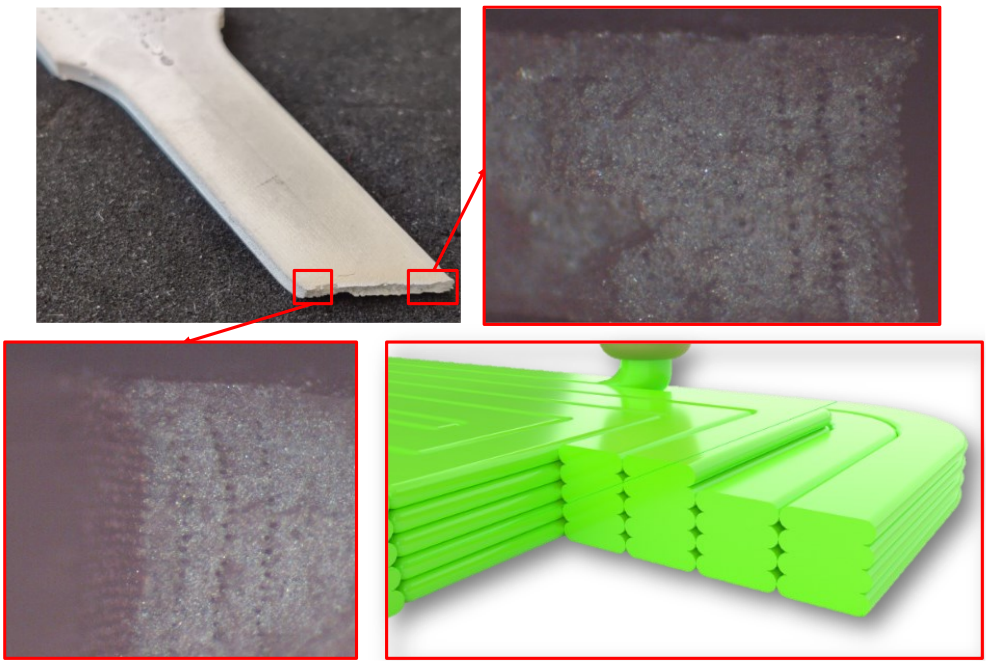

Figure 4.20: Fractures magnification where voids are distributed at the extremity of specimens with 3D explaining reconstruction

Voids are generated during the deposition of the material in printing process, and they are due to the imperfect compaction of the material between the adjacent depositions as explained in the 3D reconstruction of Figure 4.20 and by the author of this work in [46]. In fact, the deposition of the material does not create shapes with a perfect rectangular section, such as to make the whole section of the piece full and compact, but, on the contrary, generates deposition lines with elliptical or flat section with rounded edges, such as to generate voids of regular shape both between

the different layers and between the different deposition lines. Another image that reveals even more clearly the formation of voids due to deposition is the Figure 4.21 that shows the fracture section of a specimen made with a growth orientation angle of 90° where the alignment of the voids due to the linear infill pattern deposition is easily recognizable.

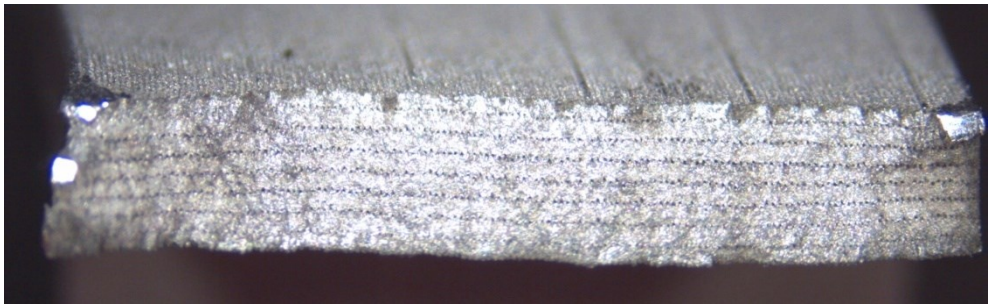

Figure 4.21: Fracture section of a 90° growth orientation angle specimen characterized by the presence of aligned voids

LCA analysis

Figure 4.22 shows the results of the comparative analysis in terms of Global Warming Potential. The trend found using the CED indicator is the same as that of the GWP, as illustrated in Table 4.10.

As expected, Scenario 2 is associated with the highest environmental load (5.70 kg CO2eq vs 5.45 kg CO2eq) because of the heat treatment phase which is not present in Scenario 1. However, the electrical energy consumption needed to carry out the aging process is low if compared to the other production phases (i.e., printing and sintering); hence, the difference in impacts between the two scenarios is less than 5% for both the considered impact categories.

Besides the H900 treatment, the two scenarios are identical, so the following considerations are valid for both of them. The most significant contributions to the carbon footprint are determined by the printing and sintering phases, which combined account for more than 82% of the total GWP and CED values.

The sintering furnace has a high energy requirement (it required a total of 71.5 kWh to complete a cycle); however, its impacts are distributed over a large number of components sintered simultaneously. On the other hand, the electrical energy

consumption per part of the printing machine does not decrease as the number of produced specimens increase (printing time and energy consumption are roughly linear with the number of specimens produced during a cycle). For this reason, despite the lower nominal power of the printer, it has an energy consumption 25% higher than the furnace. The overall impacts of the sintering phase are higher than those of the printing phase because of the inert gas consumption; argon production and transport account for about 20% of the impacts of the sintering cycle.

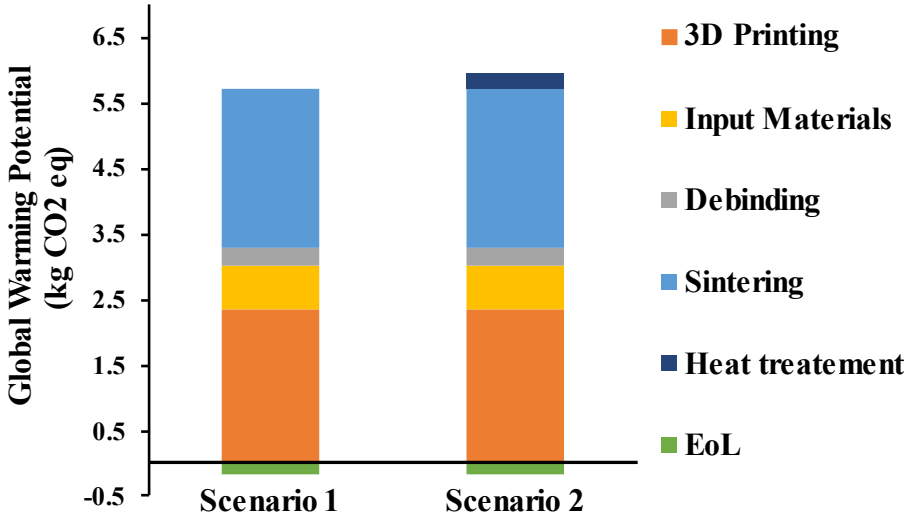

Figure 4.22: LCIA results in terms of Global Warming Potential

The debinding phase presents the lowest environmental impacts (0.28 kg CO2 eq and 6.15 MJ); the debinder is characterized by low energy consumption and a great capacity, that allows processing a large number of parts simultaneously. The organic solvent contributes for 3.11 MJ and 0.109 kg CO2 eq on the debinding phase impacts.

Table 4.10: LCIA results in terms of GWP and CED

	Global Warming Potential (kg CO2 eq)		**Cumulative Energy Demand (MJ)**	
	As sintered	Aged	As sintered	Aged
Total	5.45	5.70	98.94	103.29
3D Printing	2.34	2.34	40.46	40.46
Debinding	0.28	0.28	6.15	6.15
Input Materials	0.68	0.68	9.95	9.95
Sintering	2.41	2.41	44.58	44.58
EoL	-0.17	-0.17	-2.06	-2.06
Heat treatment	/	0.25	/	4.35

Depending on the considered scenario and impact indicator, input materials contribution ranges between 9.6% and 12.5% and it accounts for 0.68 kg CO2 eq and 9.95 MJ. These values are mainly determined by the stainless steel production (0.61 kg CO2 eq and 8.62 MJ) while the other metal rods production phases (binder production, transport, extrusion, and atomization) do not have a strong influence on the final results. Additive Manufacturing technologies use material only where needed and do not have significant scrap production as in the case of traditional chip removal techniques; for this reason, even considering the production cycle of the metal rods (including atomization, polymer production, transport and rods extrusion), input materials do not have a relevant impact in the BMD technology for what concerns CED and GWP indicators. In addition, final components can be easily recycled, further reducing raw materials environmental impacts. In this particular case, specimens recycling reduces the impacts of 0.26 kg CO2 eq and 2.2 MJ. Incineration of spent solvent determines impacts equal to 0.14 MJ for CED and 0.09 kg CO2 eq for GWP.

For what concerns the ReCiPe midpoint categories, a significant influence on the total impact of the metal rods production was observed. Specifically, it contributes for more than 80% on impact categories such as Terrestrial ecotoxicity, Marine ecotoxicity, Freshwater ecotoxicity, Human carcinogenic and Mineral resource scarcity. This behavior is mainly determined by the chromium used for the stainless steel powder. The sintering phase has a strong influence on the Ionizing radiation impact category (it accounts for more than 90% of total environmental impacts). This is attributed to inert gas production. No relevant environmental impacts were observed for solvent production and incineration. For CED and GWP, a major contribution associated with energy consumption of various production phases is usually noticed.

Sensitivity analysis

If specimens with the same load resistance are compared, i.e. able to withstand the same load before reaching the ultimate tensile strength, the Scenario 1 specimens would need a bigger cross section and they would be heavier than those of Scenario 2. This would imply greater impacts of the printing phase (which would require longer printing time and electrical energy consumption) and of the input materials. The other production phases would remain unchanged. Specifically, comparing the ultimate tensile strength of the two scenarios and considering simple mathematical relationships between cross section, stress and load, the untreated samples would require to be about 23% heavier than the aged ones to withstand the same maximum load. The environmental behavior of the latter can be easily estimated by considering a linear relationship between the part weight and the printing phase energy consumption. The results of this sensitivity analysis showed that, considering samples with the same mechanical resistance, the aged samples would have lover environmental loads according to both CED and GWP. In detail, the impact reduction would be equal to 8% and 7% according to GWP and CED respectively.

In the engineering design process, different materials or processes are typically compared by evaluating their capacity to withstand a load before reaching the ultimate tensile strength. In this context, given a defined load, the Scenario 1 specimens need a bigger cross section and, thus, they are heavier than those of Scenario 2. This implies greater impacts of the printing phase (which requires longer printing time and electrical energy consumption) and of the input materials. The other production phases remain unchanged. By comparing the ultimate tensile strength of the two scenarios and considering the engineering relationships between

cross section, stress and load, the untreated samples require to be about 23% heavier than the aged ones to withstand the same maximum load.

The environmental behavior of the latter is estimated by considering a linear relationship between the part weight and the printing phase energy consumption. The result of this analysis demonstrates that, as samples with the same mechanical resistance are concerns, the aged samples have lower environmental loads. In detail, the impact reduction is equal to 8% and 7% according to GWP and CED, respectively.

5 Conclusions

This thesis work aimed at analyzing the effect of the main parameters of the 3D printing process of the innovative BMD technology on the tensile mechanical performance of 17-4 PH stainless steel, used for this study. The analysis involved the realization of tensile specimens, compliant with the indications of the ASTM E8 standard, through the choice of the main parameters of the 3D printing process, such as the angle of orientation of growth with respect to the printing bed, the type of infill pattern, the printing speed, and the size of the diameter of the extrusion nozzle. Some of the tension specimens thus made have also been subjected to an aging process, as reported in the MPIF 35 standard, before being subjected to tensile tests together with all the other specimens, realized in the different conditions studied, always following what is indicated in the ASTM E8 standard. The main results can be summarized as follows:

- the spectrometry analysis shows that all the percentage values of 17-4 PH BMD specimens are in the range of given reference values reported in Desktop Metal technical datasheet, except for copper which is below the reported threshold.
- samples printed using a linear infill pattern, nozzle diameter at 0.4 mm, printing speed of 30 mm/s and growth orientation angle of 0 and 90° are characterized by mechanical properties in agreement with those reported in the MPIF Standard 35, characterized by similar values of Young's Modulus, yield strength, and UTS, even though samples printed at 90° exhibits a lower ductility than the 0° one, while the configuration at 45° does not exhibit values similar to those reported in the standard showing the lowest mechanical properties, with a decrease in UTS, Young's modulus and in elongation a break in respect the 0° configuration;
- for specimens realized with the infill pattern at ±45°, keeping constant nozzle diameter at 0.4 mm and printing speed of 30 mm/s, the growth orientation angles of 0° and 90° exhibit the higher UTS, Young's modulus and yield strength in respect of the 45° ones, while, if specimens realized with an infill pattern of 0°-90° are taken into account, they shown the same behavior on the elongation at break as those realized of the specimens with growth orientation angle of 90° with infill pattern of ±45°;
- the infill pattern affects the tensile mechanical properties with a slight decrease in UTS and yield strength for configurations with infill patterns of

±45° and 0°-90° compared to the linear one at 0°, while is a little more evident the decrease in Young's modulus. For the elongation at break, the reduction of ductility due to the infill pattern different from the linear one for specimens made with a growth orientation angle of 90° is remarkable;

- the influence of the printing speed is minimal on the main tensile mechanical properties' whit values very similar to each other for the different categories with a very slight tendency to decrease as the printing speed increases from 15 mm/s to 60 mm/s;
- assuming as a hypothesis that the minimum difference in mechanical performance presented by 17-4 PH to the variation of the printing speed is such as not to be appreciable, to realize n° 3 tensile specimens at a speed of 15 mm/s the printing system takes about 17 hours, time needed for the realization of n° 5 tensile specimens at a speed of 60 mm/s, and the time needed to realize n° 2 specimens at 15 mm/s is the same for printing n° 3 specimens at 30 mm/s. An increase in printing speed leads to a reduction in the quality of the parts, especially on the realization of aesthetic details that, at higher speeds, are much more evident than at low construction speeds;
- the use of a nozzle with a diameter of 0.25 mm, instead of one of 0.4 mm, shows in all the three cases a clear reduction in elongation at break, which denotes a substantial reduction in the ductility of the samples, but has left unchanged the results obtained for the tensile specimens with a growth orientation angle of 0°, while led to an improvement of performances for specimens with a growth orientation angle of 45° and worse performance for the 90° ones. This behaviour can be attributed to the fact that, by decreasing the size of the nozzle, the level of quality of the material deposition increases, thus generating a better uniformity of the layer and consequently reducing the voids that are generated with a larger diameter nozzle, with a better adhesion of the powders during the sintering phase which allows to increase the density of the part;
- H900 heat treatment increase in a remarkable way the properties UTS and yield Strength and Young's modulus of specimens, while the elongation at break undergoes an important decrease, confirming a clear increase in the fragility of the material after heat treatment;
- the EDX analysis showed the presence of second-phase oxide; from the stoichiometric ratio of silicon, present in 26%, and oxygen with about 52%, the presence of silicon oxides (SiO_2) is therefore found. These oxides are dispersed throughout the material and represent internal inclusions that could cause a reduction in mechanical performances of the material;

- Optical investigations have shown fracture surfaces characterized by the presence of aligned voids generated during the deposition of the material in 3D printing process, due to the imperfect compaction of the material between the adjacent depositions lines with elliptical or flat section with rounded edges, such as to generate voids of regular shape both between the different layers and between the different deposition lines;
- As sintered specimens performed better from the environmental point of view, but the aging process accounts for less than 5% of the total environmental impacts and improves greatly the material mechanical performances. The printing and sintering phases are those with the greatest impacts, attributed to the high electrical energy consumption of the printing machine and of the furnace.
- Input materials demonstrate low impacts and are mainly determined by the stainless steel production process.
- If specimens with the same load resistance are considered, the aging process contributes to the reduction of the environmental impacts of 3D printed metal parts and heat-treated components represent the best alternatives when high mechanical properties are required; on the other hand, aging can be avoided for non-structural parts.

Starting from these results, the next step for the research will be to evaluate the flexural and compression performance of the same material, taking into account all the conditions already studied for the tensile behavior. A further possibility that will still be taken into consideration for the continuation of this research activity is to evaluate the performance of 17-4 PH stainless steel obtained with both other 3D printing technologies and traditional ones. In fact, future work will be focused on the impacts analysis of BMD 3D printed components in comparison with the ones produced using traditional processes. The service life of the parts can be also considered in the study to evaluate the benefits of possible weight reduction achieved through metal 3D printing.

Bibliography

[1] K. V. Wong, A. Hernandez, A Review of Additive Manufacturing, ISRN Mech. Eng. 2012 (2012) 1–10. https://doi.org/10.5402/2012/208760.

[2] I. Gibson, D. Rosen, B. Stucker, Introduction and Basic Principles, Addit. Manuf. Technol. (2015) 1–18. https://doi.org/10.1007/978-1-4939-2113-3_1.

[3] A. Pellegrini, F. Lavecchia, M.G. Guerra, L.M. Galantucci, Influence of aging treatments on 17–4 PH stainless steel parts realized using material extrusion additive manufacturing technologies, Int. J. Adv. Manuf. Technol. (2023). https://doi.org/10.1007/s00170-023-11136-3.

[4] V. Di Pompeo, A. Santoni, E. Santecchia, S. Spigarelli, On the Short-Term Creep Response at 482 °C (900 °F) of the 17-4PH Steel Produced by Bound Metal Deposition, Metals (Basel). 12 (2022) 477. https://doi.org/10.3390/met12030477.

[5] M. Gabilondo, X. Cearsolo, M. Arrue, F. Castro, Influence of Build Orientation, Chamber Temperature and Infill Pattern on Mechanical Properties of 316L Parts Manufactured by Bound Metal Deposition, Materials (Basel). 15 (2022) 1183. https://doi.org/10.3390/ma15031183.

[6] T. Fongsamootr, I. Thawon, N. Tippayawong, K.Y. Tippayawong, P. Suttakul, Effect of print parameters on additive manufacturing of metallic parts: performance and sustainability aspects, Sci. Rep. 12 (2022) 19292. https://doi.org/10.1038/s41598-022-22613-2.

[7] A. Watson, J. Belding, B.D. Ellis, Characterization of 17-4 PH Processed via Bound Metal Deposition (BMD), in: Miner. Met. Mater. Ser., Springer, 2020: pp. 205–216. https://doi.org/10.1007/978-3-030-36296-6_19.

[8] F. Bjørheim, I.M. La Torraca Lopez, Tension testing of additively manufactured specimens of 17-4 PH processed by Bound Metal Deposition, IOP Conf. Ser. Mater. Sci. Eng. 1201 (2021) 012037. https://doi.org/10.1088/1757-899x/1201/1/012037.

[9] O.A. Mohamed, • Syed, H. Masood, J.L. Bhowmik, Optimization of fused deposition modeling process parameters: a review of current research and future prospects, (n.d.). https://doi.org/10.1007/s40436-014-0097-7.

[10] T. Webbe Kerekes, H. Lim, W.Y. Joe, G.J. Yun, Characterization of process–

deformation/damage property relationship of fused deposition modeling (FDM) 3D-printed specimens, Addit. Manuf. 25 (2019) 532–544. https://doi.org/10.1016/J.ADDMA.2018.11.008.

[11] C. Ziemian, M. Sharma, S. Ziemi, Anisotropic Mechanical Properties of ABS Parts Fabricated by Fused Deposition Modelling, Mech. Eng. (2012). https://doi.org/10.5772/34233.

[12] A. Decicco, J. Faust, NAG 1301 EFFECTS OF BUILD PARAMETERS ON ADDITIVE MATERIALS A Major Qualifying Project Report, (2013).

[13] L. Fernando, V. Rosas, Scholarship at UWindsor Scholarship at UWindsor Characterization of Parametric Internal Structures for Characterization of Parametric Internal Structures for Components Built by Fused Deposition Modeling Components Built by Fused Deposition Modeling, (2013). https://scholar.uwindsor.ca/etd (accessed March 17, 2023).

[14] J. Cantrell, S. Rohde, D. Damiani, R. Gurnani, L. Di Sandro, J. Anton, A. Young, A. Jerez, D. Steinbach, C. Kroese, P. Ifju, Experimental characterization of the mechanical properties of 3D printed ABS and polycarbonate parts, Conf. Proc. Soc. Exp. Mech. Ser. 3 (2017) 89–105. https://doi.org/10.1007/978-3-319-41600-7_11/COVER.

[15] Z. Quan, A. Wu, M. Keefe, X. Qin, J. Yu, J. Suhr, J.H. Byun, B.S. Kim, T.W. Chou, Additive manufacturing of multi-directional preforms for composites: opportunities and challenges, Mater. Today. 18 (2015) 503–512. https://doi.org/10.1016/J.MATTOD.2015.05.001.

[16] P.M. Pandey, N. V. Reddy, S.G. Dhande, Real time adaptive slicing for fused deposition modelling, Int. J. Mach. Tools Manuf. 43 (2003) 61–71. https://doi.org/10.1016/S0890-6955(02)00164-5.

[17] O.A. Mohamed, S.H. Masood, J.L. Bhowmik, A.E. Somers, Investigation on the tribological behavior and wear mechanism of parts processed by fused deposition additive manufacturing process, J. Manuf. Process. 29 (2017) 149–159. https://doi.org/10.1016/J.JMAPRO.2017.07.019.

[18] V. Kostakis, V. Niaros, C. Giotitsas, Open source 3D printing as a means of learning: An educational experiment in two high schools in Greece, Telemat. Informatics. 32 (2015) 118–128. https://doi.org/10.1016/J.TELE.2014.05.001.

[19] F. Ali, B. V Chowdary, J. Maharaj, Influence of Some Process Parameters on Build Time, Material Consumption, and Surface Roughness of FDM Processed Parts: Inferences Based on the Taguchi Design of Experiments,

(n.d.) 978–979.

[20] S. Kumar, Selective Laser Sintering/Melting, in: Compr. Mater. Process., Elsevier, 2014: pp. 93–134. https://doi.org/10.1016/B978-0-08-096532-1.01003-7.

[21] V. Di Pompeo, A. Forcellese, T. Mancia, M. Simoncini, A. Vita, Effect of Geometric Parameters and Moisture Content on the Mechanical Performances of 3D-Printed Isogrid Structures in Short Carbon Fiber-Reinforced Polyamide, J. Mater. Eng. Perform. (2021). https://doi.org/10.1007/s11665-021-05659-7.

[22] Y. Tang, Z. Huang, J. Yang, Y. Xie, Enhancing the Capillary Force of Binder-Jetting Printing Ti6Al4V and Mechanical Properties under High Temperature Sintering by Mixing Fine Powder, Met. 2020, Vol. 10, Page 1354. 10 (2020) 1354. https://doi.org/10.3390/MET10101354.

[23] A. I. Khadim, Adil; Ibraheem, Aysar; Hameed, Electrical Properties & Microstructure Of ZnO -Based Varistor Ceramics Doped With Rare Earth, n.d. https://doi.org/10.13140/RG.2.2.24962.53447.

[24] R.K. Lenka, P.K. Patro, T. Mahata, Shape Forming and Sintering of Ceramics, (2022) 1–54. https://doi.org/10.1007/978-981-16-1803-1_1.

[25] J.H. Martin, B.D. Yahata, J.M. Hundley, J.A. Mayer, T.A. Schaedler, T.M. Pollock, 3D printing of high-strength aluminium alloys, Nat. 2017 5497672. 549 (2017) 365–369. https://doi.org/10.1038/nature23894.

[26] S. Kumar, Selective Laser Sintering/Melting, Compr. Mater. Process. 10 (2014) 93–134. https://doi.org/10.1016/B978-0-08-096532-1.01003-7.

[27] J.A. Slotwinski, E.J. Garboczi, P.E. Stutzman, C.F. Ferraris, S.S. Watson, M.A. Peltz, Characterization of Metal Powders Used for Additive Manufacturing, J. Res. Natl. Inst. Stand. Technol. 119 (2014) 460. https://doi.org/10.6028/JRES.119.018.

[28] V. Gunenthiram, P. Peyre, M. Schneider, M. Dal, F. Coste, R. Fabbro, Analysis of laser–melt pool–powder bed interaction during the selective laser melting of a stainless steel, J. Laser Appl. 29 (2017) 022303. https://doi.org/10.2351/1.4983259.

[29] V. Gunenthiram, P. Peyre, M. Schneider, M. Dal, F. Coste, R. Fabbro, Analysis of laser–melt pool–powder bed interaction during the selective laser melting of a stainless steel, J. Laser Appl. 29 (2017) 022303. https://doi.org/10.2351/1.4983259.

[30] M.J. Matthews, G. Guss, S.A. Khairallah, A.M. Rubenchik, P.J. Depond, W.E. King, Denudation of metal powder layers in laser powder bed fusion processes, Acta Mater. 114 (2016) 33–42. https://doi.org/10.1016/J.ACTAMAT.2016.05.017.

[31] A. Dass, A. Moridi, State of the Art in Directed Energy Deposition: From Additive Manufacturing to Materials Design, Coatings 2019, Vol. 9, Page 418. 9 (2019) 418. https://doi.org/10.3390/COATINGS9070418.

[32] T. Petrat, C. Brunner-Schwer, B. Graf, M. Rethmeier, Microstructure of Inconel 718 parts with constant mass energy input manufactured with direct energy deposition, Procedia Manuf. 36 (2019) 256–266. https://doi.org/10.1016/J.PROMFG.2019.08.033.

[33] C. Schneider-Maunoury, L. Weiss, P. Acquier, D. Boisselier, P. Laheurte, Functionally graded Ti6Al4V-Mo alloy manufactured with DED-CLAD® process, Addit. Manuf. 17 (2017) 55–66. https://doi.org/10.1016/J.ADDMA.2017.07.008.

[34] S. Yin, P. Cavaliere, B. Aldwell, R. Jenkins, H. Liao, W. Li, R. Lupoi, Cold spray additive manufacturing and repair: Fundamentals and applications, Addit. Manuf. 21 (2018) 628–650. https://doi.org/10.1016/J.ADDMA.2018.04.017.

[35] B. Kevin, C. Laurent, B.A. Oussama, M. Mequignon, Z. Georges, Life cycle assessment of lighting systems and light loss factor: A case study for indoor workplaces in France, Electron. 8 (2019). https://doi.org/10.3390/electronics8111278.

[36] M. Germani, M. Mandolini, M. Marconi, E. Marilungo, A Method for the Estimation of the Economic and Ecological Sustainability of Production Lines, Procedia CIRP. 15 (2014) 147–152. https://doi.org/10.1016/J.PROCIR.2014.06.072.

[37] J.M.C. Azevedo, A. CabreraSerrenho, J.M. Allwood, Energy and material efficiency of steel powder metallurgy, Powder Technol. 328 (2018) 329–336. https://doi.org/10.1016/J.POWTEC.2018.01.009.

[38] K. Raoufi, S. Manoharan, T. Etheridge, B.K. Paul, K.R. Haapala, Cost and Environmental Impact Assessment of Stainless Steel Microreactor Plates using Binder Jetting and Metal Injection Molding Processes, Procedia Manuf. 48 (2020) 311–319. https://doi.org/10.1016/J.PROMFG.2020.05.052.

[39] I. Bianchi, A. Forcellese, M. Marconi, M. Simoncini, A. Vita, V. Castorani, Environmental impact assessment of zero waste approach for carbon fiber

prepreg scraps, Sustain. Mater. Technol. 29 (2021) e00308. https://doi.org/10.1016/J.SUSMAT.2021.E00308.

[40] D. Landi, P. Cicconi, M. Germani, Analyzing the environmental sustainability of packaging for household appliances: A test case, Procedia CIRP. 90 (2020) 355–360. https://doi.org/10.1016/J.PROCIR.2020.01.106.

[41] L. Postacchini, M. Simoncini, A. Forcellese, M. Bevilacqua, F.E. Ciarapica, G. Andreassi, A.C. Russo, Environmental assessment of an automated impregnation process of carbon fiber tows, Procedia CIRP. 88 (2020) 445–450. https://doi.org/10.1016/J.PROCIR.2020.05.077.

[42] T. Bellezze, G. Roventi, R. Fratesi, Localised corrosion and cathodic protection of 17 4PH propeller shafts, Http://Dx.Doi.Org/10.1179/1743278213Y.0000000082. 48 (2013) 340–345. https://doi.org/10.1179/1743278213Y.0000000082.

[43] C. Dudescu, L. Racz, Effects of Raster Orientation, Infill Rate and Infill Pattern on the Mechanical Properties of 3D Printed Materials, ACTA Univ. Cibiniensis. 69 (2017) 23–30. https://doi.org/10.1515/aucts-2017-0004.

[44] J. Triyono, H. Sukanto, R.M. Saputra, D.F. Smaradhana, The effect of nozzle hole diameter of 3D printing on porosity and tensile strength parts using polylactic acid material, Open Eng. 10 (2020) 762–768. https://doi.org/10.1515/eng-2020-0083.

[45] J.M. Chacón, M.Á. Caminero, P.J. Núñez, E. García-Plaza, J.P. Bécar, Effect of nozzle diameter on mechanical and geometric performance of 3D printed carbon fibre-reinforced composites manufactured by fused filament fabrication, Rapid Prototyp. J. 27 (2021) 769–784. https://doi.org/10.1108/RPJ-10-2020-0250.

[46] I. Bianchi, A. Forcellese, T. Mancia, M. Simoncini, A. Vita, Process parameters effect on environmental sustainability of composites FFF technology, Mater. Manuf. Process. 37 (2022) 591–601. https://doi.org/10.1080/10426914.2022.2049300.